ESTIMATING UNCERTAINTIES IN THE JOINT REACTION FORCES OF CONSTRUCTION MACHINERY

James Brandon Allen

Thesis submitted to the faculty of the Virginia Polytechnic Institute and State University in partial fulfillment of the requirements for the degree of

Master of Science
In
Mechanical Engineering

Dr. Corina Sandu, Chair

Dr. Mehdi Ahmadian

Dr. Alfred L. Wicks

11 May 2009
Blacksburg, Virginia

Keywords: polynomial chaos collocation, stochastic rigid body modeling, Newtonian projection method, Caterpillar 980G Series II wheel loader

Estimating Uncertainties in the Joint Reaction Forces of Construction Machinery

James Brandon Allen

ABSTRACT

In this study we investigate the propagation of uncertainties in the input forces through a mechanical system. The system of interest was a wheel loader, but the methodology developed can be applied to any multibody systems. The modeling technique implemented focused on efficiently modeling stochastic systems for which the equations of motion are not available. The analysis targeted the reaction forces in joints of interest.

The modeling approach developed in this thesis builds a foundation for determining the uncertainties in a Caterpillar 980G II wheel loader. The study begins with constructing a simple multibody deterministic system. This simple mechanism is modeled using differential algebraic equations in Matlab. Next, the model is compared with the CAD model constructed in ProMechanica. The stochastic model of the simple mechanism is then developed using a Monte Carlo approach and a Linear/Quadratic transformation method. The Collocation Method was developed for the simple case study for both Matlab and ProMechanica models.

Thus, after the Collocation Method was validated on the simple case study, the method was applied to the full 980G II wheel loader in the CAD model in ProMechanica.

This study developed and implemented an efficient computational method to propagate computational method to propagate uncertainties through “black-box” models of mechanical systems. The method was also proved to be reliable and easier to implement than traditional methods.

ACKNOWLEDGEMENTS

First and foremost I would like to thank my advisor, friend, and mentor Dr. Corina Sandu for her direction and guidance to the development and completion of this Master's Thesis. I faced a lot of hardships coming into graduate school but she lent her time and advice to help me succeed. She believed in me every step of the way, and encouraged me to go the extra mile. Her care and individual respect for students goes above and beyond the normal advisor-student relationship. To her, I owe my success and critical thinking skills throughout my entire graduate career. Thank you Dr. Corina Sandu.

I would also like to thank Dr. Mehdi Ahmadian for inviting me to come to CVeSS department and find a home here. Because of Dr. Ahmadian's care and respect for students, I found an atmosphere that developed my character as well as intellect. He aligned me with Dr. Sandu to execute the work presented in this thesis. To him, I am grateful for the opportunity to complete a master's of science in mechanical engineering.

I would like to thank my friend and PHD candidate Mr. Emmanuel Blanchard. Emmanuel helped me understand and develop the computer code necessary to perform the deterministic and stochastic analyses. The kindness and diligence that Emmanuel displayed are highly appreciated. His pleasant character was also a relief from the everyday pressures of life, and his camaraderie will never be forgotten.

I would like to thank all of the CVeSS students and Staff. I would like to thank Brian Templeton for teaching me about batch files, my colleagues Brian Sperry and Richard Lee helped keep me motivated as well as abreast of all deadlines regarding completion of the master's degree forms. I would like to thank Hyunwook Lee and Anake Umsrithong for their help with homework problems and career advice. Their personalities and friendships will also not be forgotten. I would also like to thank Ms. Sue Teel for helping and making me feel at home at CVeSS.

First, I would like to thank Ms. Cathy Hill for accommodating many meetings with me to make sure all my classes and degree requirements were being met. Her schedule is very busy, but she made plenty of time for me and did so with a smile.

I also thank Dr. Alfred Wicks for being on my committee. Dr. Wicks always has his door open and always gets excited to help a persevering student. His kindness, mentoring, and character will never be forgotten and I thank him for his help.

I would like to thank the Mechanical Engineering Department at Virginia Tech for allowing me to pursue my dreams of obtaining a Bachelor's and a Master's Degree this department.

I would like to acknowledge Caterpillar for sponsoring this project, as well as the GEM Consortium for partially supporting me through my graduate studies.

I would also like to thank my family for supporting me throughout my undergraduate and graduate years. The love and support that they provided for me, helped sustain me and keep me focused to obtain my degrees.

CONTENT

LIST OF FIGURES

LIST OF TABLES

CHAPTER 1. INTRODUCTION

1.1 Motivation

The research motivation for the work performed in this thesis is to determine the uncertainties in the reaction forces at certain joints in multibody mechanical system. The system of interest is Caterpillar's 980G II wheel loader.

For the 980G II wheel loader, Caterpillar used a Newtonian Projection surface method to address the issue the real data not satisfying the equations of moments. This surface is typically obtained with a full set of discrete algebraic equations to kinematically and dynamically represent each component with the system.

Following the projection of the forces, Caterpillar employs a simplified equation of moments to account for the dynamics of the system, while the kinematics is kept unchanged, as provided by the kinematic model of the system.

During the collection of experimental data, Caterpillar usually conducts several measurements of the same force (e.g., load force in a hydraulic actuator used to lift the liftarm) for the same conFigureuration of the equipment (e.g., position, orientation, velocity). Analyzing such data leads to the conclusion that, although the operating conditions and the system kinematics are theoretically the same, the force values collected are different. Thus, the industry identified a need to treat this system in a stochastic framework. As such, one obtains a probability density function for a specific input force at a given moment of time. The analysis of interest is, knowing the probability of the input forces, to predict the probability of the output variables of interest, such as the reaction forces in selected joints. Moreover, the difficulty of this task is increased due to two issues: first, the values collected experimentally will not identically satisfy the equations of motion for the system. Thus, more mathematical manipulation is needed to transform the available experimental data in input data for the models developed. Second, for most of the real-life applications of interest, only CAD models are available, so one needs to

propagate the uncertainties through a "black-box" model, with no access to the equations of motion.

The approximation introduced by the use of the simplified dynamics model (versus full dynamics model) in predicting the output parameters of interest is also investigated in this study. Moreover, this method cannot be implemented if no equations of motion are available for the system.

Using the linear transformation method for the mean values and the quadratic transformation to obtain the standard deviation of the stochastic outputs of interest requires off-line analysis outside the simulation model, which is costly and not computationally efficient.

1.2 Problem Statement

The motivation behind this study and the challenges posted by obtaining the uncertainties in output variables based on measured, experimental data yield the following problem statement.

In this study we will investigate quantifying and propagating uncertainties through mechanical systems treated as "black-boxes." A computationally efficient technique will be developed, that will eliminate the need of projecting forces or constructing approximate, simplified models for the systems studied.

The use of the polynomial-chaos-based Collocation approach will be analyzed. The Collocation Method involves solving a set of orthogonal polynomials to obtain a set of collocation points that are representative for the stochastic nature of the input forces. Such points will be used to define the input in the simulation model. The accuracy and ease of implementation of this approach will also be investigated.

1.3 Research Approach

The research approach used to solve the problem outlined involves a sequence of specific objectives. The first objective of this study is to build a simple 2-D double pendulum rigid body mechanism and to analyze the kinematics and dynamics of the system implemented in both Matlab and in ProMechanica. In Matlab, the model is defined with a set of differentiable algebraic equations. In ProMechanica, the system is built as a CAD model with assembly

constraints. The purpose of this objective is to validate the stochastic technique developed on a model for which we can have access to the equations of motion before we implement it on the full CAD model of the wheel loader, for which no equations of motion were available.

The second objective is to develop the stochastic framework modeling methodology using the Collocation approach and to implement it on the simple case study. As part of this objective, the approach used by Caterpillar will also be implemented, as well as for benchmarking purposes. The Collocation Method will next be applied to the full differentiable algebraic equations, instead of the reduced model (based on the equations of moments). We will consider one parameter in the DAE uncertain and will conduct a full collocation analysis in Matlab. The collocation values thus obtained for the uncertain input parameter will then used as the uncertain input into the ProMechanica version of the simple mechanism. The uncertain parameter induces a variation in the reaction forces in both Matlab and ProMechanica simple mechanisms.

The third objective is to implement the collocation approach developed to determine the uncertainties in the reaction forces in the joints of the 980G II wheel loader. There are no equations of motion available for the 980G wheel loader. Therefore, we construct a way to run a collocation analysis on the ProMechanica model in a "black-box" approach. An uncertain force acting on the liftarm of the wheel loader is assumed as stochastic. From the mean and standard deviation data provided by Caterpillar for this stochastic input force, an algorithm was developed to determine the collocation values of the uncertain force. These values, similar to simple mechanism, are used as inputs into the ProMechanica model and variations in the reaction forces are analyzed. The results from ProMechanica are post-processed to generate histograms centered about each of the resulting reaction forces, and the resulting PDF's are obtained for the reaction forces of interest.

The specific research tasks are discussed in section 1.4.

1.4 Research Tasks

The Following is a list of the research tasks necessary to achieve the research objectives ultimately leading to the analysis of the reaction joints on the full 980G II Caterpillar wheel loader.

a. Build a simple case study of a constrained mechanical system and develop the deterministic model in a differential-algebraic equations form.
b. Develop a CAD model of the same system and implement it in ProMechanica.
c. Develop an approximate simplified deterministic model (based on the Caterpillar approach) by using an equation of moments for the link of interest.
d. Benchmark the simulation results of the three deterministic models above.
e. Implement the linear transformation method for the mean and quadratic transformation for the standard deviation.
f. Develop a Monte Carlo model for the model in part c.
g. Develop a polychaos collocation model for the models developed in a) and b)
h. Develop the collocation model for the full CAD model of a 980G II wheel loader in ProMechanica.

1.5 Outline of Thesis

In Chapter 1, we presented the motivation and the problem statement for the work conducted in this thesis. The project tasks and research objective were also established in detail.

Chapter 2 focuses on a review of literature on wheel loaders. This chapter contains information for the typical assembly of a wheel loader and its subsystems. Methods of modeling a wheel loader kinematically and dynamically are reviewed. In addition, this chapter presents methods developed to control the forces acting on the wheel loader, as well as to minimize the uncertainties in these forces.

Chapter 3 presents the deterministic model for the simple case study. This chapter discusses the method of modeling the simple mechanism in Matlab as well as in ProMechanica. The results from the kinematic analysis of the Matlab and ProMechanica model are compared to establish accuracy of the ProMechanica simple mechanism. Lastly, the derivation of the reduced model based on the equation of moments is presented. The dynamic results of the reduced model for the uncertain output force of interest are compared to the force predicted by the full dynamics model (based on DAE's).

Chapter 4 presents the stochastic analysis done on the simple case mechanism. In this chapter, the linear/quadratic transformation and Monte Carlo methods are performed on the simple mechanism with the reduced equation of moments. The results from these stochastic methods are presented. The Collocation Method for the simple case mechanism is also presented with the results from both in Matlab and ProMechanica models.

In Chapter 5, the Collocation Method for the full 980G wheel loader is presented. Explanations for the basis of using ProMechanica as well as the description of the deterministic model are presented. The assumptions behind the distribution of the uncertain parameters as well as the algorithm used to generate collocation points are presented. Lastly, a comparison of the results from the uncertain input force is compared with results from Caterpillar studies. The results from applying the Collocation Method to obtain the uncertain reaction forces of interest are compared against the data published by Caterpillar.

CHAPTER 2. REVIEW OF LITERATURE

2.1 The history of wheel loaders

Wheel loaders evolved from agricultural tractors. They were introduced in the early 20th century as gasoline powered vehicles with lifting capabilities. This spawned the future design of wheel loaders in which the tractor was turned backwards and the liftarms were mounted in the rear. This design led to higher load capacity, but more safety and stability problems than the front-end wheel loader. The instability problems happened in the rear wheel steering. Manufacturers quickly abandoned the rear-mounted liftarm frame for a front-end loader. Early wheel loaders also had bigger wheels in the front than in the back, but have since maintained equal wheel size for practicality reasons in manufacturing the wheel loader [1]. A typical wheel loader is illustrated in Figure 2-1.

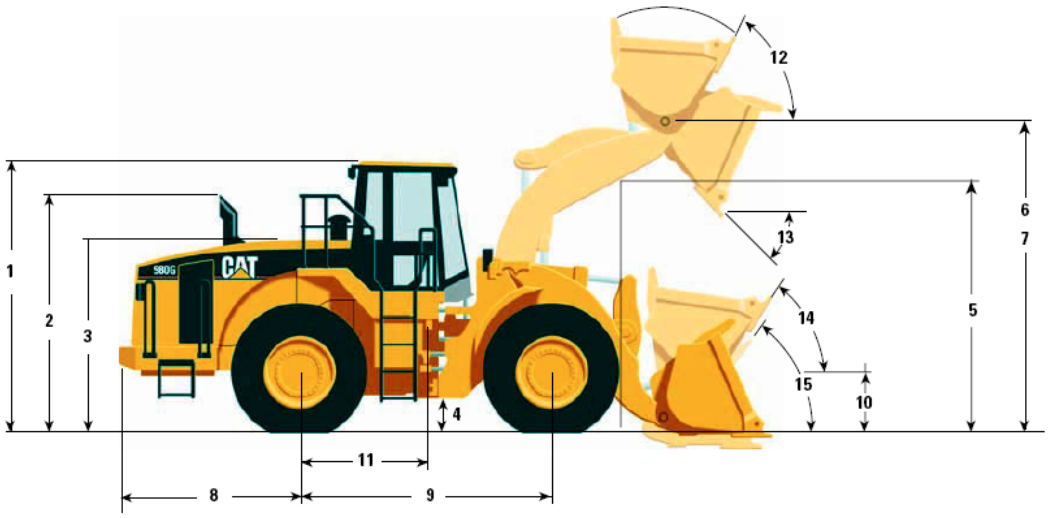

1	Height to top of ROPS	3753 mm	12'4"
2	Height to top of exhaust pipe	3390 mm	11'1"
3	Height to top of hood	2332 mm	7'8"
4	Ground clearance/ Standard tire 29.5-R25 (L-3) See Chart below for other tires	467 mm	1'6"
5	Lift arm clearance @ maximum lift	3764 mm	12'4"
6	B-Pin height	4505 mm	14'9"
7	Optional high lift	4727 mm	15'6"

8	Center line of rear axle to edge of counterweight	2493 mm	8'2"
9	Wheelbase	3700 mm	12'2"
10	Height to center line of axle	457 mm	1'6"
11	Center line of rear axle to hitch	1850 mm	6'1"
12	Rack back @ maximum lift	61°	
13	Dump angle @ maximum lift	45°	
14	Rack back @ carry	46°	
15	Rack back @ ground	36°	

Figure 2-1. Side view of modern day wheel loader (Courtesy of Caterpillar)

Today, the modern wheel loader is a rear-engine tractor with front-mounted lifting equipment. The rear axles are mounted on a pivoting joint to allow wheel contact on uneven surfaces. Average compact wheel loaders range from 2000-300 kg. Large mining wheel loaders are as large as 200,000 kg. The majority of the wheel loaders range from 10,000 kg-50,000 kg, which equates to the size of a heavy truck [1].
The maximum carrying load of a wheel loader is about 60% of the unloaded wheel loader weight. Because front-end loaders pick up loads in the front, the loads shift the center of gravity of the wheel loader.

The dynamics of a wheel loader is typically quite complex. Analyzing the dynamics of a wheel loader is difficult due to the natural frequencies of the wheel loader bodies being at the same natural frequency of the entire vehicle. Therefore, several vehicle parts can contribute to low frequency vibration, which means that more components have to be considered in analysis [1].

2.2 Modeling of lifting in wheel loaders

The main systems in a wheel loader include the engine end-frame, non-engine end-frame, and bucket. The major activators and positions of movement on a wheel loader include steering cylinders, levers, tilt link, lift cylinders, tilt lever, and hitch pin. The wheel loader turns about a central pivot called the hitch pin. The operator controls the wheel loader to execute digging and dumping cycles to remove large portions of materials [2].

During the operation of the wheel loader land dumping, the lift cylinders raise and lower the bucket, and tilt cylinders dump and rack the bucket. The tilt cylinders have dump and rack-stop forces associated with them which are examined later in the thesis. The steering cylinders move the non-engine end-frame about the hitch pin. Buckets come with many different accessories depending on the specific operation. For example, buckets with teeth are used to decrease digging resistance, while spade-shaped buckets are used for tough digging operations. Buckets also have wear plates which are separate attachments which are replaced when worn down [2].

The purpose of the hydraulic subsystem of the wheel loader is to control the position of the bucket. This hydraulic systems contains pumps, valves, and hoses which direct fluid to the lift and tilt cylinders. Lift and tilt cylinders control two different degrees of freedom of the bucket. The operator of a wheel loader can vary the amount of flow in a lift cylinder or tilt cylinder to extend or collapse them. By fully extending the tilt cylinder, the bucket dumps the material. Fully collapsing the tilt cylinders causes the tilt cylinder to rack so that material can be loaded into the bucket [2].

The purpose of the study in [2] was to understand the functionality of a wheel loader. More importantly, this work describes the scooping and digging sequences of a wheel loader, particularly the dump and rack-stop loads. The work presented on the terminology of the rack force, which is important to the understanding of the context 980G II collocation analysis. It is the rack force which is uncertain, because it is a force that is transmitted to the non-engine end-frame's liftarm components due to the material in the bucket.

2.3 Modeling Hydraulic Systems in the Bucket Assembly

To develop a reduced the kinematic model of a Caterpillar 990 wheel loader, the motions of the liftarm and the bucket are calculated in [3]. The motion of other bodies in the system was computed using the kinematic relationships between the other bodies and the new positions of the liftarm and bucket. This model required that the forces coming from the cylinder actuators be replaced by torques at the base-pin and tilt-lever pin of the liftarm.

One way to model the hydraulic subsystems is using a constant pressure to the hydraulic system with no load to the engine. Spool valves control the flow of the fluid to the cylinders which were modeled by using equations for a five-port hydraulic system, as shown in Eq. (2.1).

$$Q = Cx_1\sqrt{|p_s - p_1|}Sign(p_s - p_1) \qquad (2.1)$$

where Q is the flowrate, C is the discharge coefficient of the spool valve, x is the spool valve displacement, p_s is spool valve pressure, and D is the underlap of the valve [3].

The force generated by an actuator can be modeled using

$$f = p_1 A_1 - p_2 A_2 \tag{2.2}$$

where f is the force in the cylinder, p_1 is the pressure and A_1 is the area of cylinder 1.

It was shown in [3] that the kinematic modeling of the 990G wheel loader using a multibody generalize coordinate approach works well to model the position and velocities of a bucket/liftarm assembly. However, it was also shown that using fluid mechanics relationships to model the forces in the hydraulic actuators produces inconsistent dynamics of those compared to actual test data. However, the difference in the actual wheel loader data and the simulation was attributed to the hydraulic lines in the actual wheel loader not to the flowing hydraulic fluid correctly or splitting pressure correctly [3].

2.4 Forces Acting on a Wheel Loader

The work presented by Zhang, Carter, and Alleyne [4] focuses on four loads that affect a powertrain of a wheel loader. The four loads include power steering, drive, implement, and accessories. The power steering load is modeled to have a set of hydraulic cylinders used to coordinate the front non-engine end-frame and the engine endframe. The drive load is modeled as three subsystems: vehicle dynamics, tire model, and longitudinal force. Modeling the implement load is very important. This model consists of lift and tilt cylinders. Lifting moves the linkages and the bucket up or down. Tilting causes the bucket to rotate about its pinned joint. The loads experienced by the implement are caused by inertial effects from the linkages, bucket, and mass of the material the is dug. Models of digging forces are developed to accurately describe the implement load. These digging forces are modeled as of springs. The lift forces come from measured load profile data. Combining the digging forces, load profile data, and equations of motions for the lift cylinder, an accurate dynamic model representation of the implement load was created [4]. Figure 2-2 illustrates the earth-moving vehicle powertrain simulator developed in [4].

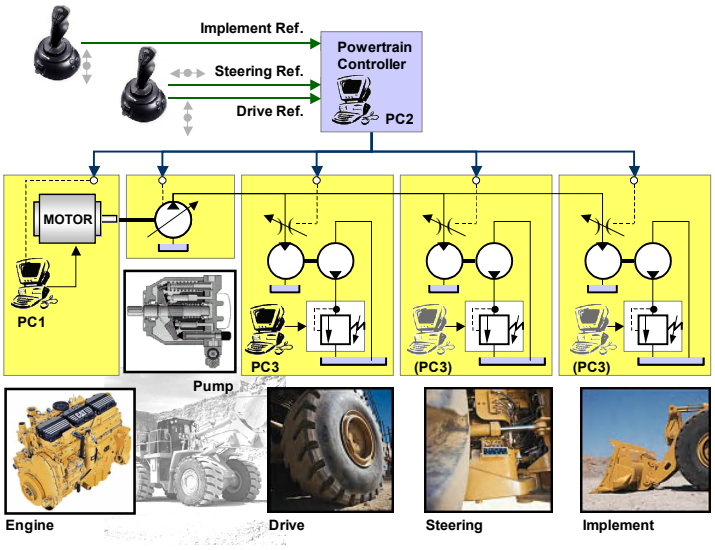

Figure 2-2. Earthmoving vehicle powertrain simulator [4]

When a wheel loader scoops pile of material during a digging operation, rimpull occurs. Rimpull, is a force exerted by the tires to propel the vehicle into a pile. Resistive force are exerted on the bucket until the resistive forces exerted on the vehicle by the pile of material equals that of the rimpull of the wheel loader.

Analyzing the resistive forces that act on the bucket of a wheel loader, one finds that there are five important forces. The pile of material transmits a force due to earth pressure and a force due to penetration during digging. Other forces exerted by the solid on the bucket are the force due to the weight of material in bucket, the force due to compaction of material, and the force due to friction between the bucket walls and the soil.

Modeling the resistive forces and running a simulation with test data shows that whenever there is no compaction force, the penetration force and the earth pressure forces are dominant in the horizontal driving direction of the wheel loader. It can also be shown that the dominant force in the vertical direction comes from the weight of the material in the bucket. Once the bucket is almost full of material, a significant increase in the earth pressure force, such as compaction of the material, will occur. One of the most important conclusions from this type of analysis shows that when the bottom of a bucket comes into contact with a pile of material, the compaction force

greatly increases, and with the earth pressure a boundary occurs which prevents the bucket from loading the material properly [4].

2.5 Internal Forces on a Wheel Loader

The internal forces on a wheel loader can be modeled using ADAMS [5]. Through extensive research, the total force acting on a wheel loader can be broken up into partial forces. These forces include, penetration force, soil cutting force and mass flow and inertia forces. The penetration force can be represented by an equation formulated by Bekker for continuous loading of soil. During the loading of a pile of soil, when the bucket retracts, loose soil falls from the bucket and the amount of the soil can be determined by bucket angle and maximum topping value determined by an internal friction angle of the material. The bucket angle determines the center of gravity and the mass of the material and center of gravity can be used to calculate inertial forces on the bucket.

In [5], a load sequence was performed by allowing the wheel loader to go forward and meet the load. The bucket is then forced into the load by wheel traction and then lifted and tilted by hydraulic cylinders. When the bucket is filled the loader reverses and continues to lift the load. The load then drives forward and empties its load. The testing was done for a cycle of 30 Hz. In testing, the author finds that there are rebound points in which the soil model and the wheel loader do not have sufficient damping. The author also shows a poor correlation between simulation results and measured data when hydraulics are not modeled in the cylinder of the lift arm [5]. Although the hydraulics are not modeled in this work, it would be advantageous to look at a reduced 980G II wheel loader model.

2.6 Computer Aided Wheel Loader Modeling

Andersson and Sellgren [6] investigated modeling a wheel loader using virtual reality or computer aided simulation programs. The main issue discussed is accurate modeling of the dynamics vehicle without knowing all of its parameters. In this article, they also discuss the use of inverse modeling though the use of computer aided in order to determine the parameters

which methods cannot be measured. The authors present a study in which they determine the reaction forces in certain bearings within the subsystems that are connected to form the liftarm of a wheel loader from VOLVO CE. The simulation in ADAMS is performed based on measured and known quantities during an experimental scooping and digging operation. The goal of the study is to determine whether the orders of magnitude of the simulation outputs are correct. In order to answer this question, the authors perform a validation based on experimentally obtained values during a real digging operation. They concluded that there was good correlation between the measured quantities, such as the force in the tilt cylinders of the wheel loader, and the simulation forces in the tilt cylinder. However, they also found that there are nonlinearities in their system that do not correlate well with the real digging sequence. The authors considered that these nonlinearities come primarily from the fluid of the hydraulic lift cylinders and were not explicitly modeled in ADAMS. The conclusion of this study is, that inverse modeling can be done effectively to determine the unknown parameters in a multibody system [6].

Some important advantages from the work presented in [6] is that ADAMS proves to be a good modeling tool for a wheel loader. The same type of kinematic analysis can be used for the 980G II wheel loader model.

2.7 Control Algorithms for Modeling Wheel Loaders

Cutting Path Trajectory

In the work presented by Ahmad Mehami [7], a control algorithm containing two levels, low and high are used to automate and control the trajectory of a wheel loader. The low level is used for normal follow trajectory and the high level is used for sensory information to adjust and correct the trajectory of the loader.

In this study, the forces that act on the bucket of a wheel loader during dumping and scooping change continuously in magnitude and direction. The trajectory can be mathematically modeled and will be a function on how much the bucket has to be raised. The material in the bucket can be approximated by the area between the stockpile of material and the trajectory of the bucket. From the volume capacity of the trajectory/load area, a new segment of the trajectory can be

calculated. From this work it was shown that the importance of calculating the trajectory can significantly reduce the resistive components that act on the load haul dumper during scooping and digging [7].

Wheel Loader Nonlinearity Control

In this study, Fales and Kelkar [8] modeled a simple wheel loader with a linkage system and hydraulics. The model has two degrees of freedom. The article discusses uncertainties due to the hydraulics of the liftarm. In order to minimize these uncertainties, Fales and Kelkar investigated a control algorithm used on the transfer function of the models dynamics and bulk modulus properties. An H-infinity controller was employed to linearize and control the uncertainty. However, linearization of the model with force control led to different system dynamics, and suggested developing a new method of linearization. The authors modified their algorithm to incorporate the nonlinearities within the valve discharge coefficient of the hydraulic lift and the bulk modulus properties of the hydraulic fluid. This modification yielded a better comparison with the original model such that the system performance criteria was met as stated at the beginning of the study. In addition, the new algorithm was more robust improving the stability of the wheel-loader simulation [8]. The use of control algorithms to minimize uncertainties in the dynamic forces of wheel loaders is a nice approach that should be further explored.

2.8 Stochastic Methods in Industry and Research

Newtonian Projection Method

A common practice in industry is to conduct load measurements at various positions in systems such as wheel loaders during field tests. However, due to time constraints, only critical load measurements can be performed. The data obtained by taking measurements at certain points may not always identically satisfy the system's equations of motions. A possible cause could be the different operating conditions affecting the measuring load sensor. A computer model is then used to run simulations of a field test. Problems arise when the computer model predicts different loads at certain points on the rigid body system than from those taken in the field test. The need to obtain realistic estimations of uncertain forces motivates the development of stochastic methods to propagate uncertainties in the measurements through the system.

Sundermeyer [9] presents a method to propagate uncertainties based on the mean values and quadratic transformation for standard deviations. The Newtonian constraint method was employed since it has been noticed that, when experimental measurements are made, the measured values do not satisfy Newton's laws exactly. The Newtonian constraint method has been employed to recover from the experimental data that load values that will satisfy Newton's laws. This method designates a constraint surface on which the true mean of the parameter of interest lies. The assumption in the method is that the uncertainty associated with the measured value is proportional to the local uncertainty associated with the true mean on the constraint surface. This allows for the measured value to be projected onto the constraint surface line. This projection can be further split up into components to be used in a root mean square fashion to determine the mean value of the uncertain parameter, as shown in Figure 2-3.

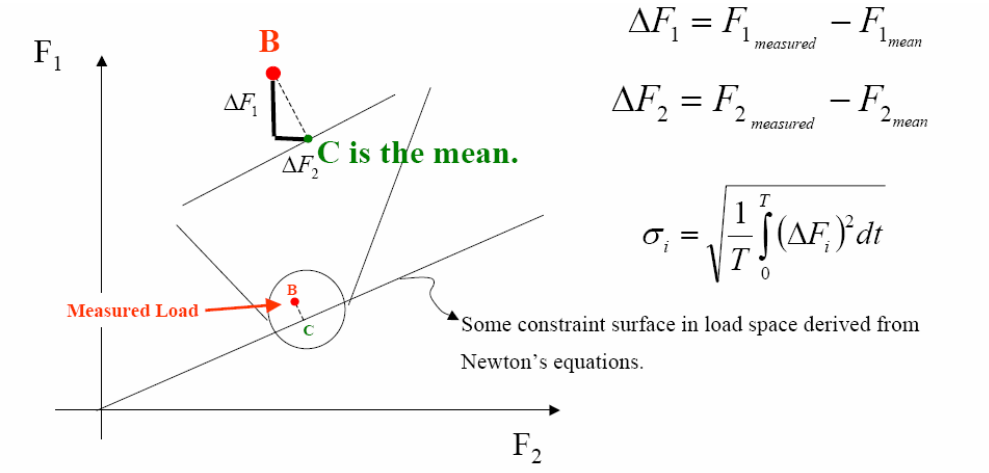

Figure 2-3. Newtonian Projection Surface [9]

In Figure 2-3, the constraint surface used in practice is the ProMechanica simulation model of the 980G series II wheel loader. The measured value, shown by B, represents data from taken from a field test. This measured value is projected onto the constraint surface by use of the standard deviation equation shown to the right in Figure 2-3.

In [9], for continuous random variables with a normal distribution, the mean of an uncertain (unknown) variable can be obtained as a linear combination of the means of the uncertain input

(or known) variables. The standard deviation can be obtained similarly, using a combination of quadratic terms containing the standard deviations known.

$$W = aX + bY + c = N(a\mu_x + b\mu_y + c, a^2\sigma_x^2 + b^2\sigma_y^2 \tag{2.3}$$

The law of linear transformations allows the true mean to be determined from a Newtonian balance of forces or balance of moments. The coefficients determined here can be used next to determine the standard deviation, as shown in Eq. (2.3). Upon obtaining the standard deviation from the projection method of a known value, this effectively allows one to quantitatively determine the true mean and the standard deviation associated with the unknown value [9].

Polynomial Chaos Theory

The fundamental idea behind the polynomial chaos method is that random processes of interest can be approximated by sums of orthogonal polynomial chaoses of random independent variables.

Second order random processes are processes with finite variance. A second order random process $X(\theta)$, viewed as a function of the random event θ, $(0<\theta<1)$, can be expanded in terms of orthogonal polynomial chaoses [10,11] as

$$X(\theta) = \sum_{j=1}^{\infty} c^j \phi^j(\xi(\theta)) \tag{2.4}$$

Here $\phi^i(\xi_{i_1} \ldots \xi_{i_n})$ are generalized Askey-Wiener polynomial chaoses of order $n(i)$, in terms of the multi-dimensional random variable $\xi = (\xi_{i_1} \ldots \xi_{i_n})$. The type of polynomials needed for the basis functions is determined by the type of distribution of the uncertain parameter of interest. In practice, a truncated expansion is used,

$$X = \sum_{j=1}^{S} c^j \phi^j(\xi) \tag{2.5}$$

This means that we consider a finite number n of random variables $\xi = (\xi_1 \ldots \xi_n)$, and sum polynomials only up to a maximal order P. It is important to notice that the total number of

terms $S = (n+P)!/(n!P!)$ increases rapidly with the number of stochastic parameters n and the order of the polynomial chaos P.

The dynamics of an unconstrained multibody system [2] can be described by a set of simultaneous fist order differential equations (ODE), shown in Eq. (2.6).

$$\dot{y} = v, \quad \dot{v} = F(t, y, v; p), \quad y\left(t^0\right) = y^0, \quad t^0 \le t \le t^F \tag{2.6}$$

Here $y \in \Re^d$ are the generalized positions, $v \in \Re^d$ are the generalized velocities, $\dot{v} \in \Re^d$ are the generalized accelerations, and $p \in \Re^e$ is a vector of system parameters. The dot notation represents derivative with respect to time.

Consider the multibody dynamic system in the ODE formulation given by Eq. (2.6) with uncertain parameters $\boldsymbol{p}$. The uncertain parameters are (functional of) random variables and can be represented using the polynomial chaos expansion as

$$p_k = \sum_{i=1}^{S} p_k^i \phi^i(\xi), \qquad 1 \le k \le e \tag{2.7}$$

The state variables of the multibody dynamic system are also functionals of the random variables that describe the sources of uncertainty, and are represented as

$$y_k(t) = \sum_{i=1}^{S} y_k^i(t)\phi^i(\xi), \quad v_k(t) = \sum_{i=1}^{S} v_k^i(t)\phi^i(\xi), \quad 1 \le k \le d \tag{2.8}$$

We use subscripts to denote the components along the deterministic (system) dimension, and superscripts to denote components along the stochastic dimension. The superscript-only notation will be used to represent the vector of stochastic coefficients,

$$y^i = \begin{bmatrix} y_1^i & \cdots & y_d^i \end{bmatrix}^T \quad \text{for all} \quad 1 \le i \le S \tag{2.9}$$

Inserting Eq. (2.9) into Eq. (2.4) leads to

$$\dot{y}_k^i = v_k^i, \quad \sum_{j=1}^{S} \dot{v}_k^j \phi^j = F_k\left(t, \sum_{m=1}^{S} y^m \phi^m, \sum_{m=1}^{S} v^m \phi^m; \sum_{m=1}^{S} p^m \phi^m\right), \quad \text{for} \quad 1 \le k \le d, \quad 1 \le j \le S \tag{2.10}$$

The equations for the time evolution of the spectral polynomial chaos coefficients $y_k^i(t)$ and $v_k^i(t)$ will be derived for this project in a collocation framework.

The collocation approach is motivated by the pseudo-spectral methods [13]. In order to derive evolution equations for the stochastic coefficients $y^i(t)$ we impose that Eq. (2.10) holds at a given set of collocation vectors

$$\mu^i = \begin{bmatrix} \mu_1^i & \cdots & \mu_d^i \end{bmatrix}^T \quad \text{for all} \quad 1 \le i \le S \tag{2.11}$$

This leads to

$$\dot{y}^i = v^i, \quad \sum_{j=1}^{S} \dot{v}^j \phi^j(\mu^i) = F\left(t, \sum_{m=1}^{S} y^m \phi^m(\mu^i), \sum_{m=1}^{S} v^m \phi^m(\mu^i); \sum_{m=1}^{S} p^m \phi^m(\mu^i) \right), \quad 1 \le i \le S \tag{2.12}$$

Consider the matrix $\mathbf{A}$ of basis function values at the collocation points

$$\mathbf{A} = \left(A_{i,j}\right), \quad A_{i,j} = \phi^j(\mu^i), \quad 1 \le j \le S, \quad 1 \le i \le S \tag{2.13}$$

The collocation points have to be chosen such that $\mathbf{A}$ is nonsingular. Then

$$\sum_{j=1}^{S} y^j \phi^j(\xi^i) = \sum_{j=1}^{S} A_{i,j} y^j \tag{2.14}$$

Equation (2.12) becomes

$$\dot{y}^i = v^i, \quad \sum_{j=1}^{S} A_{i,j}\, \dot{v}^j = F\left(t, \sum_{m=1}^{S} A_{i,m}\, y^m, \sum_{m=1}^{S} A_{i,m}\, v^m; \sum_{m=1}^{S} A_{i,m}\, p^m \right), \quad 1 \le i \le S \tag{2.15}$$

Denote the collocation points in the random system state space by

$$Y^i(t) = \sum_{j=1}^{S} A_{i,j}\, y^j(t), \quad V^i(t) = \sum_{j=1}^{S} A_{i,j} v^j(t), \quad P^i = \sum_{j=1}^{S} A_{i,j}\, p^j \tag{2.16}$$

With this notation, the collocation system (13) can be written as

$$\dot{Y}^i = V^i, \quad \dot{V}^i = F\left(t, Y^i, V^i; P^i\right), \quad 1 \le i \le S \tag{2.17}$$

Equation (2.17) shows that the direct collocation approach reduces to S independent solutions of the deterministic system. At $t = 0$, Eq. (2.16) gives the initial conditions for Eq. (2.17). After integration, the stochastic solution coefficients are recovered using:

$$y^i(T) = \sum_{j=1}^{S} \left(\mathbf{A}^{-1}\right)_{i,j} Y^j(T), \quad v^i(T) = \sum_{j=1}^{S} \left(\mathbf{A}^{-1}\right)_{i,j} V^j(T) \tag{2.18}$$

The collocation approach requires S independent runs, each using a different value for the random variables $\xi = \mu_j$. The coefficients of the polynomial chaos expansion at the final time are recovered using Eq. (2.18).

We now discuss the choice of collocation points. Let $\gamma^1, \ldots, \gamma^q$ in $[-1,1]$ be the roots of the q^{th} order one-dimensional polynomial from the family used in the construction of the basis functions. Since the basis functions ϕ^i are tensor products, the n-dimensional collocation vectors are chosen to have each component equal to one of these points

$$\mu^i = \begin{bmatrix} \mu_1^i & \cdots & \mu_d^i \end{bmatrix}^T = \begin{bmatrix} \gamma^{j_1} & \cdots & \gamma^{j_n} \end{bmatrix} \quad \text{for } 1 \le j \le S \tag{2.19}$$

There are n^q possible collocation vectors. The dimension of the stochastic space with n independent sources of uncertainty and with chaos polynomials of order up to P is smaller than the number of possible collocation points, $S < n^q$. One has to choose a subset of the vectors of form given by Eq. (2.19) as discussed in [14-16]. The alternative approach is to construct the basis functions as tensor products of one-dimensional polynomials up to order $P = q - 1$. In this case $S = n^{P+1}$ and the number of collocation points equals the base size.

For more details on the applicability of the polynomial chaos approach to multibody dynamic systems with uncertainties, as well as for the Collocation Method, reader can refer to references [17,18].

The following example illustrates the use of the Collocation Method as presented in this thesis. Suppose the polynomial expansion of the uncertain parameter has S terms and Q collocation points. The number of S terms will be 5 and the number of Q collocation points will be 15. Therefore, the ODE can be run for 15 times for each of the 15 collocation points to produce an observed value $Y^i(t)$, which is the observed behavior of a parameter in our ODE due to the

stochastic input parameter. At each time step of the ODE, a polynomial chaos expansion is recovered with 5 terms, as shown in Eq. (2.20).

$$y(t_k,\xi) = y^1(t_k)\phi^1(\xi) + y^2(t_k)\phi^2(\xi) + y^3(t_k)\phi^3(\xi) + y^4(t_k)\phi^4(\xi) + y^5(t_k)\phi^5(\xi) \tag{2.20}$$

y^i are the coefficients that describe the observed value at the collocation points. The five terms in the polynomial expansion and the l5 collocation points produce a system of equations with 15 equations and 5 unknowns as shown in Eq. (2.21).

$$\begin{cases} Y^1(t_k) = y^1(t_k)\phi^1(\mu^1) + y^2(t_k)\phi^2(\mu^1) + y^3(t_k)\phi^3(\mu^1) + y^4(t_k)\phi^4(\mu^1) + y^5(t_k)\phi^5(\mu^1) \\ \dots \\ Y^{15}(t_k) = y^1(t_k)\phi^1(\mu^{15}) + y^2(t_k)\phi^2(\mu^{15}) + y^3(t_k)\phi^3(\mu^{15}) + y^4(t_k)\phi^4(\mu^{15}) + y^5(t_k)\phi^5(\mu^{15}) \end{cases} \tag{2.21}$$

Eq. (2.21) reduces to Eq. (2.22), by use of the collocation matrix as shown below.

$$\begin{bmatrix} Y^1 \\ \vdots \\ Y^{15} \end{bmatrix} = \mathbf{A} \begin{bmatrix} y^1 \\ \vdots \\ y^5 \end{bmatrix} \tag{2.22}$$

The coefficients, y^i in Eq. (2.20) are recovered using a least-squares algorithm by use of the collocation matrix denoted by **A** in Eq. (2.22). The coefficients, y^i are thus obtained using Eq. (2.23).

$$y^j(t_k) = \sum_{j=1}^{S} \left(\mathbf{A}^{\#}\right)_{i,j} Y^i(t_k) \tag{2.23}$$

In Eq. (2.23), $\mathbf{A}^{\#}$ denotes the pseudo-inverse of **A,** which is a function of the orthogonal polynomials or basis functions at specific collocation points given by Eq. (2.13).

CHAPTER 3 SIMPLE CASE DETERMINISTIC MODEL

The final goal of this study is to identify a methodology to predict the uncertainties in the joint reaction forces in a 3-D CAD model of construction machinery without having direct access to the equations of motion of the system. The selected system for the final analysis is a Caterpillar 980G II wheel loader. The first step was to develop the methodology proposed on a simple case study for which we derive the equations of motion. Thus, we developed a Matlab model for a double pendulum linkage system, which is illustrated in Figure 3-1. The same model has also been implemented in ProMechanica. The two models have been compared to ensure similar deterministic behavior. In Chapter 4, different methods to treat the uncertainties in this system will be developed and benchmarked. Thus, the methodology developed to treat uncertainties in dynamic terms of 3-D CAD models will be validated on the simple case study considered since we have the advantage of working directly with the equations of motion in the Matlab model, by comparing the stochastic ProMechanica and stochastic Matlab models. Afterwards, the technique will be applied to the full model of the wheel loader in ProMechanica.

3.1 Model Description of Simple Case Mechanism

The simple case model is a 2-D double pendulum with a slider. There are four bodies in the system, which, to maintain a similarity with the wheel loader nomenclature are considered to represent the liftarm, bucket, rod, and cylinder. The liftarm is driven by a co-sinusoidal driver with a period of 2π radians and amplitude of 0.17453 m. A slider was defined to allow the cylinder and the rod to slide against each another. An uncut revolute joint allows the rod to rotate with respect to the liftarm. In this model, the bucket is an independent linkage and, for the purpose of this study, is maintained at a constant angle of $-5\pi/2$ radians. It is modeled so that the reaction forces can be determined similar to the real B-pin on the full 980G wheel loader. A schematic of the system considered for the simple case study is illustrated in Figure 3-1.

3.2 Constrained Equations of Motion

The system has four rigid bodies: the liftarm (body 1), the bucket (body 2), the rod (body 3), and the hydraulic cylinder (body 4). There are four revolute joints (at O, A, B, and G), and a slider joint between bodies 3 and 4. Colinearity conditions have been imposed between bodies 3 and 4 (the rod and the cylinder). This was done to assure that the rod and the cylinder positions are consistent with the geometry of the system.

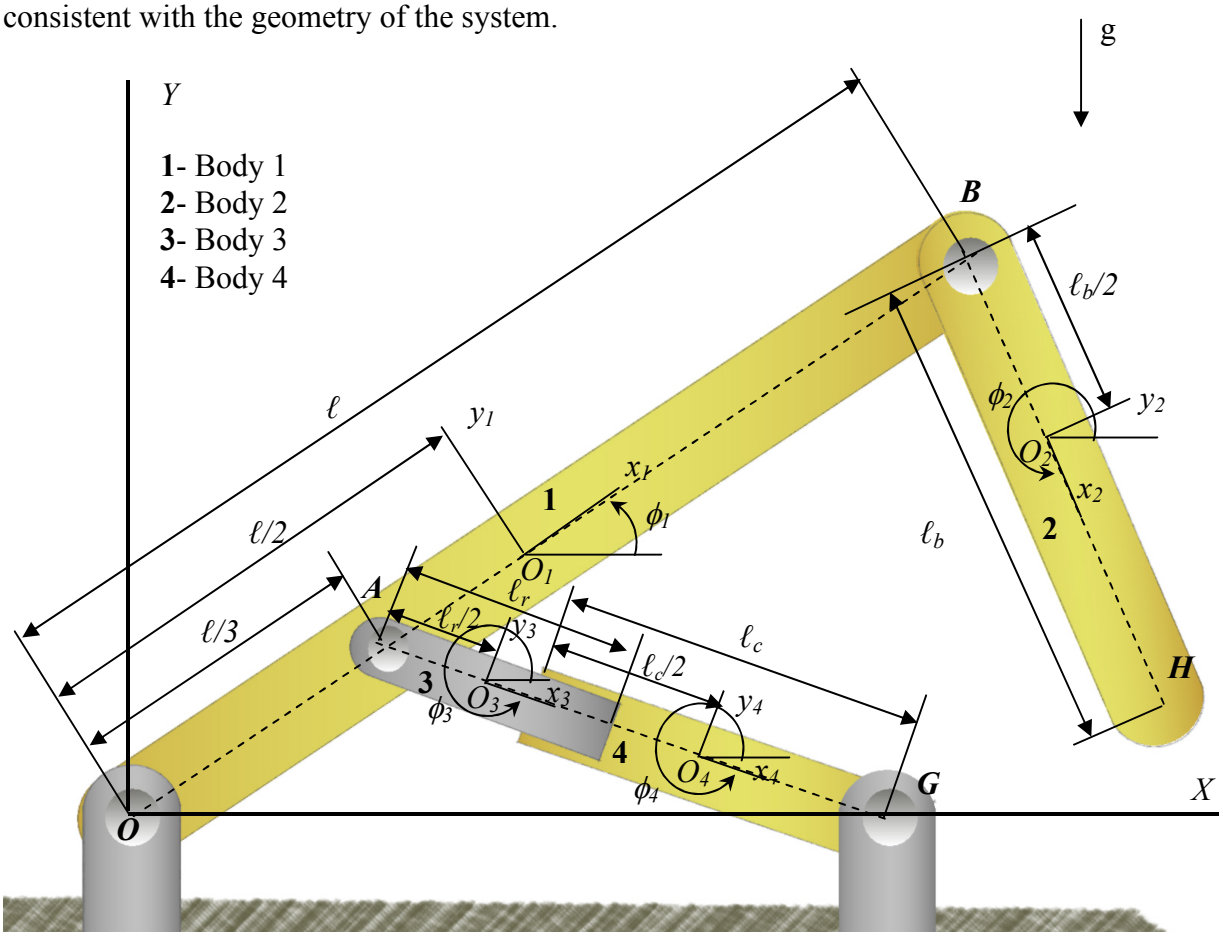

Figure 3-1.Shematic of the system used for the simple case study

The constraints of the linkage system are kinematic and driving. The 2D system has four bodies (implying 12 Cartesian coordinates to completely define the position and orientation of all the bodies) and eleven kinematic constraints. The vector of generalized Cartesian coordinates is **q**. The local reference frames are placed at the centroid of all bodies, as shown in Figure 3-1. The global reference frame has its origin at O. The vector of generalized coordinates is

$$\mathbf{q} = [x_1, y_1, \phi_1, x_2, y_2, \phi_2, x_3, y_3, \phi_3, x_4, y_4 \phi_4]^{\mathrm{T}} \tag{3.1}$$

One driving constraint is necessary to completely define the motion of the system. The driver imposed was a sinusoidal motion imposed on the liftarm. In this study the bucket was constrained at a fixed angle with respect to the liftarm. The following constraints were derived for this system Eq. (3.2). $\mathbf{\Phi}^K$ defines the kinematic constraints and $\mathbf{\Phi}^D$ defines the driving constraints. θ is defined as 2π.

$$\mathbf{\Phi}^K = \begin{bmatrix} x_1\text{-}(\ell/2)*\cos(\varphi_1) \\ y_1\text{-}(\ell/2)*\sin(\varphi_1) \\ x_2 - \ell*\cos(\varphi_1) - (\ell_b/2)*\cos(\varphi_2) \\ y_2 - \ell*\sin(\varphi_1) - (\ell_b/2)*\sin(\varphi_2) \\ x_3 - (\ell/3)*\cos(\varphi_1) - (\ell_r/2)*\cos(\theta-\varphi_3) \\ y_3 - \ell*\sin(\varphi_1) + (\ell_r/2)*\sin(\theta-\varphi_3) \\ x_4 - d + (\ell_c/2)*\cos(\theta-\varphi_4) \\ y_4 - (\ell_c/2)*\cos(\theta-\varphi_4) \\ \varphi_3 - \varphi_4 \\ y_4*x_4 - (\ell/3)*y_4*\cos(\varphi_1) + (\ell_c/2)*y_4*\cos(\theta-\varphi_4) - (\ell_c/6)*\cos(\theta-\varphi_4)*\sin(\varphi_1) \\ \varphi_2 + (5\pi/2) \end{bmatrix} = \begin{bmatrix} 0 \\ 0 \\ 0 \\ 0 \\ 0 \\ 0 \\ 0 \\ 0 \\ 0 \\ 0 \end{bmatrix} \tag{3.2}$$

$$\Phi^D = [\varphi_1 - a*\cos(\varpi*t)] = 0 \tag{3.3}$$

The complete set of constraints is thus:

$$\mathbf{\Phi} = \begin{bmatrix} \mathbf{\Phi}^K \\ \Phi^D \end{bmatrix} \equiv 0 \tag{3.4}$$

The Jacobian of these constraints equations has a full row rank, which means that the constraints considered are linearly independent, so the motion of the system can be completely predicted. The Jacobian of Eq. (3.4) is shown in Eq. (3.5).

$$\mathfrak{F}_q = \begin{pmatrix} 1 & 0 & \frac{1}{2}\,l\,\mathrm{Sin}[\phi_1] & 0 & 0 & 0 & 0 & 0 & 0 & 0 & 0 & 0 \\ 0 & 1 & -\frac{1}{2}\,l\,\mathrm{Cos}[\phi_1] & 0 & 0 & 0 & 0 & 0 & 0 & 0 & 0 & 0 \\ 0 & 0 & l\,\mathrm{Sin}[\phi_1] & 1 & 0 & \frac{1}{2}\,lb\,\mathrm{Sin}[\phi_2] & 0 & 0 & 0 & 0 & 0 & 0 \\ 0 & 0 & -l\,\mathrm{Cos}[\phi_1] & 0 & 1 & -\frac{1}{2}\,lb\,\mathrm{Cos}[\phi_2] & 0 & 0 & 0 & 0 & 0 & 0 \\ 0 & 0 & \frac{1}{3}\,l\,\mathrm{Sin}[\phi_1] & 0 & 0 & 0 & 1 & 0 & -\frac{1}{2}\,lr\,\mathrm{Sin}[\theta-\phi_3] & 0 & 0 & 0 \\ 0 & 0 & -\frac{1}{3}\,l\,\mathrm{Cos}[\phi_1] & 0 & 0 & 0 & 0 & 1 & -\frac{1}{2}\,lr\,\mathrm{Cos}[\theta-\phi_3] & 0 & 0 & 0 \\ 0 & 0 & 0 & 0 & 0 & 0 & 0 & 0 & 0 & 1 & 0 & \frac{1}{2}\,lc\,\mathrm{Sin}[\theta-\phi_4] \\ 0 & 0 & 0 & 0 & 0 & 0 & 0 & 0 & 0 & 0 & 1 & \frac{1}{2}\,lc\,\mathrm{Cos}[\theta-\phi_4] \\ 0 & 0 & 0 & 0 & 0 & 0 & 0 & 0 & 0 & 0 & 0 & -1 \\ 0 & 0 & -\frac{1}{6}\,l\,lc\,\mathrm{Cos}[\phi_1]\,\mathrm{Cos}[\theta-\phi_4] + \frac{1}{3}\,l\,\mathrm{Sin}[\phi_1]\,y_4 & 0 & 0 & 0 & 0 & 0 & 0 & y_4 & -\frac{1}{3}\,l\,\mathrm{Cos}[\phi_1] + \frac{1}{2}\,lc\,\mathrm{Cos}[\theta-\phi_4] + x_4 & -\frac{1}{6}\,l\,lc\,\mathrm{Sin}[\phi_1]\,\mathrm{Sin}[\theta-\phi_4] + \frac{1}{2}\,lc\,\mathrm{Sin}[\theta-\phi_4]\,y_4 \\ 0 & 0 & 0 & 0 & 0 & 1 & 0 & 0 & 0 & 0 & 0 & 0 \\ 0 & 0 & 1 & 0 & 0 & 0 & 0 & 0 & 0 & 0 & 0 & 0 \end{pmatrix}$$

(3.5)

Hydraulic Cylinder Force Computation

As mentioned in the review of literature, one way to model the hydraulic forces in a hydraulic subsystem is by use of fluid motion equations for flow rate and pressure. However, in the simple case model, the hydraulic nature of the cylinders was approximated with a translational spring damper actuator (TSDA). The equation used to determine the force in this actuator is shown in Eqs. (3.6-3.9). The TSDA acts between bodies 3 and 4. The spring has the length l given by Eq. (3.7) and the force produced by the TSDA computed with Eq. (3.9).

$$\mathbf{d}_{34} = \begin{bmatrix} x_4 - x_3 \\ y_4 - y_3 \end{bmatrix} \tag{3.6}$$

$$l = \sqrt{(x_4 - x_3)^2 + (y_4 - y_3)^2} \tag{3.7}$$

$$\dot{l} = \left[(x_4 - x_3) \cdot (\dot{x}_4 - \dot{x}_3) + (y_4 - y_3) \cdot (\dot{y}_4 - \dot{y}_3) \right] / l \tag{3.8}$$

$$f = k \cdot (l - l_o) + c \cdot (\dot{l}) \tag{3.9}$$

$\mathbf{d}_{34}$ is the distance vector between bodies 3 and 4, l_0 is the unstretched length of the TSDA spring, k is the stiffness of the TSDA, and c is the damping coefficient of the TSDA.

3.3 Generalized Forces

In multibody dynamics, the generalized force vector on the right hand side of the equation of motion (EOM) contains all forces acting on the system, including forces coming from TSDAs .

$$\mathbf{Q}_3 = \frac{f}{l}\begin{bmatrix} \dot{\mathbf{d}}_{34} \\ \mathbf{d}_{34}\mathbf{B}_3\mathbf{s'}_3 \end{bmatrix}, \quad \mathbf{Q}_4 = -\frac{f}{l}\begin{bmatrix} \dot{\mathbf{d}}_{34} \\ \mathbf{d}_{34}\mathbf{B}_4\mathbf{s'}_4 \end{bmatrix}, \quad \text{where} \quad \mathbf{s'}_3 = \mathbf{s'}_4 = \mathbf{0} \tag{3.10}$$

where $\dot{\mathbf{d}}_{34}$ can be computed from Eq. (3.6), and $\mathbf{s}_i$' represents the distance between the center of gravity and the location of the local reference frames, and $\mathbf{B}_i$ is the time derivative of the transformation matrix $\mathbf{A}_i$, for i=3,4.

The generalized forces also take into account the force due gravity which acts at the center of gravity for each body. Therefore, the total generalized force vector is constructed as shown in Eq. (3.11).

$$\boldsymbol{Q}^{A} = \begin{bmatrix} 0 \\ m_1 g \\ 0 \\ 0 \\ m_2 g \\ 0 \\ \frac{f}{l}(\dot{x}_3 - \dot{x}_4) \\ m_3 g + \frac{f}{l}(\dot{y}_3 - y_4) \\ 0 \\ -\frac{f}{l}(\dot{x}_3 - \dot{x}_4) \\ m_4 g - \frac{f}{l}(\dot{y}_3 - y_4) \\ 0 \end{bmatrix} \tag{3.11}$$

3.4 Differential Algebraic Equations

In order to perform the direct dynamic analysis of the system described in Figure 3-1, a system of Differential Algebraic Equations (DAE) was assembled and solved for the accelerations and Lagrange multipliers. The Lagrange multipliers are introduced to account for the constraints, and are associated with the reaction forces in the joints. $\mathbf{M}$ is the generalized mass matrix, as shown in Eq. (3.12) .

$$\mathbf{M} = diag\left(m_1, m_1, J_1, m_2, m_2, J_2, m_3, m_3, J_3, m_4, m_4, J_4\right) \tag{3.12}$$

where, m_i is the mass of the body, and J_i is the mass moment of inertia, i=1,…,4.

Θ_q is the Jacobian matrix shown in Eq. (3.5). The generalized accelerations $\ddot{\mathbf{q}}$, are calculated numerically using a Hilbert -Hughes integrator and are shown in the vector in Eq. (3.13).

$$\ddot{\mathbf{q}} = [\ddot{x}_1, \ddot{y}_1, \ddot{\phi}_1, \ddot{x}_2, \ddot{y}_2, \ddot{\phi}_2, \ddot{x}_3, \ddot{y}_3, \ddot{\phi}_3, \ddot{x}_4, \ddot{y}_4, \ddot{\phi}_4]^{\mathrm{T}} \tag{3.13}$$

The Lagrange multipliers $\boldsymbol{\lambda}$ are calculated numerically using a Hilbert-Hughes integrator and may physically represent a force or a torque. They correspond to the number of constraints as shown in Eq. (3.14).

$$\boldsymbol{\lambda} = \left[\lambda_1, \lambda_2, \lambda_3, \lambda_4, \lambda_5, \lambda_6, \lambda_7, \lambda_8, \lambda_9, \lambda_{10}, \lambda_{11}, \lambda_{12}\right]^{\mathrm{T}} \tag{3.14}$$

The generalized force vector $\mathbf{Q}^{A}$, is shown in Eq. (3.11).

The accelerations $\boldsymbol{\gamma}$, are also calculated numerically using a Hilbert-Hughes integrator correspond to the number of constraints and are shown in Eq. (3.15) as.

$$\boldsymbol{\gamma} = \left[\gamma_1, \gamma_2, \gamma_3, \gamma_4, \gamma_5, \gamma_6, \gamma_7, \gamma_8, \gamma_9, \gamma_{10}, \gamma_{11}, \gamma_{12}\right]^{T} \tag{3.15}$$

Theoretically, $\boldsymbol{\gamma}$ can be calculated using the relations in Eq. (3.16).

$$\boldsymbol{\gamma} \equiv -(\boldsymbol{\Phi}_{\mathbf{q}}\dot{\mathbf{q}})_{\mathbf{q}}\dot{\mathbf{q}} - 2\boldsymbol{\Phi}_{\mathbf{q}t}\dot{\mathbf{q}} - \boldsymbol{\Phi}_{tt} = \boldsymbol{\Phi}_{\mathbf{q}}\ddot{\mathbf{q}} \tag{3.16}$$

Finally, in its matrix form, the system of DAE's developed can be written as shown in Eq. (3.17).

$$\begin{bmatrix} \mathbf{M} & \boldsymbol{\Phi}_{\mathbf{q}}^{\mathbf{T}} \\ \boldsymbol{\Phi}_{\mathbf{q}} & \mathbf{0} \end{bmatrix} \cdot \begin{bmatrix} \ddot{\mathbf{q}} \\ \boldsymbol{\lambda} \end{bmatrix} = \begin{bmatrix} \mathbf{Q}^{\mathbf{A}} \\ \boldsymbol{\gamma} \end{bmatrix} \tag{3.17}$$

3.5 Initial Conditions

Initial conditions are needed to start a simulation. The initial conditions selected for the four bodies are presented in Table 3-1.

Table 3-1. Initial Conditions

Body(n)	X- Position	Y- Position	ϕ_n
1	l/2*cos(10π/180)	l/2*sin(10π/180)	10π/180
2	l+(lb/2)* cos(5π/2)	l+(lb/2)*sin(5π/2)	5π/2
3	(l/3)+(lr/2)* cos(10π/180)	(l/3)+(lr/2)* sin(10π/180)	$2\pi - \phi_3$
4	d-(lc/2)* cos(10π/180)	d-(lc/2)* sin(10π/180)	$2\pi - \phi_4$

Once the system in Eq. (3.17) is solved for $\ddot{\mathbf{q}}$ and $\boldsymbol{\lambda}$, the Lagrange multipliers can be used to recover the reaction force in the joints. For the joint at B, which is a revolute joint, there is no reaction torque, but two reaction forces can be computed as shown in Eq. (3.18).

$$\mathbf{F}^{"k}{}_{i} = -\mathbf{C}_{i}^{T}\mathbf{A}^{T}\boldsymbol{\Phi}_{\mathbf{r}i}^{kT}\boldsymbol{\lambda}^{k} \tag{3.18}$$

Integration With Hilbert Hughes Integrator

To integrate the DAE given in Eq. (3.17), a Hilbert Hughes numerical integrator was used to solve for the position, velocity, and acceleration of all bodies in the system. A paper describing the internal mechanism of this integrator is [19].

3.6 Computer-Aided Modeling

Upon implementing the simple case study model in Matlab, ProMechanica 2.0 was used to build the simple case mechanism as a CAD model. The model in ProMechanica was used to compare the simulation results of the MATLAB model with outputs from ProMechanica. The ProMechanica model contains the liftarm, bucket, rod, and cylinder bodies as in the Matlab model. This model was built using the same dimensions of the MATLAB model.

Each component of the simple case mechanism was built independently in ProMechanica and then assembled together with proper constraints. Unlike the Matlab model, where the geometry of the linkages is less relevant, the ProMechanica model uses a hollow cylinder for the lift-cylinder and a cylindrical rod for the lift rod. In assembling the simple mechanism in ProMechanica, a liftarm pivots off of the lift rod. The bucket is constrained to keep a constant orientation of $-5\pi/2$ radians with respect to the x axis of the liftarm, as shown in Figure (3-2). The red arrows facing downward are gravitational forces acting on the individual bodies in the system. The model was derived using SI units. A perspective and a side view of the ProMechanica model are included in Figures 3-2 and 3-3.

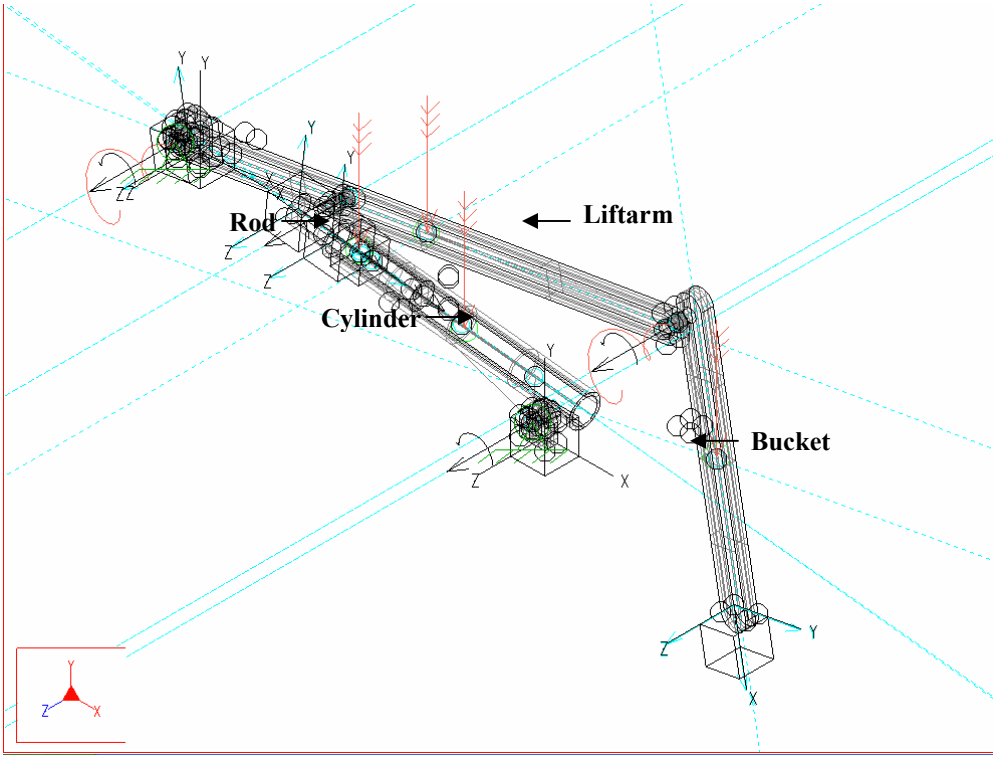

Figure 3-2. ProMechanica model of simple mechanism

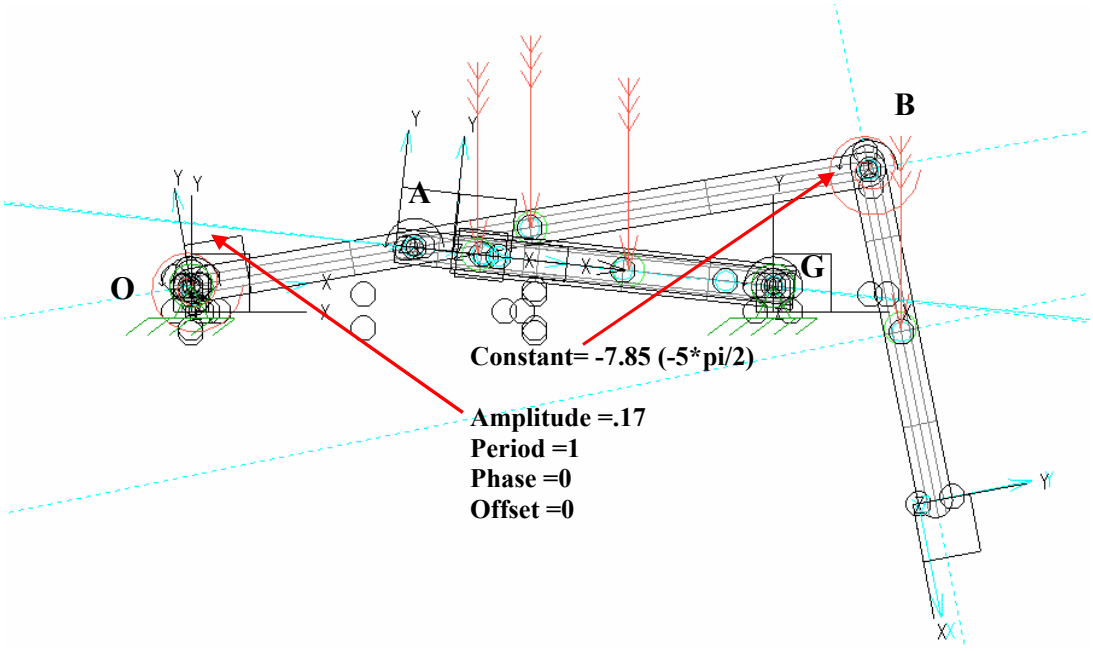

Figure 3-3. Side view of simple mechanism in ProMechanica

3.7 Comparison between the Results of the ProMechanica Deterministic Model and those of the Matlab Deterministic, DAE Model

Liftarm

The position of the liftarm in the x direction as obtained from the MATLAB model described by the DAE Eq. (3.17), and the one from the ProMechanica model are shown in Figure 3-4. The two plots illustrate similar behavior. Figure 3-5 illustrates the position of the liftarm along the y direction for the two models.

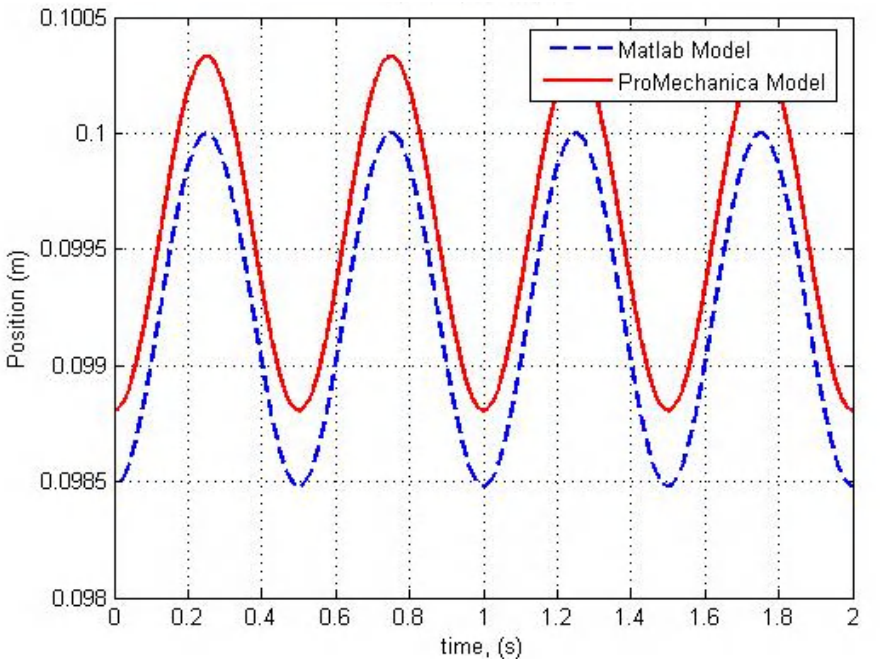

Figure 3-4. Liftarm x position using the MATLAB model

It was considered that the small differences noticed in the displacement of the liftarm are due to slightly different inertia properties in the ProMechanica model.

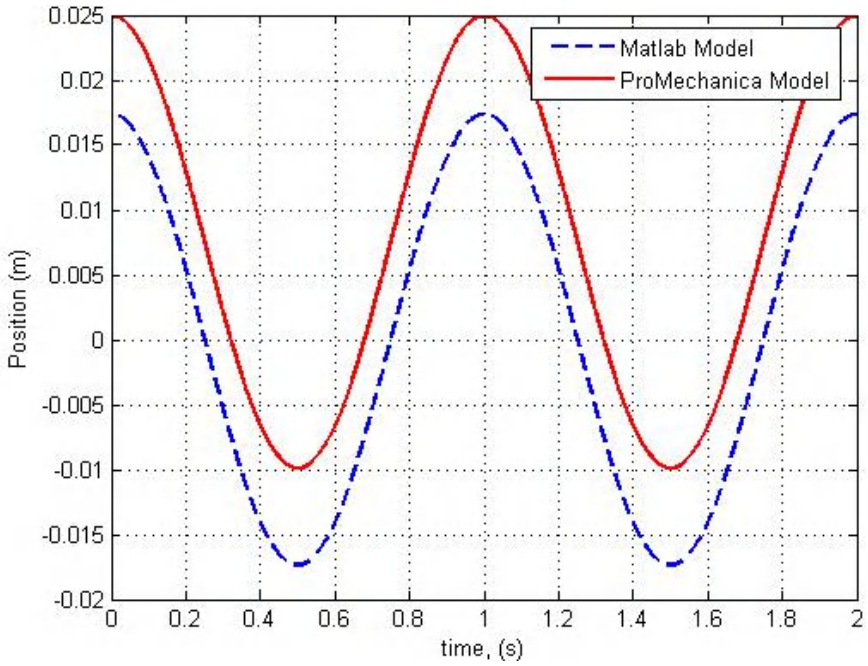

Figure 3-5. Liftarm y position using the MATLAB model

Rod

Figure 3-6 illustrates the position of the rod in the x direction, while Figure 3-7 shows its position along the y direction.

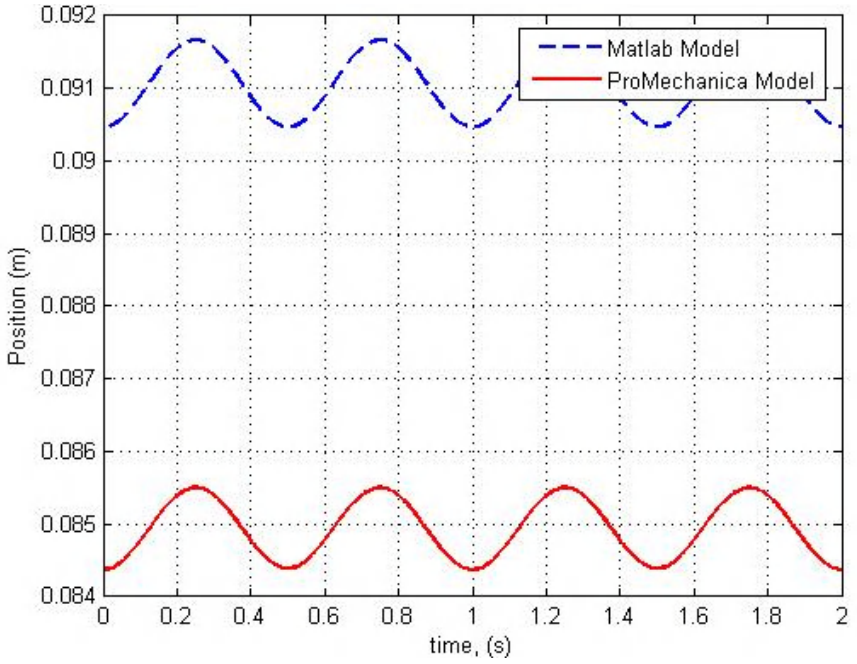

Figure 3-6. Rod x position using the MATLAB model

The magnitudes are again slightly different, but the order of magnitude is the same for both models. This is due to a slight difference in the implementation of the actuator in ProMechanica.

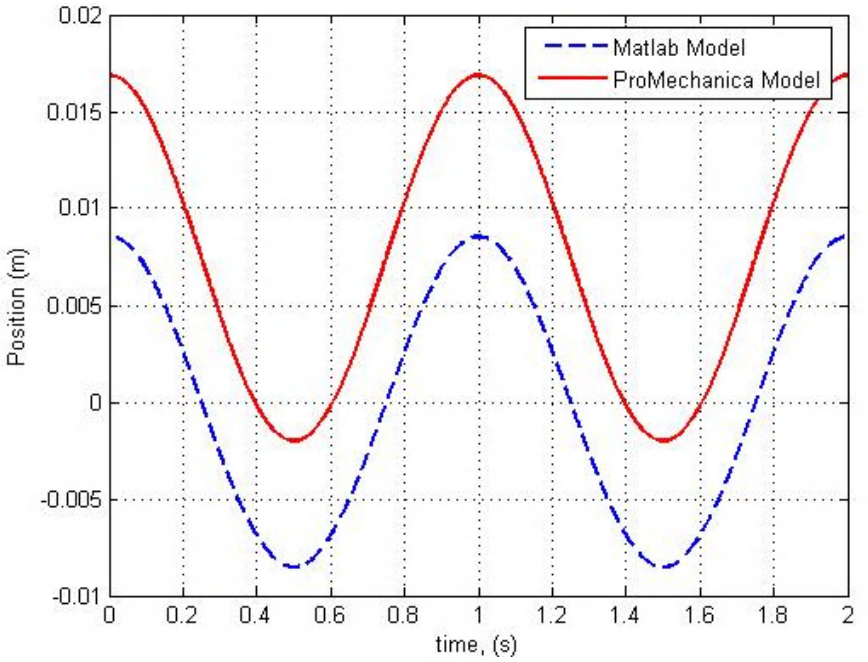

Figure 3-7. Rod y position using the MATLAB model

3.8 Dynamic Analysis of Reduced Simple Mechanism

The simple case mechanism was modeled at the beginning of this chapter using a full set of differentiable algebraic equations to predict position, velocity, and acceleration of all 4 bodies within the system. From the Lagrange multipliers obtained solving the differentiable algebraic equations we can also determine the reaction forces at the joints between the bodies. However, for practical applications, one may not have access to the discrete algebraic equations to determine the kinematics and dynamics of the system. A reduced model, based on equilibrium of moments could be a simple alternative, when the kinematics is known from separate simulations. Therefore, before moving into the stochastic framework for the full set of differentiable algebraic equations, we develop a reduced dynamic model, basically a relationship between the measured force used as input and the calculated output force.

Decomposition of Forces for Reduced Model

In Figure 3-8 we represent the liftarm. The liftarm is pinned at O. At A, a hydraulic cylinder applies external load to the liftarm; this load, decomposed in its global horizontal component (F_{r3x}) and vertical component (F_{r3y}) is considered an uncertain input. Point A is located at a third of the length of the liftarm from point O. Point B is the joint between the liftarm and the second link (the bucket). The reactions at B are the output forces of interest, and they are also decomposed in the global horizontal (F_{r2x}) and vertical (F_{r2y}) components. The orientation angle between the global horizontal axis X and the lift-arm is denoted by Φ_1. The reason behind selecting F_{r3} as uncertain is the fact that Caterpillar usually collects load data for the actuator that lifts the liftarm.

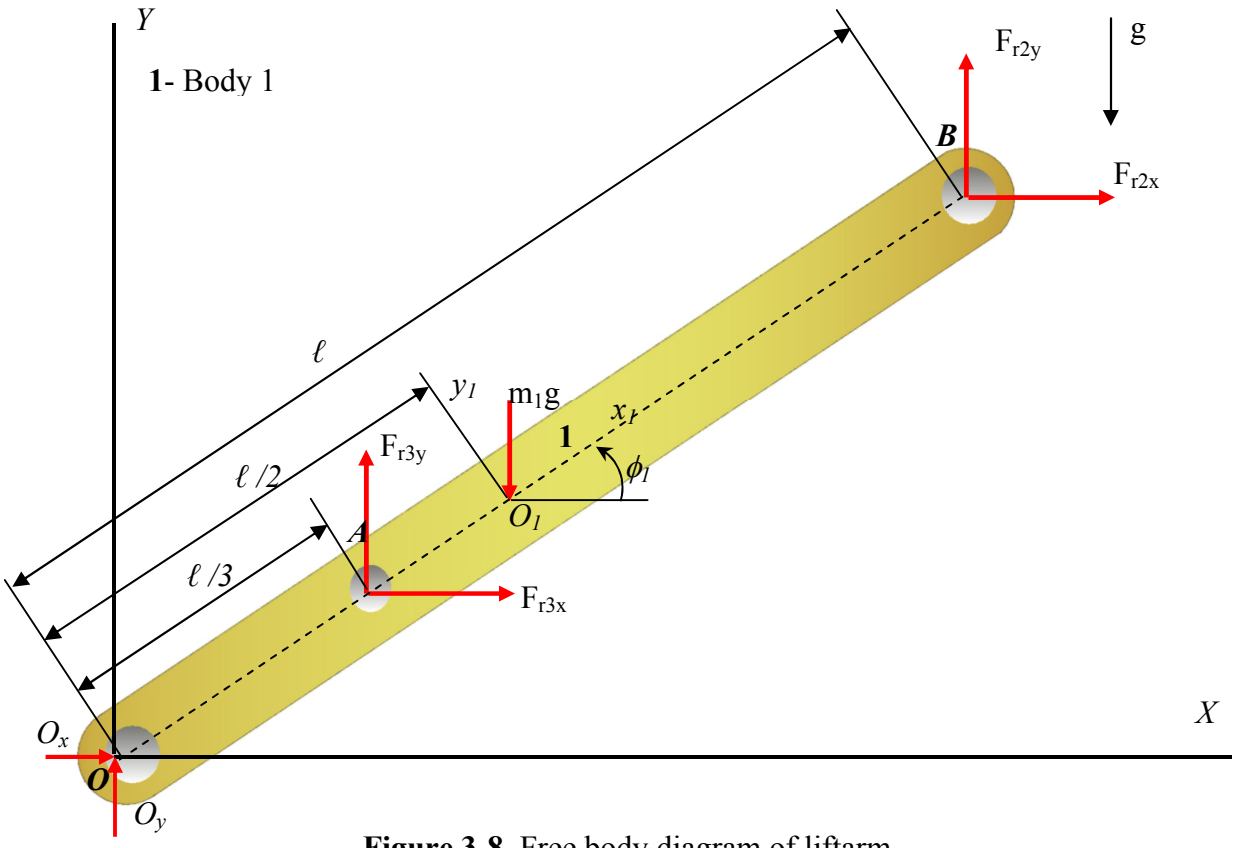

Figure 3-8. Free body diagram of liftarm

Referring to Figure 3-8, we assume that the force at A can be measured, and thus it is considered known for the purpose of this study. In the same time, to be as realistic as possible, the forces at A are assumed to be stochastic. The uncertainty introduced in the prediction of the system

dynamics (including reaction forces in other joints) due to the sensing of the actuator force is the main effect that we try to understand in this study.

The goal of the study is to predict the reaction force at B at a given moment in time. Thus, on components, we need to determine F_{r2x} and F_{r2y}. Both components are easily obtained in the full deterministic DAE model, as shown before. Now we assume that the component in the X direction, F_{r2x}, will have a deterministic value. The effect of the uncertainties in F_3 will only be reflected in the uncertainty in F_{r2y}.

From Figure 3-8 we can write the equation of moments (3.19) about point O as:

$$\sum M_o = \frac{\ell}{3}\cos(\varphi_1)F_{r3y} - \frac{\ell}{3}\sin(\varphi_1)F_{r3x} + \ell\cos(\varphi_1)F_{r2y} - \ell\sin(\varphi_1)F_{r2x} - m_1 g\frac{\ell}{2}\cos(\varphi_1) = J_1\alpha_1 \qquad (3.19)$$

where $\Im_1$ is the mass moment of inertia shown in equation (3.19), ℓ is the length of the lift-arm, ϕ_1 is the orientation angle in the global reference angle, and α_1 is the angular acceleration, also shown in equation (3.20).

$$J_1 = \frac{m_1\ell^2}{3}, \quad \alpha_1 = \ddot{\varphi}_1 \qquad (3.20)$$

From Eq. (3.19) we can compute the unknown vertical component of F_2 as shown in Eq. (3.21).

$$F_{r2y} = \frac{m_1\ell\alpha}{3\cos(\varphi_1)} - \frac{F_{r3y}}{3} + \frac{\tan(\varphi_1)F_{r3x}}{3} + \tan(\varphi_1)F_{r2x} + \frac{m_1 g}{2} \qquad (3.21)$$

Cross Product Method for Reduced Model Forces

The cross-product method for determining the equations of moments comes from an example demonstrated by Caterpillar [9]. The method is presented below.

Figure 3-9 represents a free body diagram of the system shown in Figure 3-8. The angles ϕ_{3*} and ϕ_{2*} are the angles between the F_{r3} and F_{r2} forces and the liftarm (body 1). The derivation of the equation of moments for the F_{r2} is shown next.

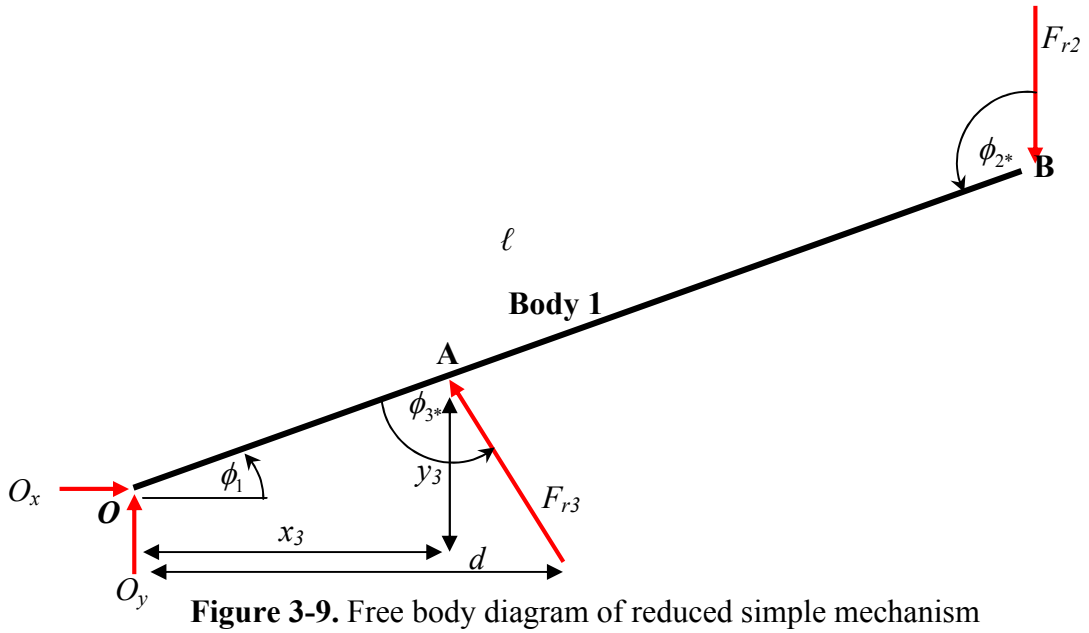

Figure 3-9. Free body diagram of reduced simple mechanism

Using cross products $\tau = r \times F$ becomes $\tau = rF\sin(\theta)$ (3.22)

r is the moment arm with respect to point 0, θ is the angle between the force and the moment arm. Here, θ is replaced by ϕ_{3*} or ϕ_{2*} in Figure 3-9, for our application.

Solving for ϕ_{3*} $$x_3 = d - \frac{\ell\cos(\phi_1)}{3} \quad , \quad y_3 = \frac{\ell\sin(\phi_1)}{3} \tag{3.23}$$

d is the distance between point *O* and the end of cylinder of body 4 from Figure 3-1, point G. ℓ is the length of the liftarm also shown in Figure 3-1.

$$\phi_{3*} = \arctan 2\left(\frac{y_3}{x_3}\right) + \left(\frac{\pi}{2} - \phi_1\right) \tag{3.24}$$

Solving for ϕ_{2*} $$\pi = \frac{\pi}{2} + \phi_1 + \phi_{2*}, \quad \phi_{2*} = \frac{\pi}{2} - \phi_1 \tag{3.25}$$

Where ϕ_1 is the angle between the liftarm and ground as shown in Figure 3-1.

Equations of Moments about *O*:

$$\sum M_o = F_{r3}\frac{\ell}{3}\sin(\phi_{3*}) - F_{r2}\ell\sin(\phi_{2*}) - \frac{m_1 g\ell\sin(\phi_{2*})}{2} = \frac{m\ell^2}{3}\ddot{\phi}_1 \tag{3.26}$$

Where m_1 is the mass of the liftarm.

$$F_{r2} = \frac{F_{r3}\sin(\phi_{3*})}{3\sin(\phi_{2*})} - \frac{m_1 \ell \ddot{\phi}_1}{3\sin(\phi_{2*})} - \frac{m_1 g}{2} \tag{3.27}$$

$$F_{r2y} = \cos(\phi_1) * F_{r2} \tag{3.28}$$

The inputs into both derivations for the equations of moments (decomposition and cross product) come from the kinematic analysis of the full DAE for the simple mechanical system and the measured input force for F_{r3}. These inputs were F_{r3}, F_{r2x} assumed known or measured for the decomposition method, angular acceleration $\ddot{\phi}_1$, angular position ϕ_1, mass of liftarm m_1, and length of liftarm ℓ. To recover the reaction forces from the DAE at points A and B in Figure 3-1, the following relationship was used,

$$\mathbf{F}^{"k}{}_i = -\mathbf{C}_i{}^T \mathbf{A}^T \mathbf{\Phi}_{\mathbf{r}i}{}^{kT} \boldsymbol{\lambda}^k \tag{3.29}$$

Where the subscript i refers to the respective bodies in the system. In this case, the subscript refers to bodies 1 and 2 when computing the reaction forces at B, and bodies 1 and 3 when computing the reaction force at A.. The position vectors are denoted as,

$$\mathbf{r}_2 = \begin{bmatrix} x_2 \\ y_2 \end{bmatrix}, \mathbf{r}_3 = \begin{bmatrix} x_3 \\ y_3 \end{bmatrix} \tag{3.30}$$

Therefore, from Eq. (3.30), the x and y components of the reaction forces for bodies 2 and 3 can be derived.

$\mathbf{C}_i$ is an identity matrix here. The matrix $\mathbf{A}_i$ from Eq. (3.29) is the transformation matrix between the local reference frame for bodies 2 and 3, respectively, to the global reference frame. This transformation matrix can be written as:

$$\begin{aligned} \mathbf{A}_2 &= \begin{bmatrix} \cos(\phi_2) & -\sin(\phi_2) \\ \sin(\phi_2) & \cos(\phi_2) \end{bmatrix} \\ \mathbf{A}_3 &= \begin{bmatrix} \cos(\phi_3) & -\sin(\phi_3) \\ \sin(\phi_3) & \cos(\phi_3) \end{bmatrix} \end{aligned} \tag{3.31}$$

The matrix $\mathbf{\Phi}_{\mathbf{r}i}$ is the differential of the kinematic constraints with respect to the position components x and y for bodies 2 and 3. Lastly, $\boldsymbol{\lambda}^k$ are the Lagrange multipliers resulting from the DAE.

In Figure 3-10, we represented the variation of the F_{r2y} reaction force in the joint B using the full DAE model and the reduced model. It is clear from this Figure that the assumptions made in deriving the reduced model lead to a severe underestimation of the reaction force in the y direction in pin B. This is an important observation indicating that the use of simplified representations, such as those obtained with the Newtonian projection method, should be avoided, since they cannot accurately capture the dynamics of the system.

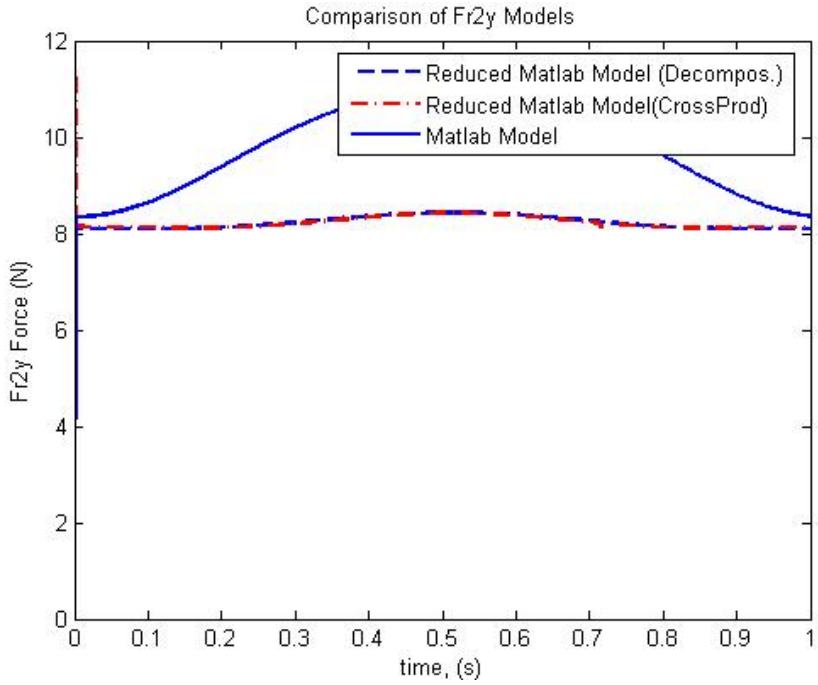

Figure 3-10. Comparison of cross product method and decomposition (reduced model) methods versus Matlab DAE for F_{r2y}

In this chapter, a deterministic model for a simple multibody mechanism was developed. Using a set of differentiable algebraic equations (DAE), the kinematics and dynamics of the system were analyzed using Matlab. The same model was constructed in ProMechanica and the kinematics and dynamics were verified to be consistent with the Matlab model. Due to the limitations imposed by testing capabilities and the complexity of real-life construction machinery, a reduced form of the multibody system was constructed, with only one equation of moments for the liftarm. It has been noticed from the simulation results that the reduced form of the simple mechanism underestimates reaction forces compared to the full DAE model. It was important to validate the deterministic Matlab model through the benchmark with the ProMechanica model before the stochastic models are developed. Moreover, knowing that there is a significant

difference between the full and the reduced model for the simple case study indicates that it is very important to identify techniques to propagate the uncertainties through a model without having to derive reduced "off-line" approximations to use as a starting point.

CHAPTER 4. STOCHASTIC MODELING OF SIMPLE CASE MECHANISM

An important part of this work was to compare different approaches in treating uncertainties in multibody dynamic systems. The complete case study model and its deterministic equations of motion have been described in detail in Chapter 3.

Before discussing the stochastic analysis methods developed and the results obtained in this study, the following terminology is defined. A histogram represents the number of occurrences a stochastic parameter displays within a distribution. Probability density function refers to the area of the distribution normalized to 1. Temporal distribution refers to the distribution of a stochastic parameter at each time step.

The stochastic analysis is initially conducted on just the liftarm of the simple case mechanism using the reduced model (equation of moments), similar to what Caterpillar would have used following the projection method employed to adjust the measured forces such that they satisfy the equation of moments. It is assumed that the equation of moments can accurately predict the reaction forces at B, the bucket, assuming the input forces at A, the rod, are known.

As mentioned before, it was realized that there was a significant difference in the predicted values at the B pin versus the actual values obtained by the forward dynamics Matlab DAE model. Therefore, two methods were developed in assessing the validity of the stochastic nature in the equations of moments for the simple mechanism. An outline of the different stochastic modeling approaches applied on the case study model is given here:

I. *Caterpillar's approach to propagate uncertainty through equation (3.21*).

In this approach, F_{r3x} and F_{r3y} are uncertain known inputs and F_{r2x} is a known deterministic input obtained from the forward dynamics Matlab model. Also, as known inputs are the angular orientation of the liftarm, φ_1, and the angular acceleration α, obtained from the forward dynamics deterministic Matlab model for the respective moment for the time at which we write the equation of moments (3.19). We also know the mass m_1 and the length ℓ of the liftarm. F_{r3x} and F_{r3y} are considered to be uncertain

with a normal distribution within ±5% of their deterministic value at that specific moment in time, which is a typical distribution of measured loads, as we learned from Caterpillar. The mean values for F_{r3x} and F_{r3y} are calculated as the mean of the normal distribution considered. (In reality, measured values of forces such as F_3 at that specific moment in time are available to Caterpillar, who uses them next in the Newtonian projection method to estimate the mean value that satisfies the equation of moments and the standard deviation for these forces.) The mean for F_{r2y} is computed using the linear transformation shown in Eq. (3.21), with the coefficients given in Eq. (4.4). The standard deviation is computed using the quadratic transformation, as shown in equation (4.3).

II. *Mixed approach to estimate the uncertainty in F_{r2y}.*

Version 1: The forward dynamics Matlab model was run to obtain the deterministic values for F_{r3x}, $F_{r3y,}$ F_{r2x}, and F_{r2y}; this F_{r2y} was considered to be the "calculated" value in Eq.(4.3). Next, F_{r2y} was computed using Eq. (3.21); this was considered to be the "measured" value in Eq. (4.3). In this case we take the mean of the stochastic input forces at A to be equal to the deterministic values obtained for a specific moment in time at A. Using Eq. (4.3), the standard deviation of F_{r2y} was computed.

Version 2: In this case we assume that the "true" mean of F_{r2y} is calculated from Eq. (4.13) disregarding the computation done for this force in the forward dynamic Matlab model.

The reason to develop this approach (in its two versions) was to illustrate the difference between propagation of uncertainties in F_{r3x} and F_{r3y} through the entire Matlab model, versus the "reduced approach" which uses only Eq. (3.21)

III. *Monte Carlo approach to propagate uncertainty through equation (3.21).* The main difference between this method and the Caterpillar's approach is in the calculation of the mean value for the uncertain unknown force F_{r2y}. A Monte Carlo simulation is run on Eq. (3.21) at a given moment in time, with F_{r3x} and F_{r3y} randomized between ±5% of their deterministic value, as

above, and the mean and the standard deviation for the uncertain output force F_{r2y} is obtained directly from the simulation.

4.1 Employing the Linear Transformation Method to Propagate the Mean and Quadratic Transformation Method to Propagate the Standard Deviation on the 2-D Two-linkage System Matlab Model

Obtaining the Distribution for the "Measured Force"

As mentioned above, the "measured" force in this study is $F_{3.}$ In order to obtain a distribution with time held constant, a set of random values were generated to create a normal distribution for F_{r3x} and F_{r3y} within ±5% of their deterministic value. We next assumed that their mean values are the mean of the distributions of the "measured" forces considered.

Obtaining Stochastic Properties for the "Unknown Force"

Equation (4.1) represents the linear transformation law used in [9] to obtain the mean values of uncertain unknown parameters, when the mean values of the uncertain input forces are known. The relation also includes the quadratic transformation for the standard deviation. Eq. (4.1) has been customized for the purpose of this study in Eq. (4.2). The coefficients m_x, m_y, and c are given in equation (4.4).

$$W = aX + bY + c = N(a\mu_x + b\mu_y + c,\ a^2{\sigma_x}^2 + b^2{\sigma_y}^2) \tag{4.1}$$

$$W = N(m_x\mu_x + m_y\mu_y + c,\ {m_x}^2{\sigma_x}^2 + {m_y}^2{\sigma_y}^2) \tag{4.2}$$

$$\sigma^2 = m_y(F_{measured} - F_{calculated})^2 \tag{4.3}$$

$$m_x = \frac{\tan(\phi_1)}{3}; \qquad m_y = \frac{1}{3}; \qquad c = \frac{m_1 \ell \alpha}{3\cos(\varphi_1)} + \tan(\varphi_1)F_{r2x} + \frac{m_1 g}{2} \tag{4.4}$$

The mean values of F_{r3x} and F_{r3y} were directly used to calculate the value of the unknown stochastic force component F_{r2y} using Eq. (3.21), as illustrated in Figure 3-8. The standard deviation was calculated using Eq. (4-3).

4.2 Results from Benchmarking the Linear Quadratic Transformation and Monte Carlo Methods

Figures 4-1 and 4-2 represent the histogram and the Probability Density Function (PDF) of the input stochastic forces. It is important to note that the histogram and the PDFs of these forces remained unchanged for the stochastic methods analyzed. Later in this section, a histogram and a PDF are presented at different instants of time for the F_{r2y} using the Monte Carlo and the linear/quadratic methods.

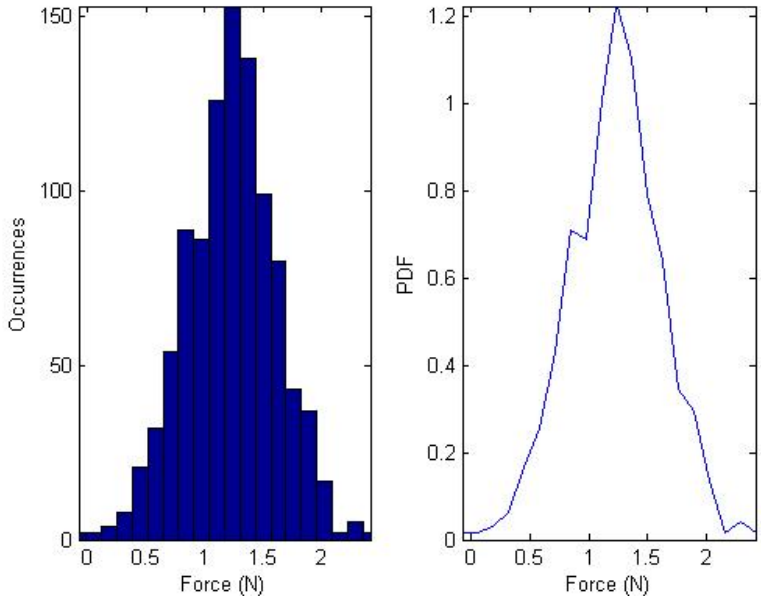

Figure 4-1. Histogram and PDF of the F_{r3x} reaction force at time t=0.1 sec

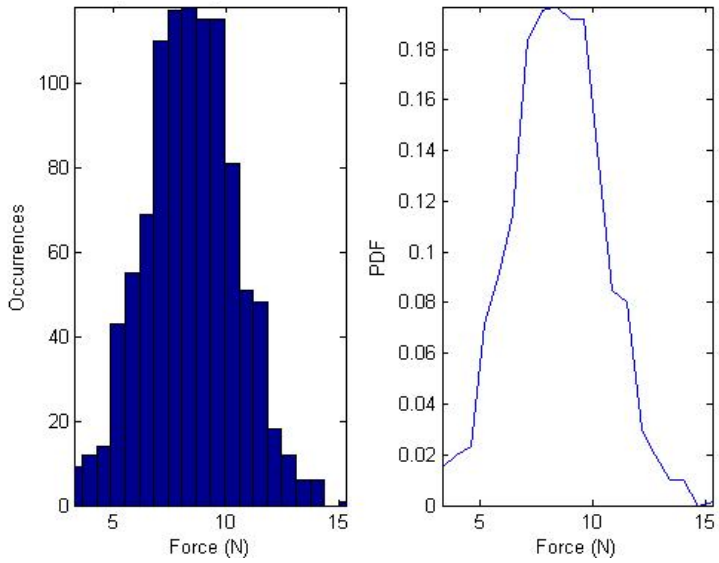

Figure 4 -2. Histogram and PDF of the F_{r3y} reaction force at time t=0.6 sec

Caterpillar's Approach

Figure 4-3 shows a schematic of the implementation of the linear transformation approach at any selected time step to obtain the mean of a stochastic output PDF by solving the reduced model (equation of moments) using as input the mean of the known (measured) stochastic force.

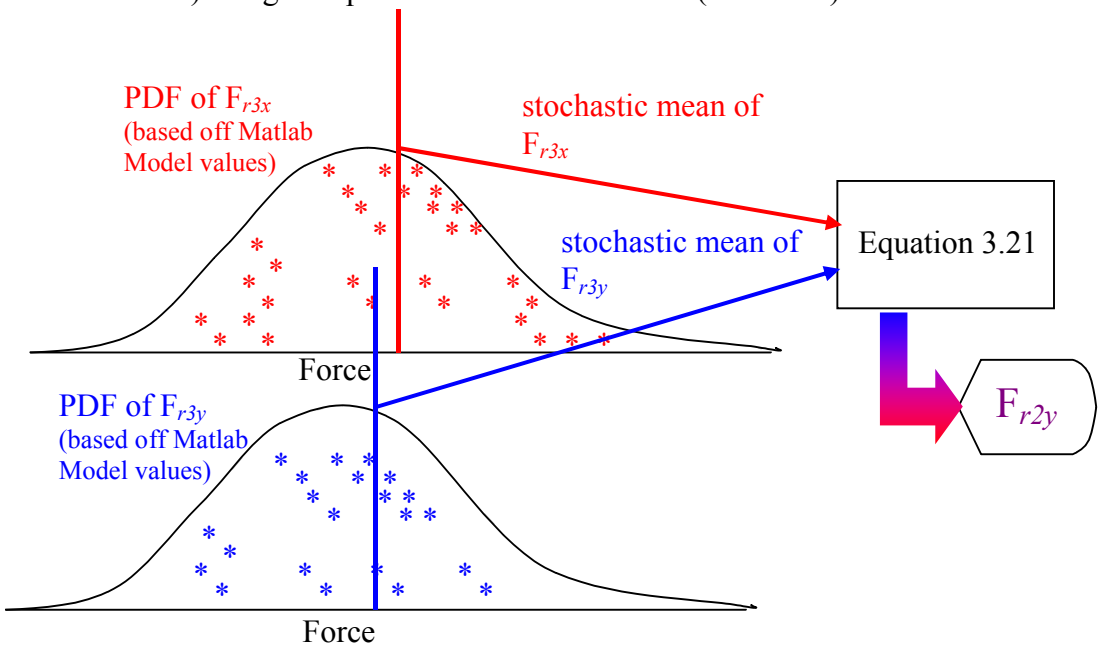

Figure 4-3. Graphical illustration of Caterpillar's method [3] to estimate the uncertainty in F_{r2y} This figure is only intended to graphically visualize the computational approach, and it does not include real data or distributions of the forces in this study.

Mixed Matlab Model

As described earlier, there are two versions of the "Mixed Matlab Model". A graphical illustration of the implementation of the mixed method is given in Figure 4- 4.

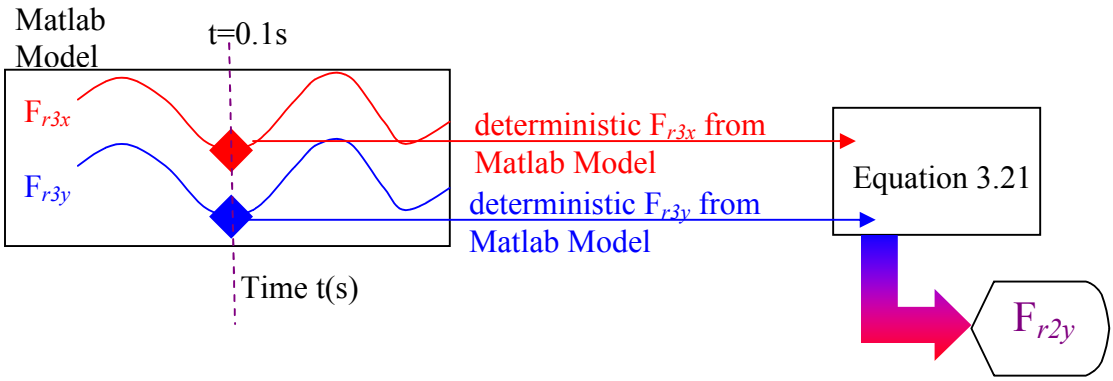

Figure 4-4. Graphical illustration of the mixed method to estimate the uncertainty in F_{r2y}

Monte Carlo Method

A graphical illustration of the implementation of the Monte Carlo method is given in Figure 4-5.

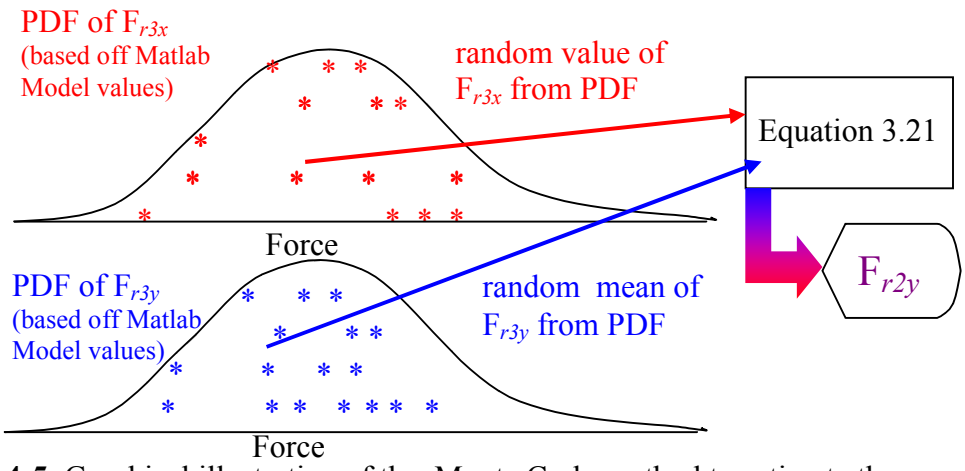

Figure 4-5. Graphical illustration of the Monte Carlo method to estimate the uncertainty in F_{r2y}

This figure is only intended to graphically visualize the computational approach, and it does not include real data or distributions of the forces in this study.

Comparison of Caterpillar, Mixed, and Monte Carlo Methods

The main reason for implementing the uncertainty propagation methods described above is to compare the results obtained under different assumptions and using different strategies. For example, one important aspect is to assess the differences in the results when we rely on the full multibody dynamics model versus the "reduced" model (when we only employ equation (3.21). The complete Matlab model takes into account all bodies in the system and the constraints associated with them.)

Relevant plots obtained with each method are discussed next. Simulations were run for 1000 milliseconds. The stochastic known input forces F_{r3x} and F_{r3y} are the same in all cases and are illustrated in Figure 4-6. The probability density function (PDF) of the forces at each moment in time is shown. In the context of this work, we will refer to the representation of a stochastic force mean and standard deviation through time as the evolution of that force. Such an illustration is presented in Figure 4-6 for the stochastic input force F_{r3}.

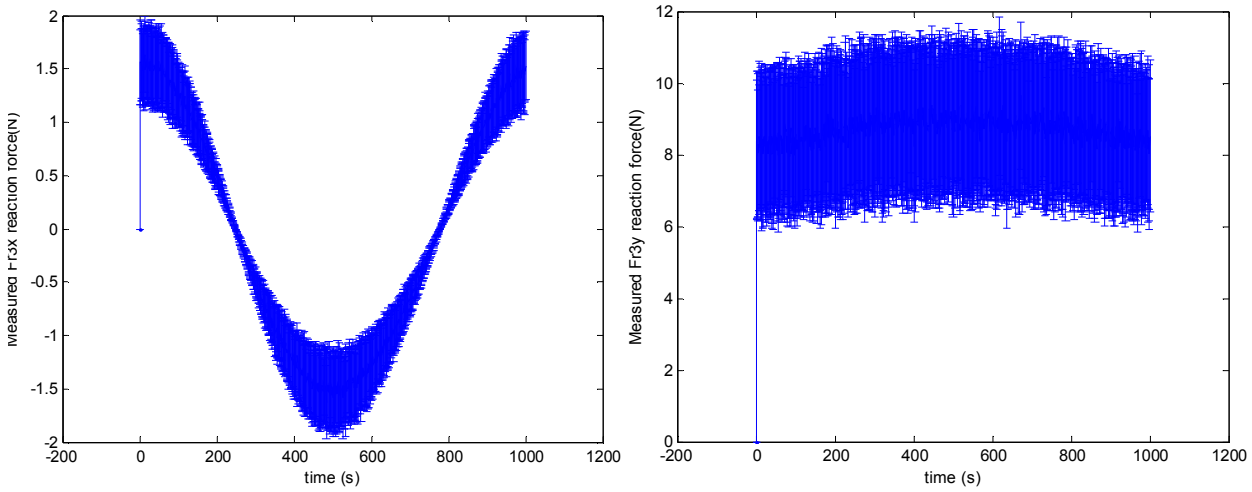

a. F_{r3x} b. F_{r3y}

Figure 4-6. Evolution of the stochastic input (known, measured) force F_{r3} components

It is important to note that for this study, the distributions of the input functions, as well as those of the output functions were not obtained through propagation in time, but rather considered independent at each moment in time. For the input forces, the distribution can be extracted from the experimental data, while for the output forces, the distribution is obtained from the simulation results.

Using the Mixed Matlab Method (version 1) we obtained the evolution of the reaction force F_{r2y}, as illustrated in Figure 4-7.

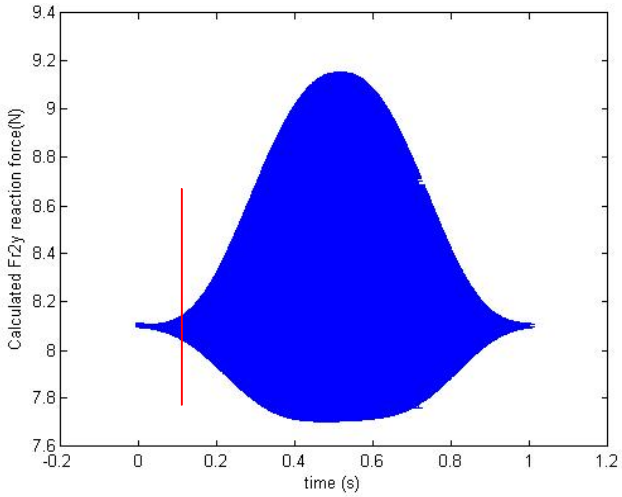

Figure 4-7. Evolution of F_{r2y} using the Mixed Matlab Method (version 1)

This plot represents the baseline for comparing the method developed using the Linear/Quadratic transformation and the Monte Carlo Method. An ensemble of 1000 runs was performed for the Monte Carlo simulation. The vertical red line denotes t=0.1 sec. This moment of time has been arbitrarily selected to illustrate the analysis in this part of our study, but the conclusions are general, and do not depend on the time chosen.

Figure 4-8 presents the evolution of F_{r2y} obtained using the Caterpillar uncertainty propagation approach. Figure 4-9 presents the PDF of F_{r2y} obtained using the Monte Carlo Method. As before, the vertical red line denotes t=0.1 seconds for Figure 4-8 and Figure 4-9.

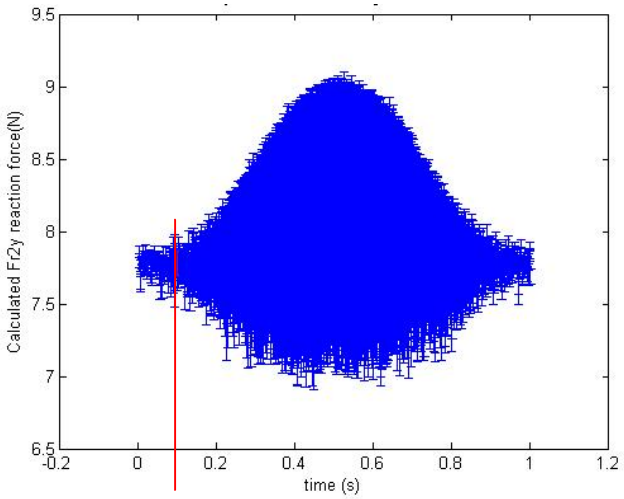

Figure 4-8. Evolution of F_{r2y} using Linear/Quadratic Method

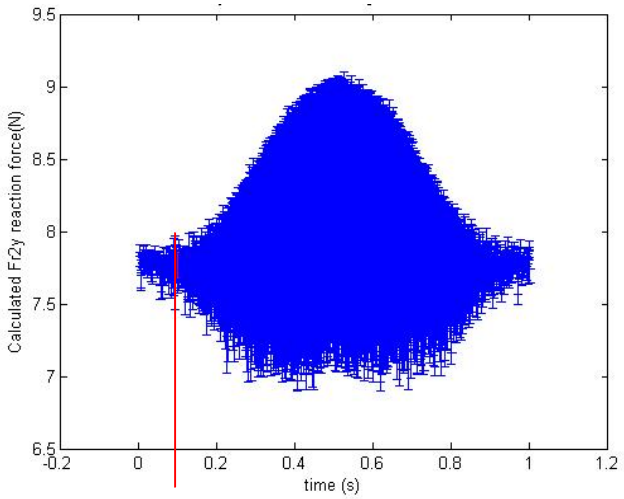

Figure 4-9. Evolution of F_{r2y} using Monte Carlo Method

As it can be noticed, the results presented in Figures 4-7 through 4-9 for the three methods implemented are very similar.

In Figure 4-10 we present a comparison between the histogram and PDF of F_{r2y} with the linear/ quadratic transformation and with the Mixed Methods at t=0.1 sec. This histogram was obtained by randomizing 1000 points with a normal distribution within the standard deviation at t= 0.1sec.

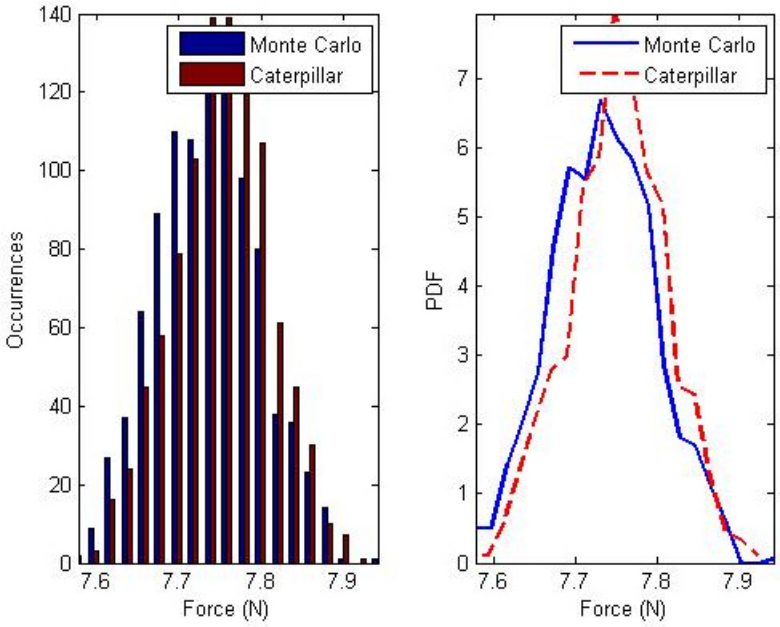

Figure 4-10. Histogram and PDF of the F_{r2y} reaction force at time t=0.1 sec

In Figure 4-11 we present a comparison between the histogram and PDF of F_{r2y} with Linear/Quadratic and with the Mixed Methods at t=0.6 sec.

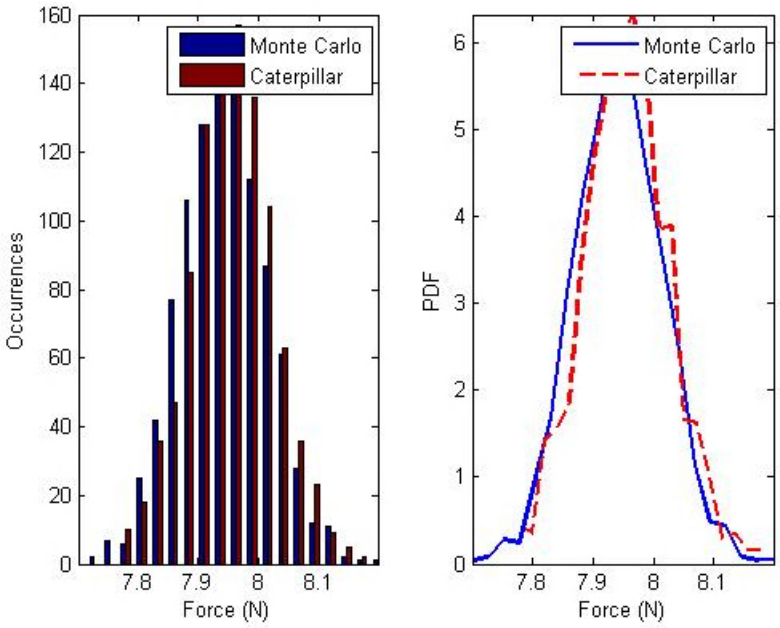

Figure 4-11. Histogram and PDF of the F_{r2y} reaction force at time t=0.6 sec

In Table 4-1 we summarize the results for the three methods for two discrete moments of time: t=0.1sec and t=0.6 sec. Since the parameter of interest is the unknown reaction force F_{r2y}, Table 4-1 illustrates the values of the mean and standard deviation for this force in each case discussed above.

Table 4-1. Comparison Results of Linear/Quadratic Transformation, Mixed (ver. 1), and Monte Carlo Methods

Unknown Uncertain Force [N]	**Matlab Mixed Method 1** Mean	**Matlab Mixed Method** Std. Dev.	**Caterpillar Method** Mean	**Caterpillar Method** Std. Dev	**Monte Carlo** Mean	**Monte Carlo** Std. Dev.
1. F_{r2y} t=0.1sec	8.0936	0.0338	7.7816	0.0829	7.7658	0.0860
2. F_{r2y} t=0.6sec	8.3910	0.6737	7.9904	0.9107	7.9796	0.9176

It can be seen from Table 4-1 that the mean value of the reaction force is the same for the linear/quadratic transformation and for the Monte Carlo methods, and slightly different for the Mixed method (version 1). Similar conclusions can be drawn for the standard deviation. We attribute these differences to the limiting assumptions made in the Mixed method, while the very good correlation of the other two methods validate the correct implementation of those methods on the two-link system model.

As mentioned, in the discussion of the results in Table 4-1 above we assumed that the "true" value for the mean of the unknown stochastic force F_{r2y} was the deterministic value obtained from the full forward dynamics Matlab model. Next, as described in the Mixed Method version 2 section, we assume that the "true" value of the mean of the unknown force is obtained by simply using the deterministic values from the forward dynamics of the "measured" (known) forces F_{r3x} and F_{r3y} and the deterministic component F_{r2x} in Eq. (3.21) to obtain a new value for F_{r2y}. The evolution of F_{r2y} thus obtained is deterministic, and presented in Figure 4-12.

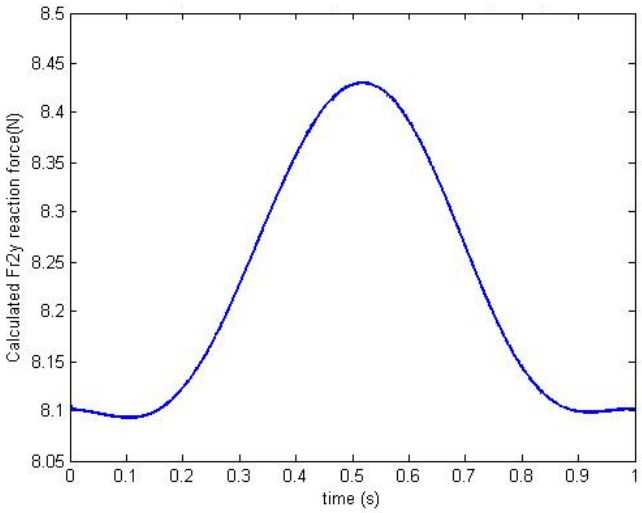

Figure 4-12. Evolution of Fr2y obtained using equation (3.21)

In Figures 4-13 and 4-14 we present the evolution of the F_{r2y} obtained using the Caterpillar and the Monte Carlo Methods, where, as a starting point for the mean value of F_{r2y} we used the value obtained directly from Eq. (3.21).

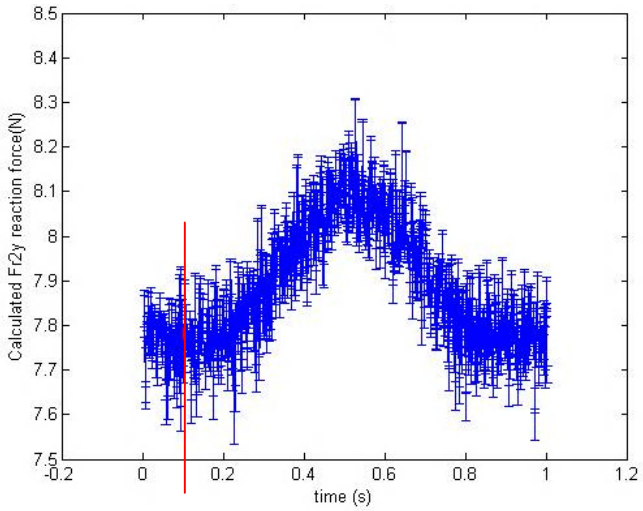

Figure 4-13. Evolution of F_{r2y} using Linear/Quadratic method (with Mixed Method version 2)

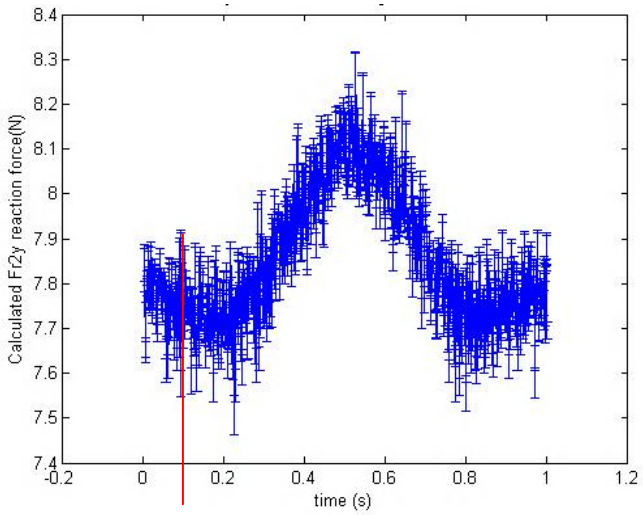

Figure 4-14. Evolution of F_{r2y} using Monte Carlo Method (with Mixed Method version 2)

In Figures 4-15 and 4-16 we present the histogram and the PDF of F_{r2y} for t=0.1 sec, and respectively for t=0.6 sec with the mixed version 2. This histogram was obtained by randomizing 1000 points with a normal distribution within the standard deviation at t= 0.1sec.

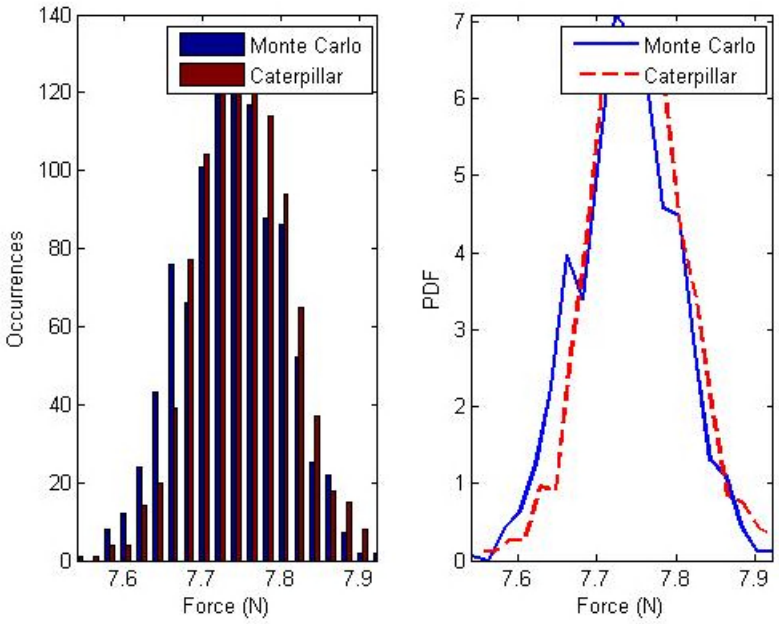

Figure 4-15. Histogram and PDF of F_{r2y} using Caterpillar and Monte Carlo (with Mixed Method version2)

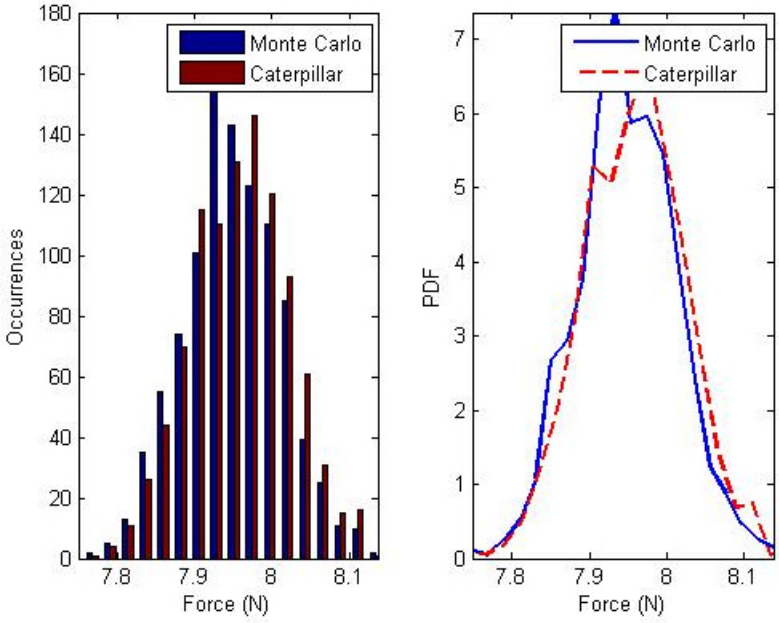

Figure 4-16. Histogram and PDF of F_{r2y} using Caterpillar and Monte Carlo (with Mixed Method version 2)

In Table 4-2 we summarize the results at t=0.1 sec and t=0.6 sec.

Table 4-2. Comparison Results of the Caterpillar, Mixed (ver. 2) and Monte Carlo Methods

Unknown Stochastic Force [N]	**Matlab Mixed Method 2** Mean	**Matlab Mixed Method 2** Std. Dev.	**Caterpillar Method** Mean	**Caterpillar Method** Std. Dev	**Monte Carlo** Mean	**Monte Carlo** Std. Dev.
1. F_{r2y} t=0.1 sec	8.0936	0	7.6895	0.0108	7.6736	0.0119
2. F_{r2y} t=0.6 sec	8.3910	0	8.0503	0.0178	8.0394	0.0188

As before, one can notice the very good correlation between the linear/quadratic transformation and the Monte Carlo Methods, in terms of both standard deviation and mean value, while the Mixed Method gives slightly different values.

4.3 Polynomial Chaos Approach for the Simple Case study Mechanism

Collocation Procedure – For Uniform Distribution of F_{r3x} and F_{r3y} at the Rod/Cylinder Assembly (A-Pin)

The polynomial chaos approach to treat uncertainties in multibody dynamic systems was implemented using the collocation technique on the Matlab model of the two-link mechanism. The uncertain input parameter was considered to be the amplitude of the driver of the lift arm, with a uniform distribution. Such a distribution requires orthogonal Legendre polynomials for the Karhunen-Loeve (KL) expansion. To implement the Collocation Method, the uncertain input was approximated using a KL expansion. The polynomials used as bases functions in the KL expansion were of order five. The coefficients of the independent variable in the polynomial expansion were solved using collocation points selected from the distribution. For more details on the process of selecting the collocation points the reader can refer to [17].

The DAE from Eq. (3.17) was run for 15 uncertain driver amplitudes at the collocation points taken from a stochastic distribution. Without restricting the validity of our analysis, the stochastic distribution considered first was uniform. From the 15 different amplitudes, 15 reaction forces for F_{r3} and F_{r2} can be computed at the collocation points. A polynomial chaos expression was obtained for each time step for F_{r3} and F_{r2}. Using the procedure outlined in the

example provided in the Polynomial chaos section 2.8, the number of terms in the polynomial expansion is 5 and the number of observed F_{r3} values was 15. Therefore, a system of 15 equations and 5 unknowns were obtained for the F_{r3} force as shown in Eq. (4.5)

$$\begin{bmatrix} F_{r3}{}^{1} \\ \vdots \\ F_{r3}{}^{15} \end{bmatrix} = \mathbf{A} \begin{bmatrix} f_{r3}{}^{1} \\ \vdots \\ f_{r3}{}^{5} \end{bmatrix} \tag{4.5}$$

The uppercase F_{r3} refers to the stochastic values at the collocation points, **A** is the collocation matrix from Eq. (2.13), and the lowercase f_{r3} refers to the 5 coefficients obtained from a least-squares analysis that will satisfy the collocation points with the following expansion

$$F_{r3}(t_k,\xi) = f_{r3}{}^{1}(t_k)\phi^1(\xi) + f_{r3}{}^{2}(t_k)\phi^2(\xi) + f_{r3}{}^{3}(t_k)\phi^3(\xi) + f_{r3}{}^{4}(t_k)\phi^4(\xi) + f_{r3}{}^{5}(t_k)\phi^5(\xi) \tag{4.6}$$

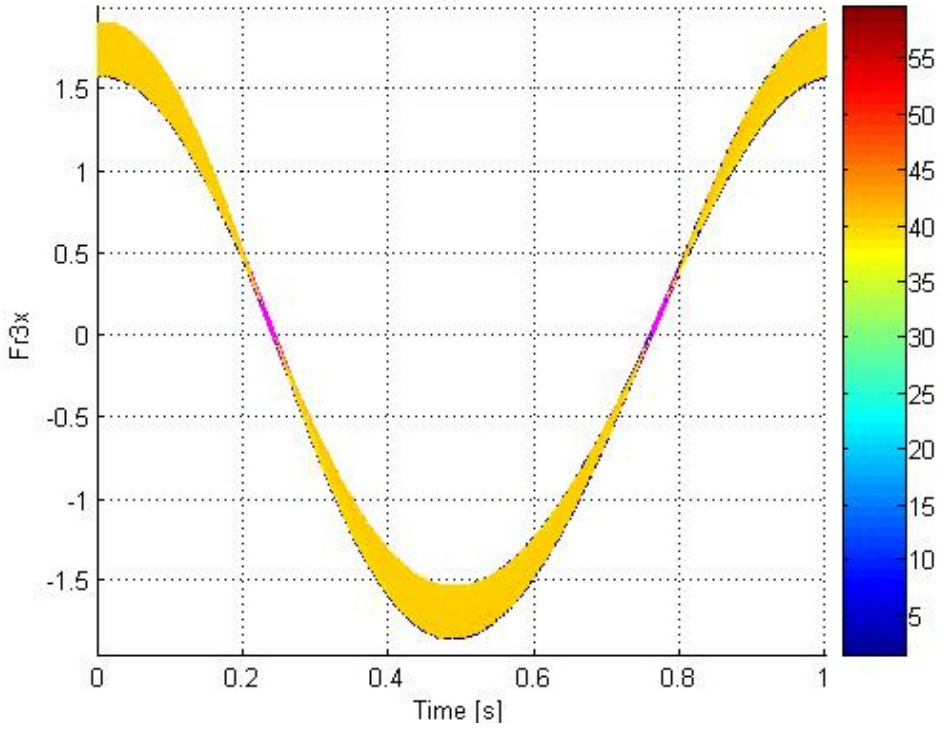

Figure 4-17. Temporal distribution of F_{r3x} obtained using the Collocation Method for a uniform distribution of F_{r3x} at each moment of time

The expansion in Eq. (4.6) represents the total magnitude and direction of F_{r3}. The DAE can calculate the reaction forces along the x and y components as shown in Eq. (3.30) at the collocation points. Therefore, upon obtaining the expansion illustrated in Eq. (4.6) for F_{r3x} and

F_{r3y}, an ensemble of 4000 points for ξ from the stochastic uniform distribution were used as input. In Figures 4-17 and 4-18 we present the temporal distribution of the stochastic input forces F_{r3x} and F_{r3y} resulting from the Monte Carlo simulations performed at each time step.

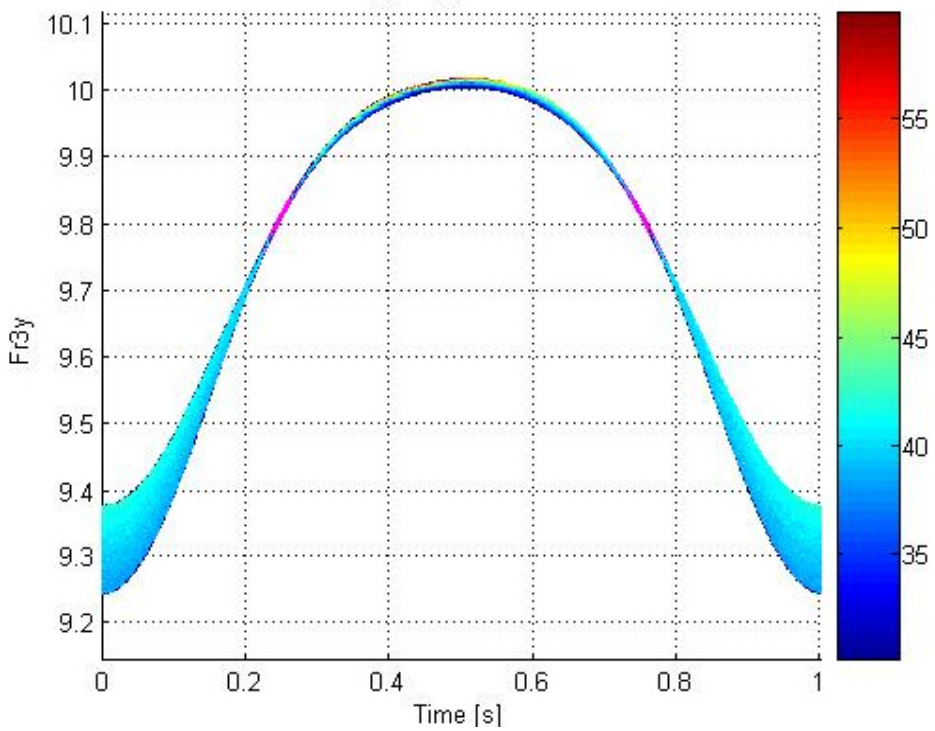

Figure 4-18. Temporal distribution of F_{r3y} obtained using the Collocation Method for a uniform distribution of F_{r3y} at each moment of time

The interpretation of these graphics can be done using the color coding illustrated to the right of the plots. At each moment in time, the probability of a certain force value to occur, within the range of possible values is color coded. Thus, the closer to red, the higher the probability of the force component consider having the value indicated on the vertical axes at a given moment in time. The magenta line that appears in Figures 4-17 and 4-18 represents the value of the F_{r3x}, respectively of the F_{r3y} from the deterministic model.

Collocation Procedure for Beta Distribution of F_{r3x} and F_{r3y} at the Rod/Cylinder Assembly (A-Pin)

To further illustrate the techniques analyzed in this study, the second simulation conducted used Beta distributions for F_{r3x} and F_{r3y} at the A-Pin. The Beta distribution implies using orthogonal Hermite polynomials, for the KL expansion. The same form of the expansion for the F_{r3} force

was obtained, as the one given by Eq. (4.6). An ensemble of 4000 points for ξ from the Beta distributions was input to the expansion at each time step during the 1 second duration of the simulation. Figures 4-19 and 4-20 illustrate the temporal distribution of F_{r3x} and $F_{r3y,}$ when the Beta distribution was used. As before, red indicates a higher probability and blue indicates a lower probability for the occurrence of a force value.

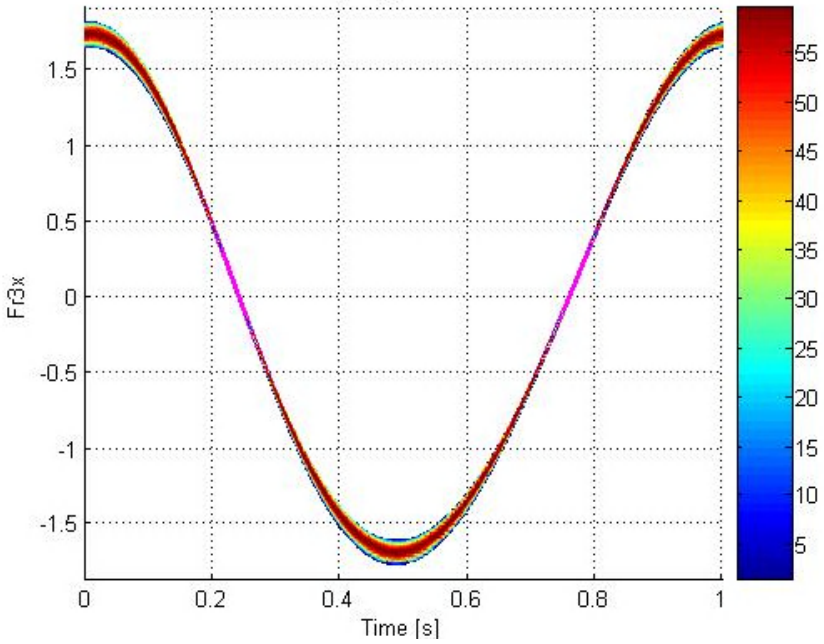

Figure 4-19. Temporal distribution of F_{r3x} obtained using the Collocation Method for a Beta distribution of F_{r3x} at each moment of time

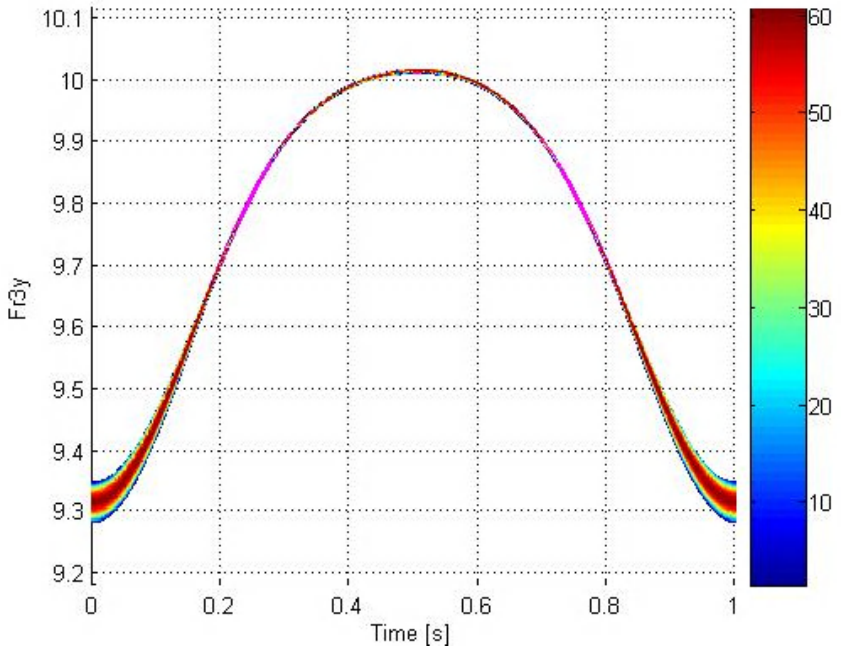

Figure 4-20. Temporal distribution of F_{r3y} obtained using the Collocation Method for a Beta distribution of F_{r3y} at each moment of time

We notice from Figures 4-19 and 4-20 that the highest probability occurs near the center of the distribution. Also, the distribution of the input reaction forces, as seen in these figures, illustrates the fact that, as previously considered, their standard variation is within ±5% from the values obtained with the deterministic model (magenta line in Figures 4-19 and 4-20).

Collocation Results for Reactions at Bucket/ Lift arm Assembly (B-Pin) For Uniformly Distributed Inputs

The collocation procedure for treating the uncertainties in the two-link system has been further employed to estimate the uncertainties in the reaction forces at the B-Pin. The focus in this section is to see how the uncertain parameter (considered as input) applied to the sinusoidal driver affects the reactions at the B-pin. The "bucket" (body 2) is constrained in one position for the entire duration of the simulation. The "liftarm" (body 1), however, is moving as prescribed by the uncertain driver. The first test on this portion of our simple Matlab model was done using a uniform distribution for the uncertain input.

The same procedure that was explained for recovering the coefficients of the polynomial chaos expansion for F_{r3} is employed this time for F_{r2}. In this case, the observed stochastic value is F_{r2} and thus leads to Eq.(4.7), where

$$\begin{bmatrix} {F_{r2}}^{1} \\ \vdots \\ {F_{r2}}^{15} \end{bmatrix} = \mathbf{A} \begin{bmatrix} {f_{r2}}^{1} \\ \vdots \\ {f_{r2}}^{5} \end{bmatrix} \tag{4.7}$$

Therefore, the polynomial chaos expansion for F_{r2} can be obtained from the expression shown in Eq. (4.8).

$$Fr_2(t_k,\xi) = {f_{r2}}^{1}(t_k)\phi^1(\xi) + {f_{r2}}^{2}(t_k)\phi^2(\xi) + {f_{r2}}^{3}(t_k)\phi^3(\xi) + {f_{r2}}^{4}(t_k)\phi^4(\xi) + {f_{r2}}^{5}(t_k)\phi^5(\xi) \tag{4.8}$$

Figures 4-21 and 4-22 illustrate the temporal distribution of the predicted reaction forces F_{r2x} and F_{r2y} in the B-pin. These figures were generated as before with an ensemble of 4000 points for ξ from the uniform distribution at each time step. When compared with the results presented earlier, the distribution of the uncertain reaction forces F_{r2x} and F_{r2y} estimated based on the polynomial chaos method seems to converge to the deterministic value mid-cycle.

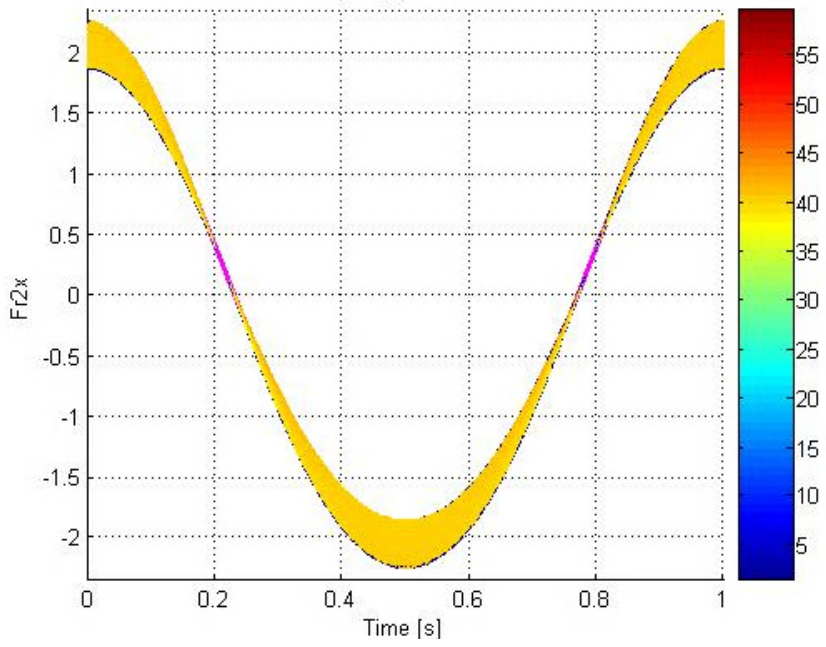

Figure 4-21. Temporal distribution of F_{r2x} obtained using the Collocation Method for a uniform distribution of F_{r2x} at each moment of time

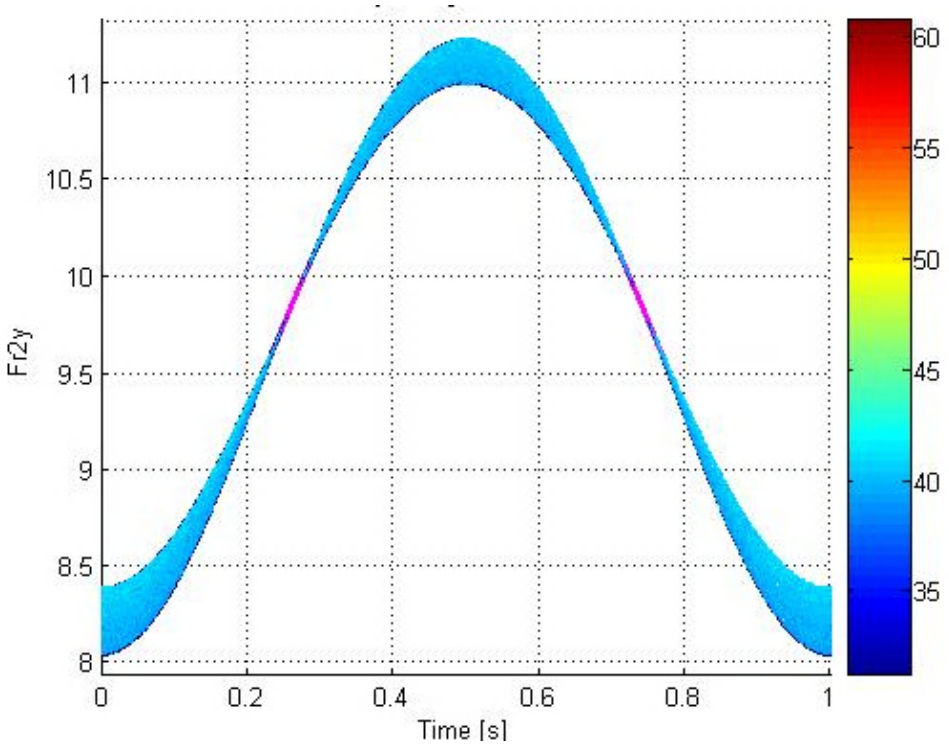

Figure 4-22. Temporal distribution of F_{r2y} obtained using the Collocation Method for a uniform distribution of F_{r2y} at each moment of time

Collocation Results for Reaction at the Bucket/ Lift Arm (B-Pin) Assembly for Beta Distributed Inputs

In Figures 4-23 and 4-24 we present the temporal distribution of the reaction forces in the B-Pin obtained using a collocation approach, similar to the one employed in the previous section. The only difference was in the type of distribution of the uncertain inputs, which, in this case, was a Beta distribution.

We can notice that, for this case study, the reaction forces at the B-pin have a higher probability toward the center of the distribution, at each time step.

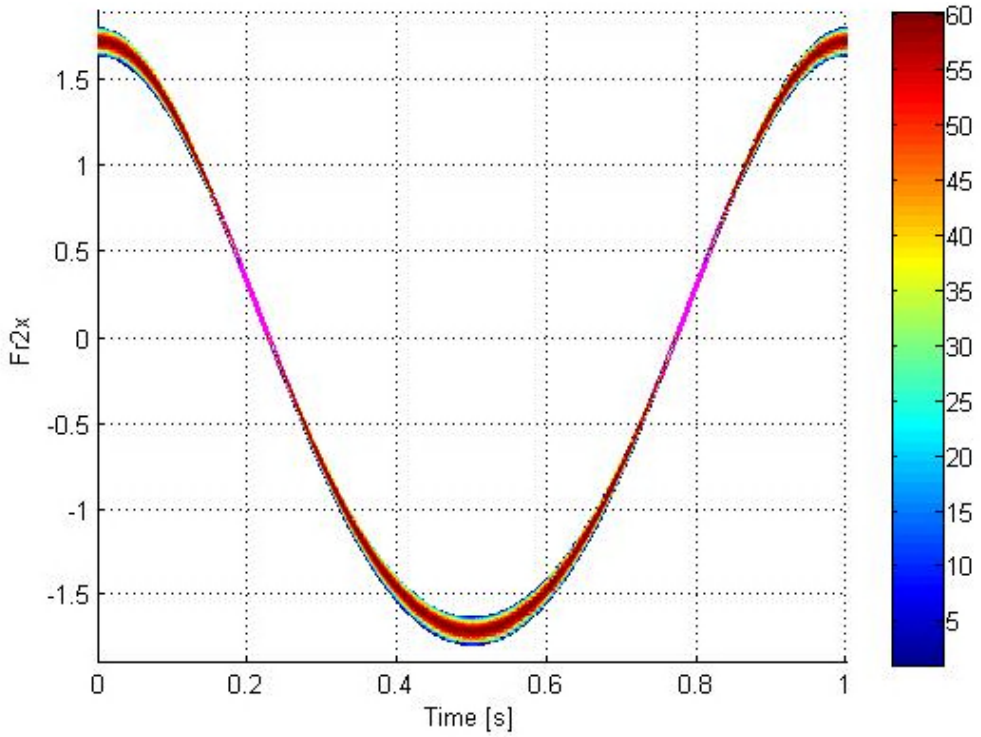

Figure 4-23. Temporal distribution of F_{r2x} obtained using the Collocation Method for a Beta distribution of F_{r2x} at each moment of time

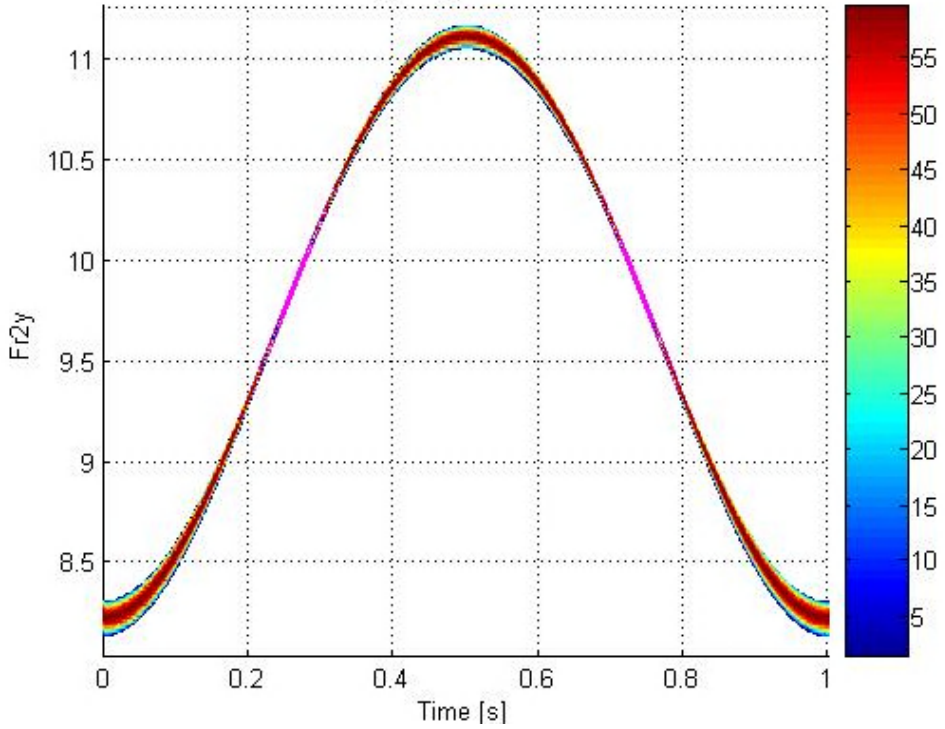

Figure 4-24. Temporal distribution of F_{r2y} obtained using the Collocation Method for a Beta distribution of F_{r2y} at each moment of time

4.4 Stochastic Analysis of the ProMechanica Simple Mechanism Model using Collocation Points

To gain confidence in the collocation approach proposed to treat uncertainties in "black-box" type models, a simple case ProMechanica model was run with the same collocation points as in the simple case Matlab model. The simulation time for the ProMechanica model was 1 second, just as for the simple case Matlab model.

It is important to recall that the source of uncertainties considered in this study is the variability in the measurements of the actuator force at a given instant. Thus, the input force of interest F_{r3}, was to have an independent distribution at each moment in time. The goal of this study was to estimate the distribution of the output forces of interest, (e.g., joint reaction forces), based on the knowledge about the input, and the system dynamics. The stochastic parameter considered was the amplitude of the driver. The amplitude is part of a continuously differentiable trigonometric function. Performing an individual independent stochastic analysis at each point in time using the 15 different collocation points in ProMechanica would be equivalent to generating 15 time evolving "deterministic" curves for the uncertain parameter which was the amplitude of the driver. However, it is important to note that the basic principle is that we assume the same distribution for the collocation analysis in both models, (Matlab and ProMechanica).

Using the information obtained on polynomial chaos from the literature review, random variables can be expressed as functions of some random events of a known probability distribution. In this study, this random variable is the amplitude of the driver, which is denoted by the variable $Y^i(t)$. The coefficient matrix that allows the amplitude of the driver to be uncertain is expressed as $\mathbf{A}_{i,j}$. The collocation values can be recovered using Eq. (4.9).

$$y^j(t_k) = \sum_{j=1}^{S} \mathbf{A}^{\#}{}_{i,j} Y^i(T) \tag{4.9}$$

$\mathbf{A}^{\#}{}_{i,j}$ is the pseudo-inverse of $\mathbf{A}_{i,j}$. The value, $Y^i(T)$ contains a vector of collocation amplitude values which are used as the input to the ProMechanica kinetic model. In this analysis, the number of collocation points was 15.

The 15 different collocation points were found for each time step ranging from 0 to 1000 milliseconds with a time step of 0.02 seconds. The stochastic driver amplitude was used as the input into the ProMechanica model. Fifteen different sets of data were generated for the stochastic amplitude at each point in time. Those files were read into ProMechanica and produced 15 different sets of reaction forces at the bucket (body 2) and at the revolute joint connecting the liftarm (body 1) and the rod (body 3).

The 15 collocation points obtained for the reaction forces F_{r3} and F_{r2} from ProMechanica were then read back into Matlab to process the temporal distribution plots. The polynomial chaos expansion for the reaction forces were derived using the same methodology described in section 4.3 for the Matlab DAE reaction forces F_{r3} and F_{r2}. The number of bins, and bin range were determined by an algorithm developed in [20]. The algorithm used a Beta (2,2) distribution in order to approximate a Gaussian distribution. Again, this was only an approximation to compare the simple case Matlab collocation results with those of the simple case ProMechanica collocation results. The results are presented in Figures 4-25 and 4-26.

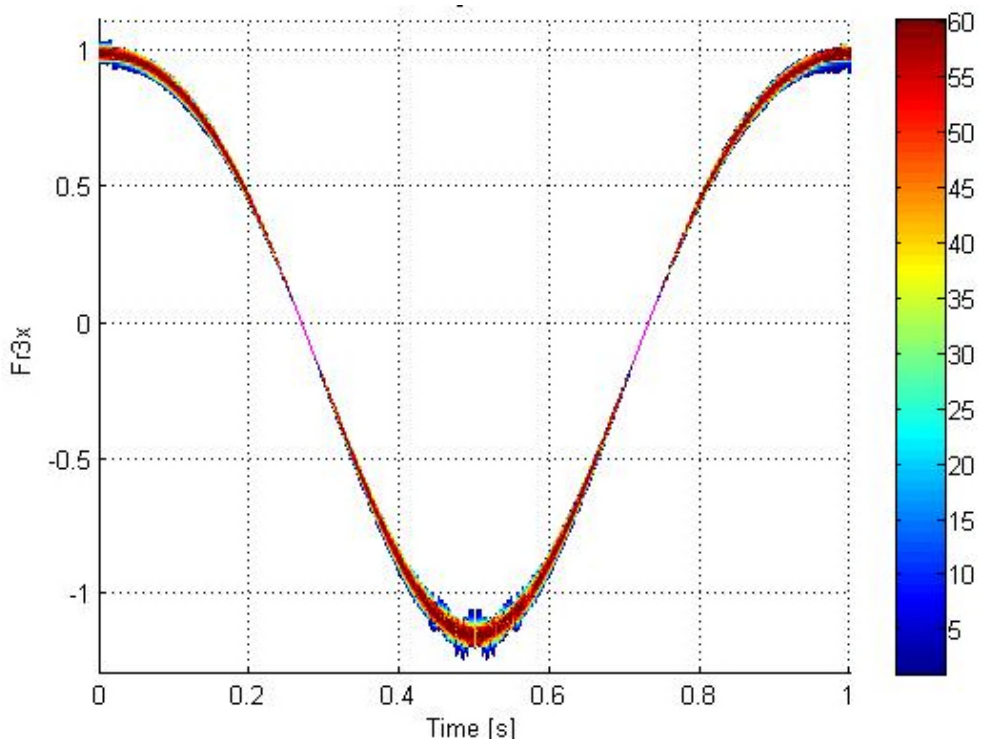

Figure 4-25. Temporal distribution of ProMechanica F_{r3x} obtained using the Collocation Method for a Beta distribution of F_{r3x} at each moment of time

The ProMechanica values for the input forces F_{r3x} and F_{r3y} presented in Figure 4-26 input forces show a high probability density of the true mean indicated by the red color. There are points where the color density indicates that the highest probability of the force value is close to (converges to) the deterministic result at that point in time. While the shape of the graph is similar to that of the Matlab collocation results, there is a slight offset in the F_{r3y} forces, most likely due to the geometry of the bodies in the ProMechanica model, which have slightly different centers of mass compared to the Matlab Model. This can also be attributed to the complex geometry of the hydraulic lift cylinder/rod configuration in ProMechanica, as opposed to a simple planar relationship in Matlab. Unlike the model in ProMechanica, the simple case Matlab model has 2-dimensional bodies with no thickness in the z-direction. The hydraulic cylinder/rod assembly in Matlab has only a revolute constraint connecting the rod and liftarm, while the liftarm of the simple mechanism in ProMechanica has a small pinion about which the rod to rotates. From Figure 4-27 we can see that the high areas of probability occur towards the center of the distribution. The red indicates a high probability and the blue indicates a low probability.

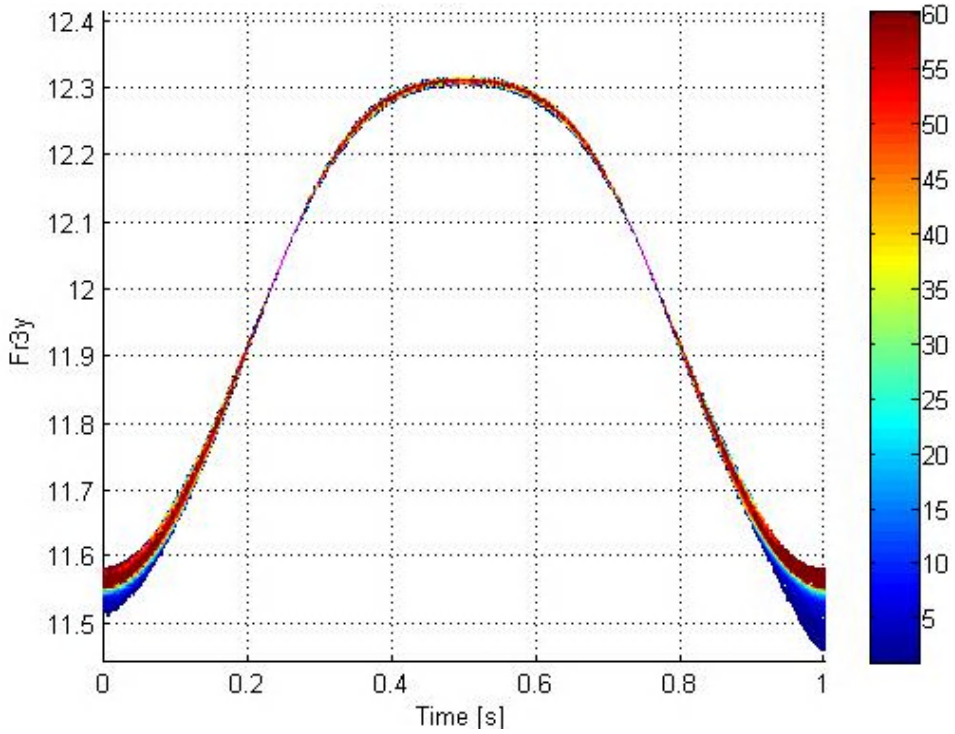

Figure 4-26. Temporal distribution of ProMechanica F_{r3y} obtained using the Collocation Method for a Beta distribution of F_{r3y} at each moment of time

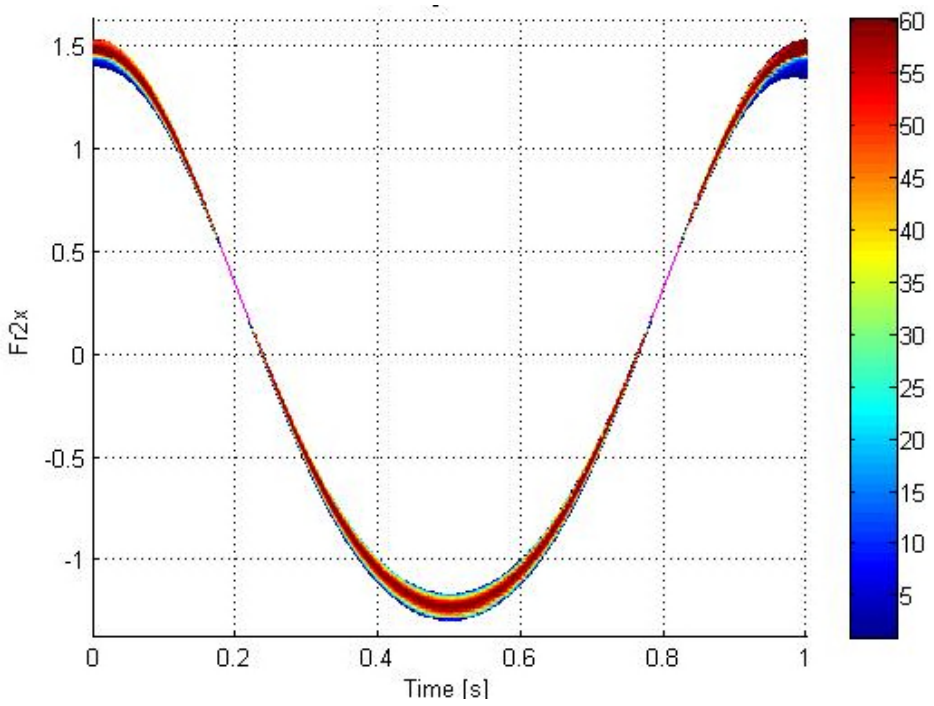

Figure 4-27. Temporal distribution of ProMechanica F_{r2x} obtained using the Collocation Method for a Beta distribution of F_{r2x} at each moment of time

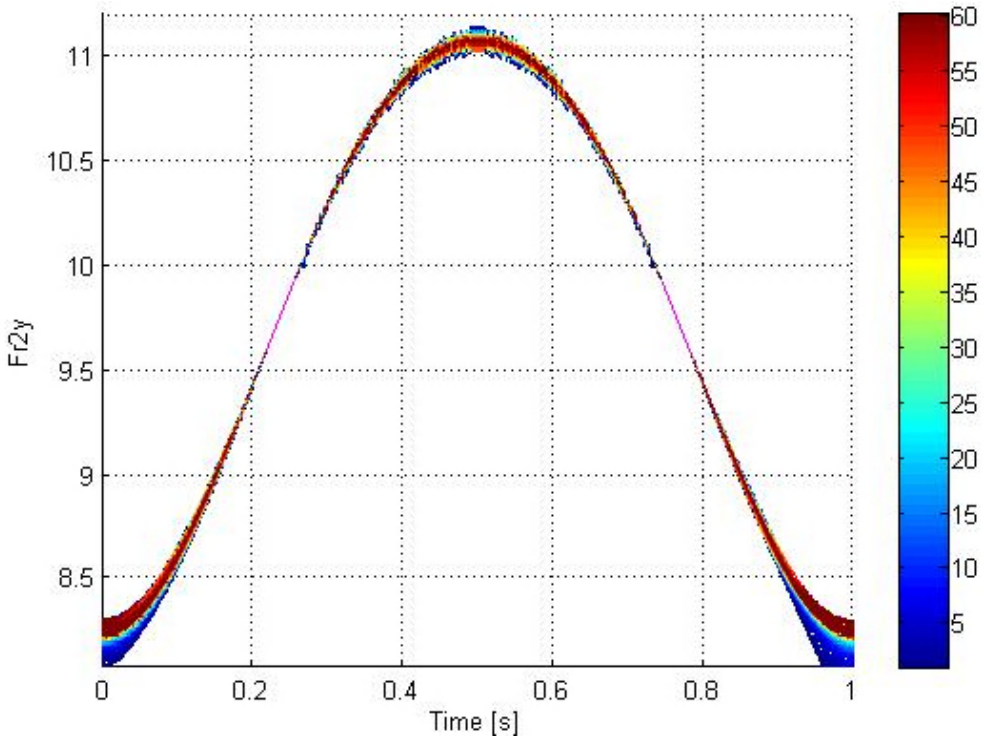

Figure 4-28. Temporal distribution of ProMechanica F_{r2y} obtained using the Collocation Method for a Beta distribution of F_{r2y} at each moment of time

If the collocation points are very close, the output is almost the same in all cases. We postulate that this phenomenon is likely the result of the system reaching an equilibrium position.

The same phenomena observed in Figure 4-27 is noticed in Figure 4-28. From the results presented in this chapter, one can see that the same distributions are generated when we have equations of motion in Matlab, and when we do not have them, in the ProMechanica model. This is a very important result, since the next step in our study is to estimate the stochastic reaction forces stochastic in the full 980GII wheel loader, for which we do not have the equations of motion. Moreover, the complexity of the stochastic model derivation is reduced, and the accuracy of the deterministic model is preserved.

CHAPTER 5. COLLOCATION APPROACH ANALYSIS ON THE FULL 980G II WHEEL LOADER MODEL IN PROMECHANICA

In this chapter we implement the collocation methodology illustrated in Chapter 4 on the full 980G II wheel loader model developed in ProMechanica. We analyze the rackstop force, introduced in the literature review chapter, and consider it an uncertain parameter. Using the Collocation Method, we obtain a probability density function of the rackstop force. The uncertain rackstop force is used as an input and propagated through the ProMechanica model of the wheel loader to determine the resulting probability function for the reaction forces at the joint between the bucket and the liftarm of the non-engine end-frame of the wheel loader. This point is called the B-Pin, similar to the joint in the simple case study discussed in previous chapters.

5.1 Deterministic Model of 980G II Wheel Loader

The deterministic model was developed by Caterpillar in ProMechanica and it consists of only the non-engine end frame of the entire 980G II wheel loader. It has a total of 34 bodies. The kinematic model has all rigid bodies connected by pre-defined joints in ProMechanica. It is driven by actuators acting at certain joints. For example, for the motion between the bucket and the liftarm, the model uses a table containing field test data to rotate the bucket in time. In the kinetic model, each of the pre-defined joints are broken apart into independent 6 degree of freedom joints. The reaction forces are then imposed on components of the 6 degree of freedom joints. The purpose of the kinematic model is to generate the positions, orientations, velocities, and accelerations of all bodies as well as the reaction forces at the joints not measured during field test. The reaction forces from the kinematic model are imposed on the 6 degree of freedom joints in the kinetic model to keep the system at zero degrees of freedom. The kinematic model is shown in Figure 5-1 and the kinetic model is shown in Figure 5-1.

The ProMechanica kinematic and kinetic models for the wheel loader are the only available means of obtaining deterministic outputs. Due to the complex nature of the 980G wheel loader, no equations of motion were derived. (At the beginning of this project, it was suggested exporting the equations of motion could be obtained from ProMechanica. However, further investigation of this option showed that it was not possible.)

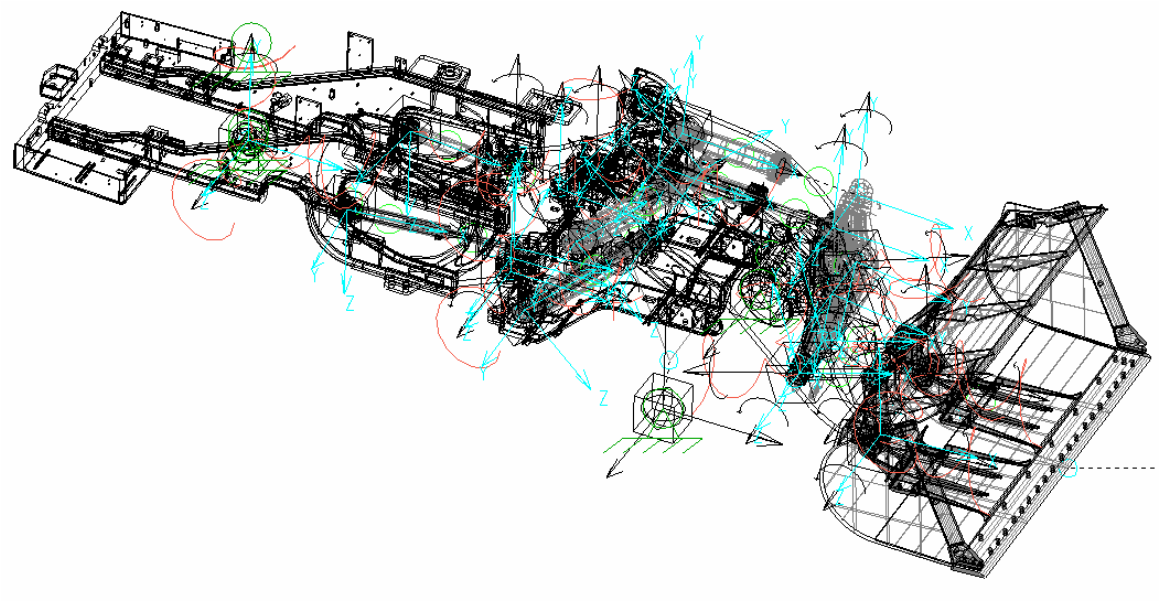

Figure 5-1. Kinematic model of non-engine end frame in ProMechanica

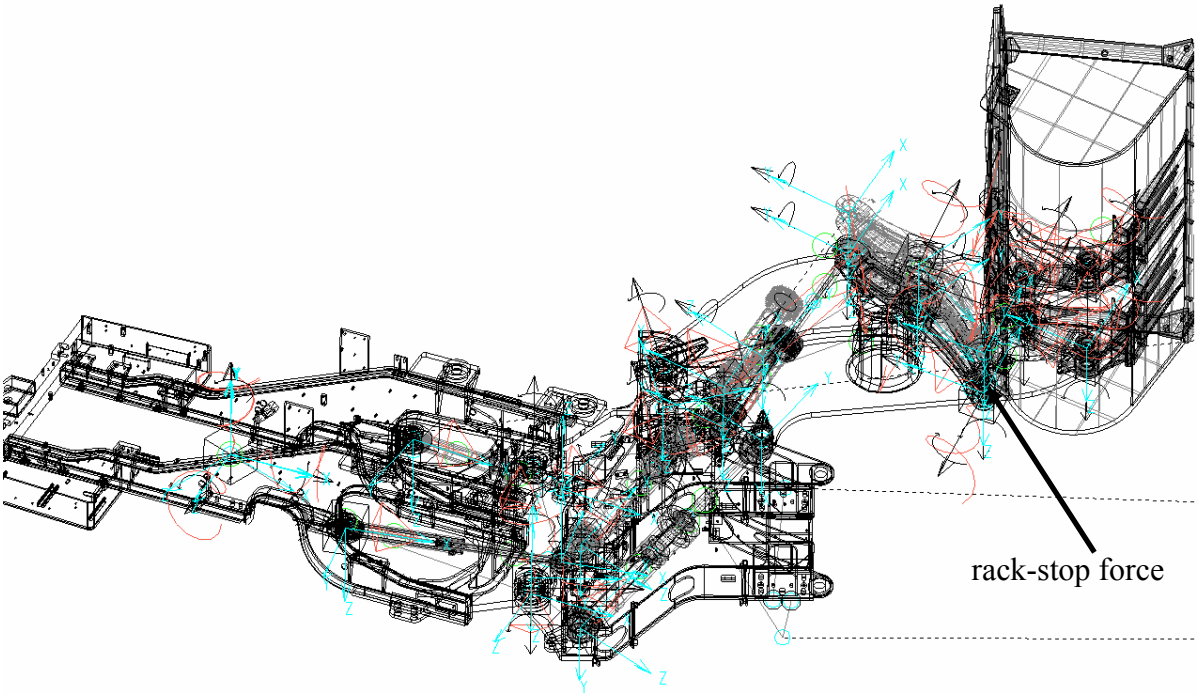

Figure 5-2. Kinetic model of non-engine end frame in ProMechanica

5.2 Stochastic Collocation Analysis on 980G II Wheel Loader

As for the simple case mechanism, the Collocation Method simply expresses a particular force of interest that acts on the wheel loader as an uncertain parameter. By making the uncertain force stochastic, other reaction forces of interest on the wheel loader can be investigated and a PDF can be obtained through post-processing. The main ideas behind using the Collocation Method are that it is computationally efficient and that it can be applied to systems for which one has only access to the input files, and not the equations of the model.

The uncertain parameter chosen for the collocation analysis on the full wheel loader was the rack-stop force. The rack-stop force is the force that the material being scooped initially exerts on the liftarm of the bucket assembly. This force was also chosen because it is an impact force which occurs at specific instants during the scooping and digging process. This force only has one component and the mean and standard deviation data was made available by Caterpillar.

To develop the collocation framework for the full wheel loader, a known distribution had to be assumed. The literature review revealed that, for continuous random variables, a Gaussian or normal distribution was assumed for continuous random variables. This was the distribution used by Caterpillar [9] in their analysis. Therefore, the normal distribution was used to obtain the collocation points.

When using the polynomial chaos approach, a random variable can be expressed as functions of some random event, with some type of distribution. The process associated with this random variable is the rack stop force which is denoted by the variable $R^i(t)$. The coefficient matrix is expressed as $A_{i,j}$, I and j are the indices of the matrix based on the number of terms in the basis polynomial functions. The number of terms in the polynomial expansion for the rack-stop force is 5, and 15 collocation points were chosen from an assumed Gaussian distribution. The coefficient values in the polynomial expression can be obtained using Eq. (5.1).

$$r^j(T) = \sum_{j=1}^{S} \mathbf{A}^{\#}{}_{i,j} R^i(T) \tag{5.1}$$

The polynomial chaos expansion of the stochastic rack-stop force thus becomes

$$R(t_k,\xi) = r^1(t_k)\phi^1(\xi) + r^2(t_k)\phi^2(\xi) + r^3(t_k)\phi^3(\xi) + r^4(t_k)\phi^4(\xi) + r^5(t_k)\phi^5(\xi) \qquad (5.2)$$

Here, R is denoted as the stochastic rack-stop force. The matrix A is the collocation matrix from Eq. (2.13) and $R^i(T)$ contains a vector of collocation rack-stop force values which are next used as the input to the ProMechanica kinetic model.

To obtain the necessary collocation points, fifteen rack-stop force collocation points were generated from an algorithm shown in Appendix B. This algorithm also produced a histogram by running an ensemble of 4000 points for ξ on Eq. (5.2). This histogram was obtained using the 15 rack-stop collocation points from the mean and standard deviation data for the rack-stop force provided by Caterpillar.

Fifteen rack-stop collocation input files were generated for the full 980G wheel loader model. Each file contained data for two discrete moments in time and the corresponding rack-stop uncertain force values obtained from the previously mentioned collocation procedure. The first file contained data for 26.78 sec and 26.8 sec. The second file contained data for 50.16 sec and 50.18 sec. The third file contained data for 70.26 sec and 70.28 sec. The last group of times was 92.06 sec and 92.08 sec. Each file was run for the respective times. The reaction forces at the B-pin were output and plotted, as shown later in the results section. These moments of time were selected because they correspond to moments when impact forces act on the liftarm.

5.3 Results of Collocation Method on 980G II Wheel Loader

Each probability density function comes from its respective slice in time and is independent of the time step before it. From the plots of the histograms and PDFs of the rack-stop force, it is evident that at some time steps, a Gaussian envelope is visible, while at other time steps the PDF is skewed resembling a Beta distribution.

In Figure 5-3 the rack uncertainty of the rack-stop force is evaluated at t=26.78 sec. Both the histogram and the probability density function show a Gaussian distribution. This indicates that

the mean is spread according to a uniform deviation. This observation is also reflected in the PDF.

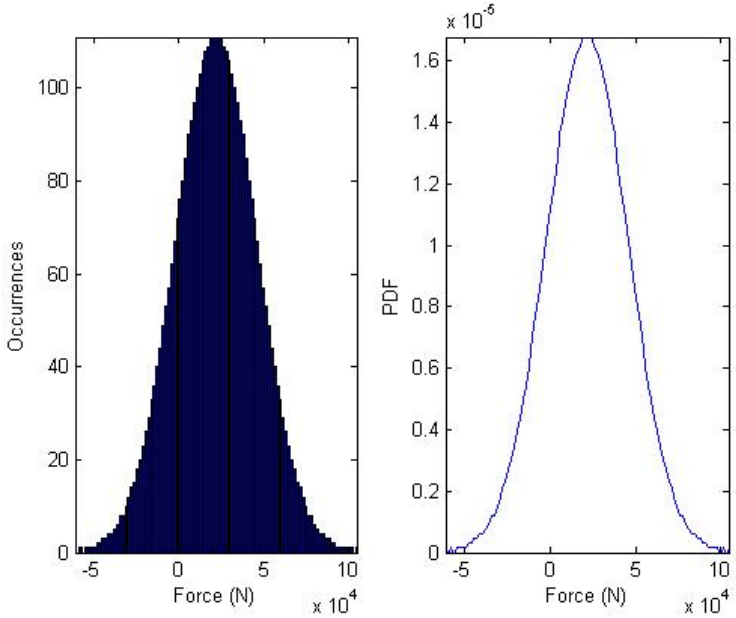

Figure 5-3. Histogram and PDF of uncertain rack-stop force at t=26.78 sec

In Figure 5-4, the same symmetry in the rack-stop force occurs at t=26.8 sec. This behavior was expected as the time values are only hundredths of a second apart. Again, the behavior is reflected in the PDF.

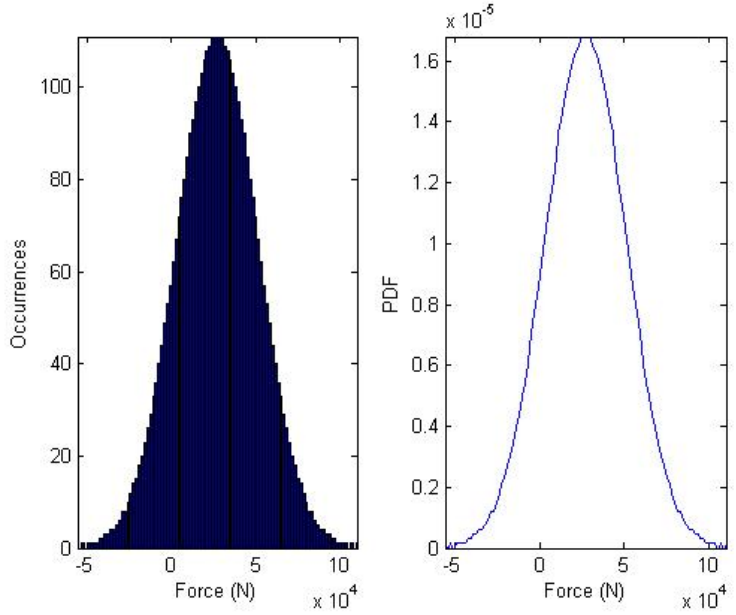

Figure 5-4. Histogram and PDF of uncertain rack-stop force at t=26.8 sec

In Figure 5-5, the uncertainty in the rack-stop force is evaluated at t=50.16 sec. In this figure, a Gaussian behavior is evident in the histogram of the rack-stop force. The same behavior is evident in the PDF representation.

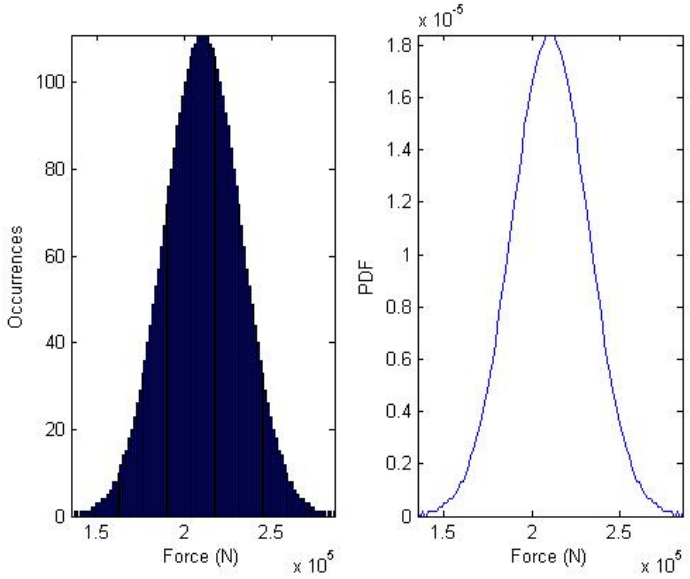

Figure 5-5. Histogram and PDF of uncertain rack-stop force at t=50.16 sec

In Figure 5-6, the same behavior is also evident at t=50.18 sec. Again, because of the small increment in time, this behavior would be expected to be similar to the previous time step.

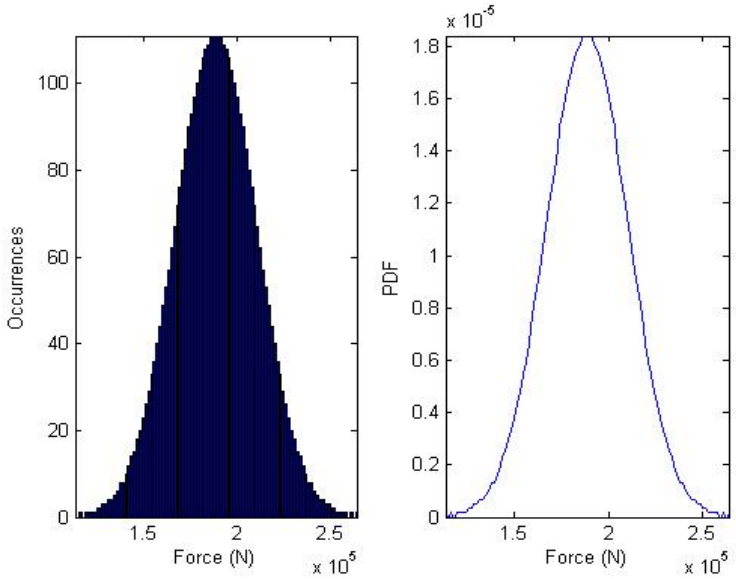

Figure 5-6. Histogram and PDF of uncertain rack-stop force at t=50.18 sec

Standard Deviation for Rack-stop Impacts

The moments of time for which the stochastic rack-stop force is shown correspond to the impact cycle of the rack-stop is force. The PDF plots generated by Caterpillar [9] for the rack-stop force are used for benchmarking purposes.

In Figure 5-7 mean values of the first and the second rack-stop impacts are plotted, with the corresponding standard deviations. The standard deviations are plotted for the first impact at t=26.78 sec and 26.8 sec. The standard deviations are also plotted for the second impact at t=50.16 sec and 50.18 sec. The mean and standard deviation of the rack-stop force for one standard deviation, provided by Caterpillar from their study [9] are plotted for the first and second impacts in Figure 5-8. The line running through the center of the outermost lines is the mean. The outermost lines running parallel to the mean are standard deviations at each time step. Figures 5-7 and 5-8 prove that the standard deviations generated by the Collocation Method and by the Caterpillar Method are similar.

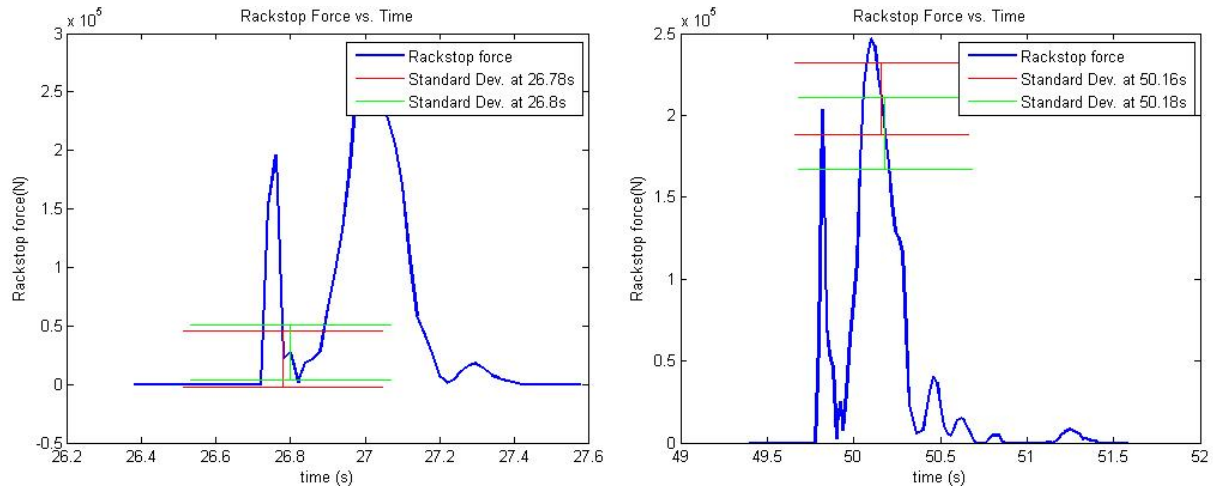

(a) t=26.78 sec and 26.8 sec, first impact (b) t=50.16 sec and 50.18 sec, second impact

Figure 5-7. Mean values and standard deviation of rack-stop force obtained with the Collocation Method

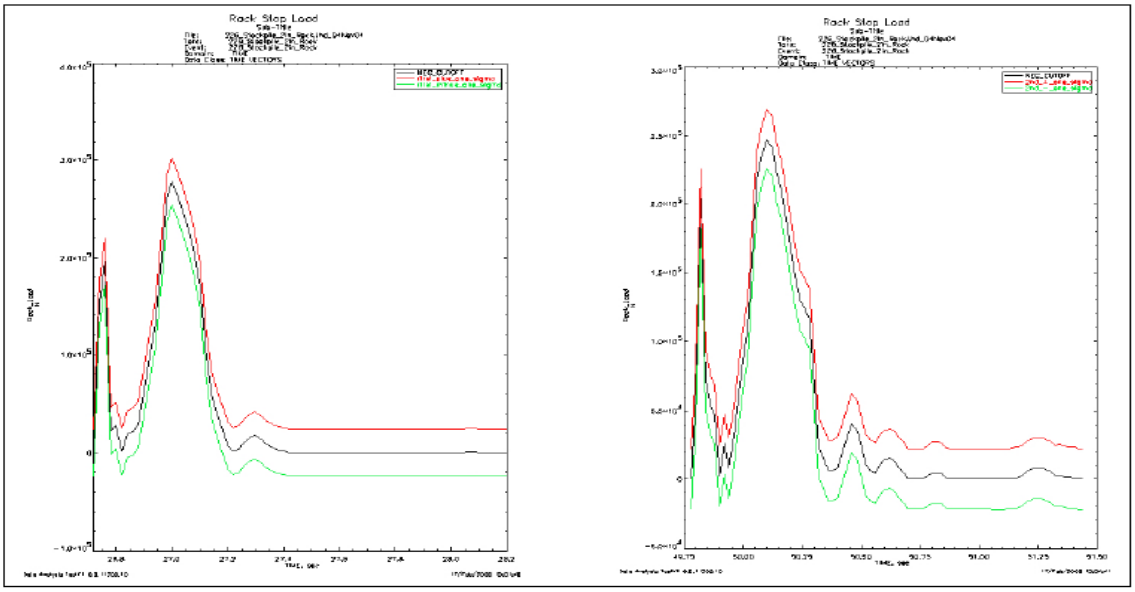

(a) First impact (b) Second impact

Figure 5-8. Mean values and standard deviation of rack-stop force from the Caterpillar study [9]

The rack-stop force is plotted for the third and fourth impacts. Standard deviation is designated as the upper and lower limits of the horizontal lines at t=70.26 sec and 70.28 sec for the third impact. The mean and the standard deviations for the fourth impact are plotted for t=92.06 sec and 92.08 sec. Like the first and second impact, the plot in Figure 5-9 shows all deviations of the rack-stop force at each time step, as provided in the Caterpillar study [9]. Again, the line running in the middle of the two outermost lines is the mean of the rack stop force. The outermost lines are the upper and lower standard deviations.

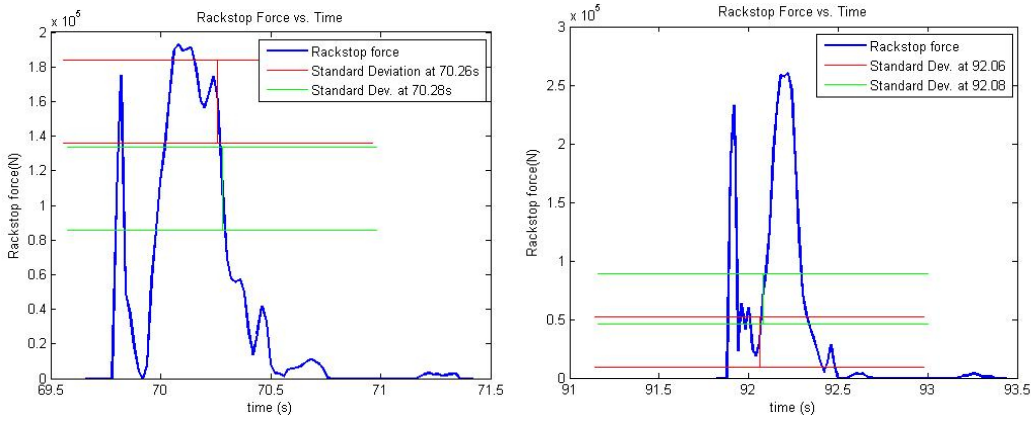

(a) t=70.26 sec and 70.28 sec, third impact (b) t=92.06 sec and 92.08 sec, fourth impact

Figure 5-9. Mean values and standard deviation of rack-stop force obtained with the Collocation Method

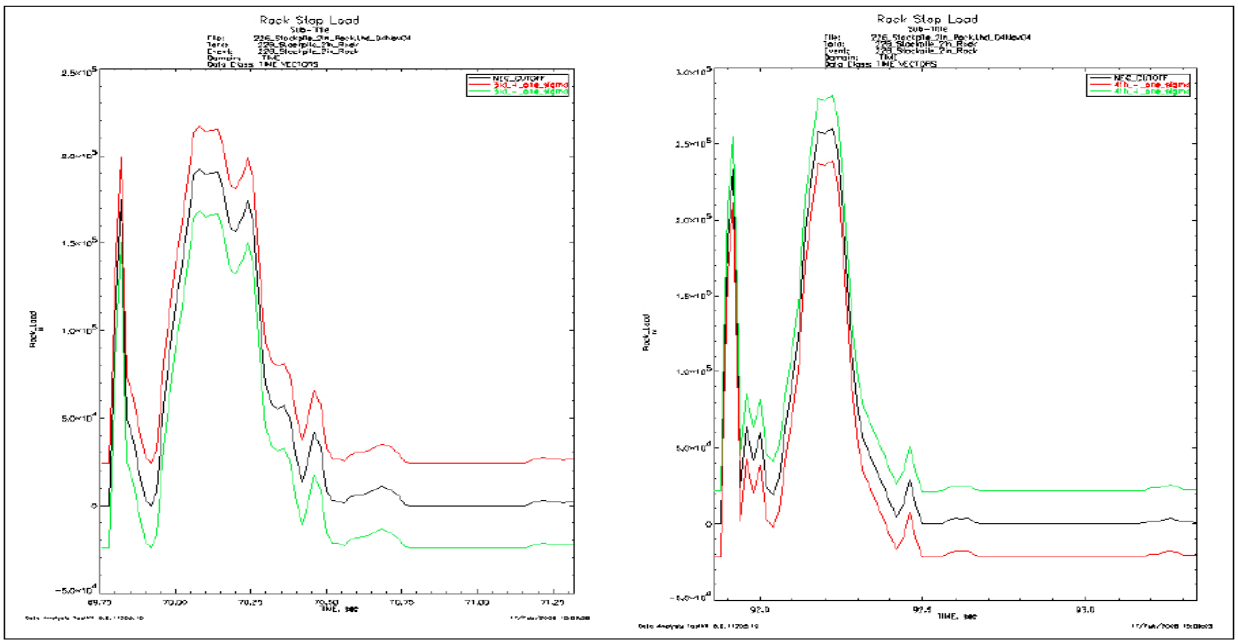

(a) Third Impact (b) Fourth Impact

Figure 5-10. Mean values and standard deviation of rack-stop force from the Caterpillar study [9]

Collocation Analysis Results at B Pin

The fifteen rack-stop collocation points used on the ProMechanica model produced variations in the reaction forces in the B-pin as expected. Fifteen different magnitudes in the forces were produced at the B-pin, and were post-processed by the same algorithm used to produce the histograms and PDF plots for the rack-stop force. Only the results of the B-Pin X force was examined because of the assumption that the forces in the x direction hold for a first-order approximation. However, because of the nature of the Collocation Method developed, any reaction force of interest could be represented in a similar manner.

The observed values of the variation in the B-pin relate to the coefficients necessary for the polynomial chaos expansion of the B-pin X force as shown in Eq.(5.3).

$$\begin{bmatrix} B_x^{\,1} \\ \vdots \\ B_x^{\,15} \end{bmatrix} = \mathbf{A} \begin{bmatrix} b_x^{\,1} \\ \vdots \\ b_x^{\,5} \end{bmatrix} \tag{5.3}$$

Here, B_x is denoted as the stochastic B-pin X force and A is the Collocation matrix from Eq.(2.13). The least-square algorithm is then employed as shown for the rack-stop force to obtain the coefficients in the polynomial chaos expansion shown in Eq. (5.4).

$$B_x(t_k,\xi) = b_x{}^1(t_k)\phi^1(\xi) + b_x{}^2(t_k)\phi^2(\xi) + b_x{}^3(t_k)\phi^3(\xi) + b_x{}^4(t_k)\phi^4(\xi) + b_x{}^5(t_k)\phi^5(\xi) \quad (5.4)$$

An ensemble of 4000 points for ξ from the assumed Gaussian distribution was the input to Eq. (5.4). An algorithm shown in Appendix B, produced the representative histogram and PDF at the same time step where the rack-stop forces were analyzed.

In Figure 5-11, the reaction force in the B-Pin X component is spread out normally about the mean. The complimentary PDF indicates the points in the histogram create a Gaussian envelope.

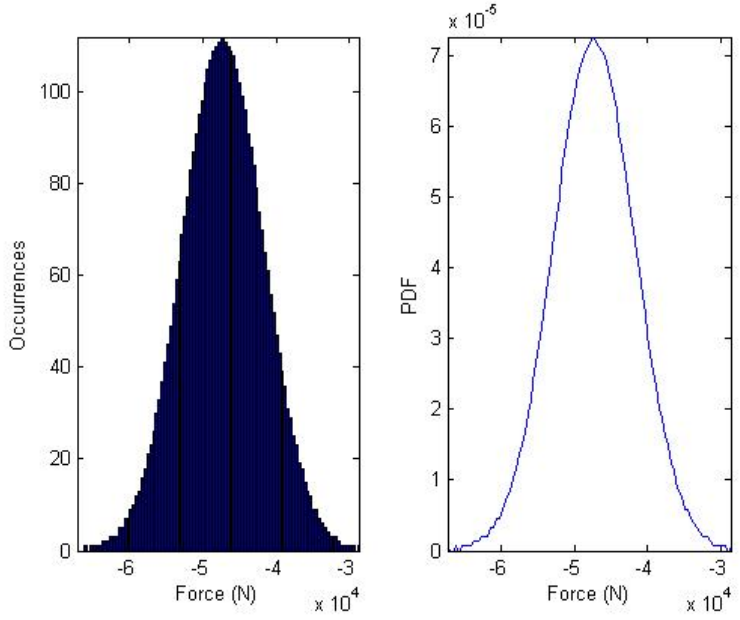

Figure 5-11. Histogram and PDF of uncertain B-Pin X force at t=26.78 sec

Similar to Figure 5-11, Figure 5-12 shows a Gaussian spread of the reaction forces in the B-Pin X force at t=26.8 sec.

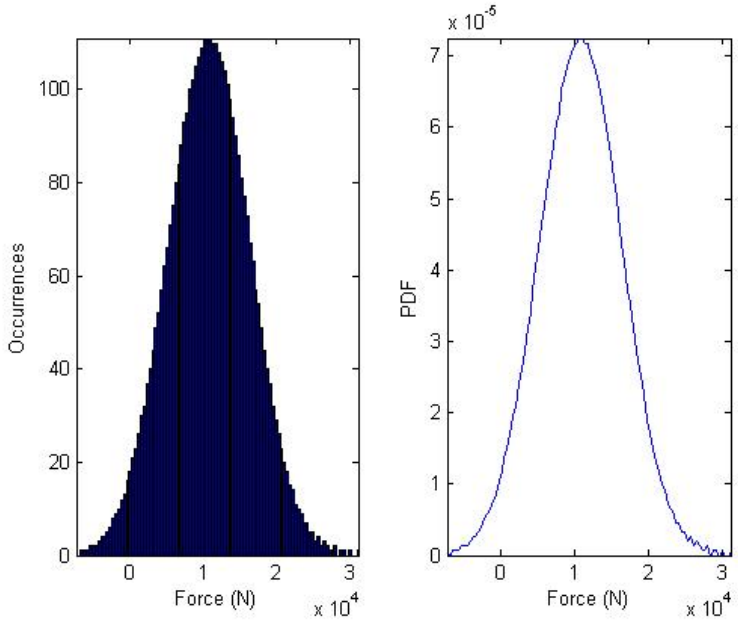

Figure 5-12. Histogram and PDF of uncertain B-Pin X force at t=26.8 sec

In Figure 5-13, the uncertainty in the B-Pin X reaction force is observed at t=50.16 sec. The data shows a bit tighter distribution. The resulting PDF also displays a Gaussian distribution.

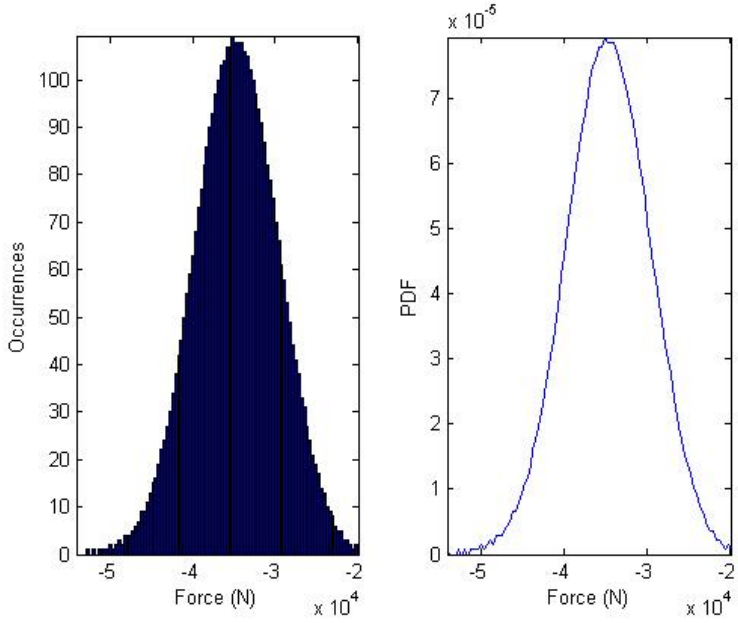

Figure 5-13. Histogram and PDF of uncertain B-Pin X force at t=50.16 sec

In Figure 5-14, the reaction force in the x direction at the B-pin at t=50.18 sec is presented and it also has a Gaussian distribution.

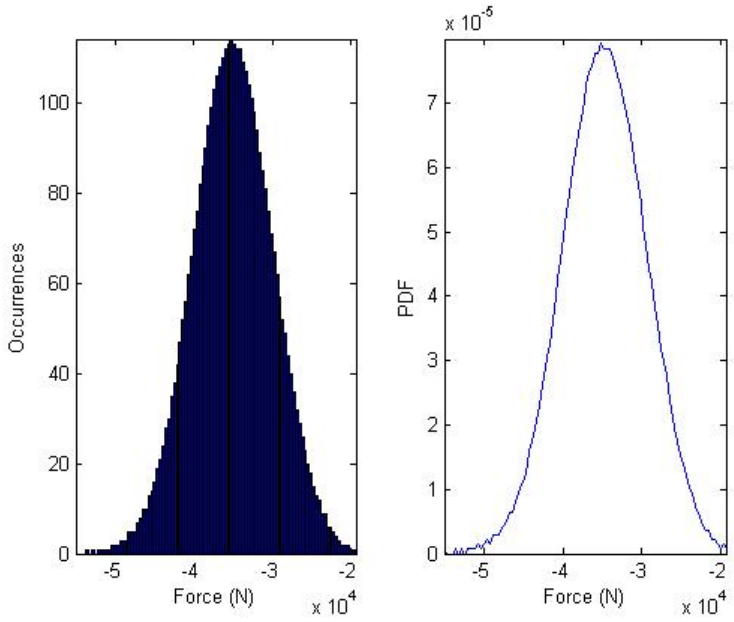

Figure 5-14. Histogram and PDF of uncertain B-Pin X force at t=50.18 sec

As a final consistency check, the standard deviations of the PDFs of the B-pin X force were plotted against the mean values obtained from the kinetic analysis performed in ProMechanica on the full 980G II wheel loader model. Although only a few moments of time for the full wheel loader model were analyzed in the Collocation procedure, it is important to see how the standard deviation from the random rack-stop force compares with the standard deviation obtained by Caterpillar with the Newtonian projection method followed by the quadratic transformation method [9]. The results obtained with the Collocation approach are presented in Figures 5-15 through 5-18.

In Figure 5-15 we focus on the upper and lower limits of the standard deviation of the B-Pin X force at times t=26.78 sec and 26.8 sec.

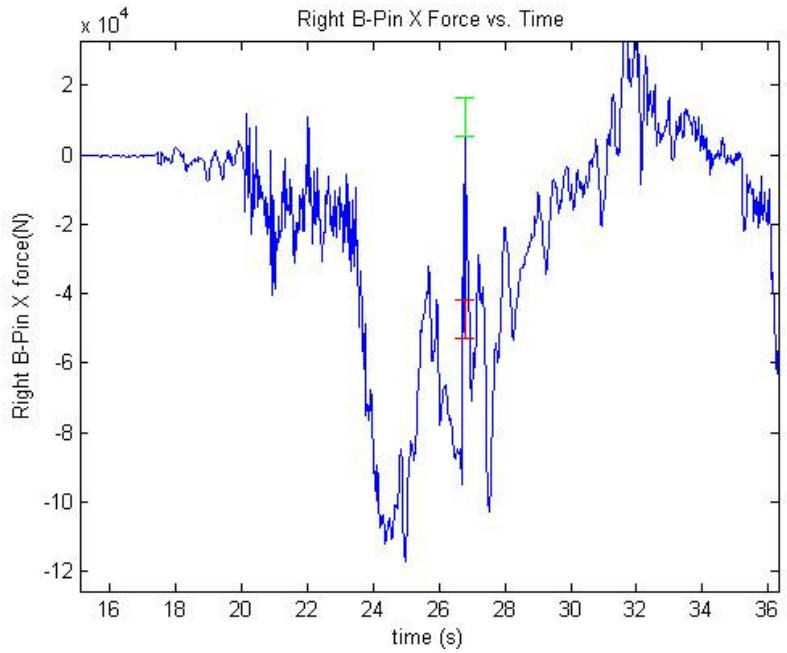

Figure 5-15. Mean values and standard deviation of B-Pin X force at t=26.78 sec and 26.8 sec

In Figure 5-16 we focus on the upper and lower limits of the standard deviation of the B-Pin X force at times t=50.16 sec and 50.18 sec.

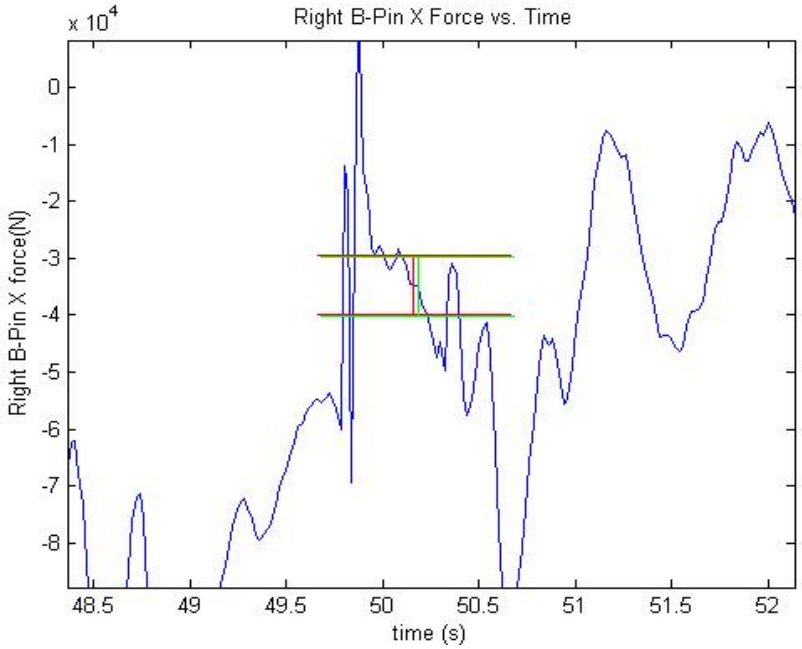

Figure 5-16. Mean values and standard deviation of B-Pin X force at t=50.16 sec and 50.18 sec

In Figure 5-17 we focus on the upper and lower limits of the standard deviation of the B-Pin X force at times t=70.26 sec and 70.28 sec.

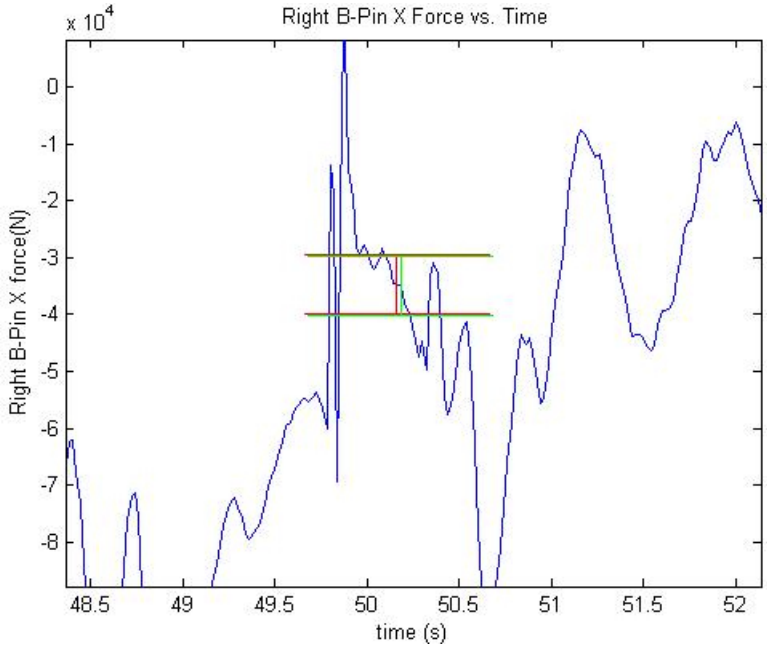

Figure 5-17 Mean values of B-Pin X force and standard deviation at t=70.26 sec and 70.28 sec

In Figure 5-18 we focus on the upper and lower limits of the standard deviation of the B-Pin X force at times t=90.26 sec and 90.28 sec.

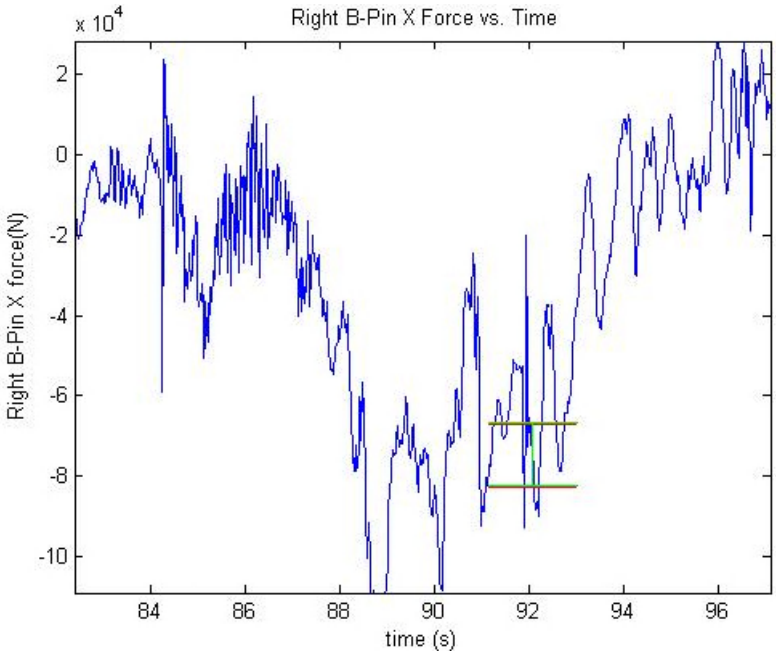

Figure 5-18. Mean values and standard deviation of B-Pin X force at t=92.06 sec and 92.08 sec

In Figure 5-19, the deterministic output of the B-Pin X force is plotted for all 100 seconds of simulation time with standard deviations at the specific times that were presented in the previous four Figures. Comparing Figure 5-19 with Figure 5-20 it is evident that the stochastic behavior of the B-Pin X force due to a random rack-stop input force predicted with the Collocation Method is consistent with the method used by Caterpillar [9]. Thus, we achieved the final objective of this study, showing that the Collocation technique can be used to estimate uncertainties in "black-box" models of complex mechanical systems such as the 980G II wheel loader.

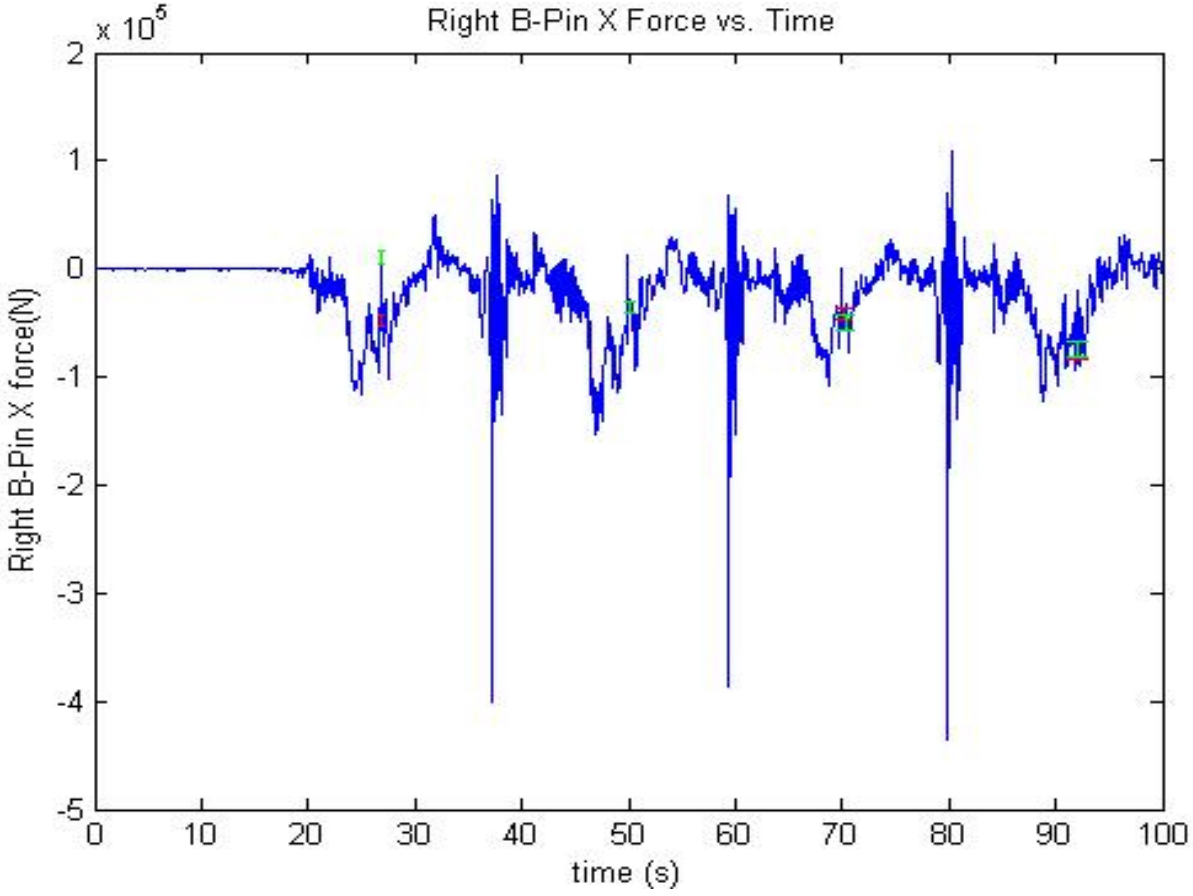

Figure 5-19. Mean values of B-Pin X force with standard deviation at t=26.78, 26.8, 50.16, 50.18, 70.26, 70.28, 92.06 and 92.08 seconds obtained from the Collocation Method

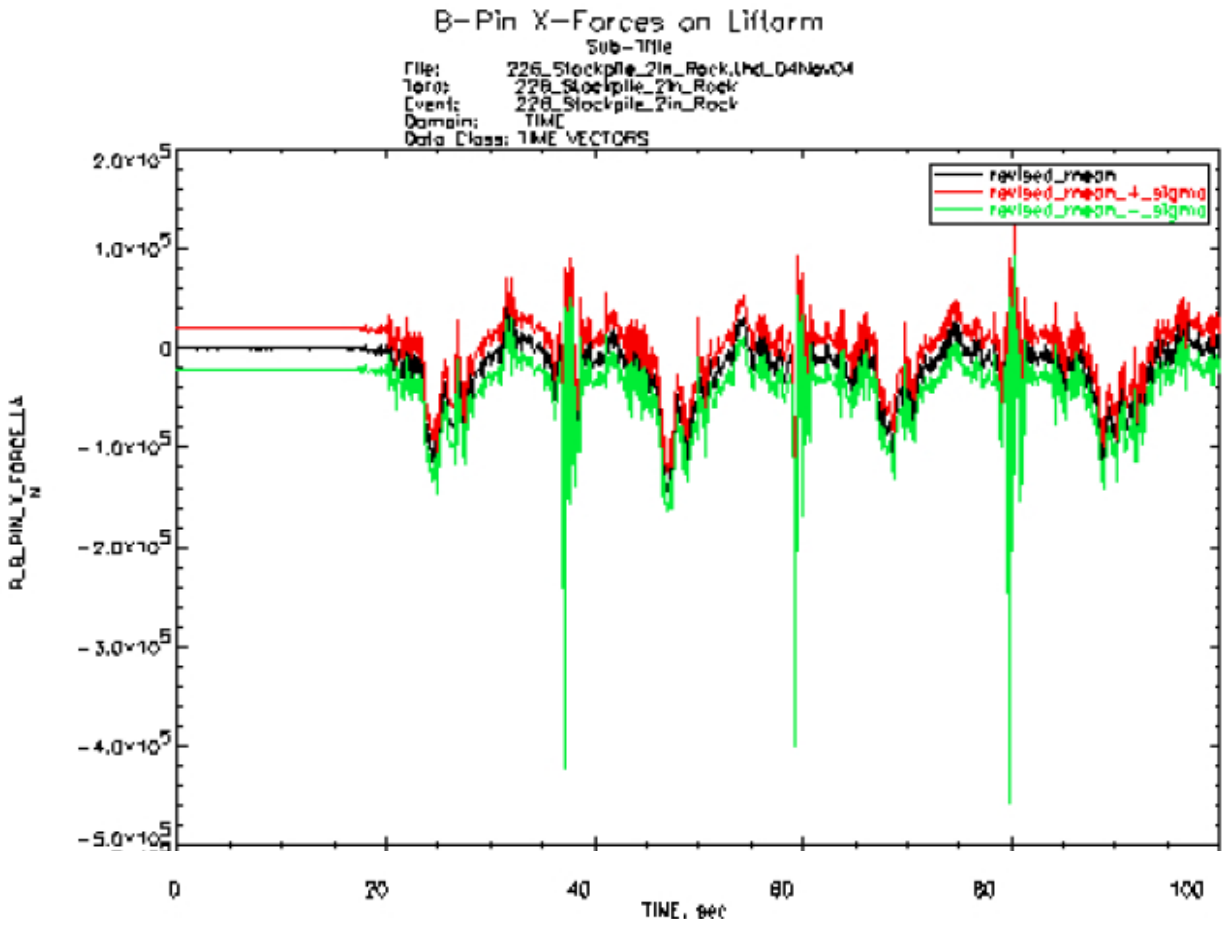

Figure 5-20. Mean values of B-Pin X force with standard deviation from Caterpillar [9]

CHAPTER 6 CONCLUSIONS AND FUTURE WORK

This study was motivated by the need to estimate the impact of uncertainties in input forces of construction machinery on the reaction forces in various joints. The main contributions of this thesis are outlined below.

The project started from our communications with researchers at Caterpillar. They noticed that, when collecting field data for different loads on the wheel loaders, different values are recorded for the system in the same configuration and under the same kinematic conditions. Thus, it has been noticed that there is uncertainty in the input forces, such as those produced by the hydraulic actuators that lift the liftarms. While many points on a vehicle can be instrumented, it is not practical, or possible to measure the forces at all desired locations, such as the reaction forces in the joints. This prompted Caterpillar to investigate methods to predict those uncertainties through simulation. The studies that Caterpillar shared with illustrated the fact that, if one tries to use the measured forces directly in the equations of motion of a system, they may realize that, due to the uncertainties in the measurement, those equations will not be identically satisfied. To alleviate this, they employed a Newtonian projection method to extract from the measurements the values of the forces that will satisfy the equations of moments. To propagate the uncertainties in the input forces and obtain the uncertainties in the output forces of interest, Caterpillar used a linear transformation method for the mean values, and a quadratic transformation method for the standard deviation.

In this study we investigated the application of the polynomial chaos–based Collocation approach to propagate the uncertainties through a construction vehicle, and to use the measured data to predict the uncertainties in the reaction forces without modifying the mathematical model of the system. The approach was to first validate our proposed technique on a simple case study. The simple case study consisted of a double pendulum linkage system driven by an actuator modeled as a two-body rod and cylinder sub-system. The motion of the second link was not considered of interest for this study, and thus was kept at a constant angular orientation with respect to the driven link. This system was modeled using differential algebraic equations, implemented in Matlab and it was also modeled in ProMechanica. The two deterministic models

were compared and only slight differences were noticed in their outputs, mainly due to a different way of defining the inertia properties of the bodies in ProMechanica. Further, the results of the Matlab model were compared with the results obtained from a reduced model that was intended to mimic the approach followed by Caterpillar (using the projection method). It has been shown that the reduced model cannot accurately capture the behavior of the system, when compared to the Matlab and ProMechanica full models.

The stochastic analysis considered that the amplitude in the actuator force in the Matlab model, and respectively of the driver in the ProMechanica model is uncertain. Two different types of distributions for the stochastic input force (normal and Beta) were analyzed. The output of interest was the reaction force in the joint between the two links in the simple case study (B-pin, between the liftarm and the bucket). The technique used by Caterpillar, a Monte Carlo approach, and a mixed approach were implemented on the reduced model. Next, the Collocation approach was developed and implemented on the full Matlab model, and on the ProMechanica model, and they showed very consistent results, with differences mainly due to implementation of the deterministic models.

Finally, once the Collocation approach was validated on the simple case study, we implemented it on the full ProMechanica model of a Caterpillar 980 G II wheel loader. The procedure involved obtaining the standard distribution of the input values from the experimental data, using it to calculate a number of Collocation points (in this case, fifteen), use the Collocation points in the input file of the ProMechanica, run the ProMechanica kinetic model, and predict corresponding output forces for the reactions in the joints of interest, for each of the Collocation points considered. The uncertainties in the input forces were obtained from data provided by Caterpillar, and the stochastic joint reaction forces were output (in terms of mean values and standard deviations) for several moments in time (i.e., at different kinematic configuration of the system). A final comparison was performed between the results obtained with the Collocation Method and the results presented in the Caterpillar report [9] and a very good correlation has been found. Moreover, the Collocation approach is non-intrusive, no model equations have been modified in the process, it is computationally efficient, and it can be applied on the full model, with no simplifying assumptions.

Future work may be performed to further investigate more efficient means of creating and using the Collocation points in the input files. Also, it is of interest to study means of being able to use the same model for both kinematic and dynamic analysis of the vehicle, rather than two different models, which is the current practice employed by Caterpillar. This will not only lead to a more realistic simulation of the system, but it will also allow the estimation of uncertainties in kinematic parameters.

APPENDIX A. CATERPILLAR 980 G II WHEEL LOADER TOPOLOGY

Nomenclature (Top View)

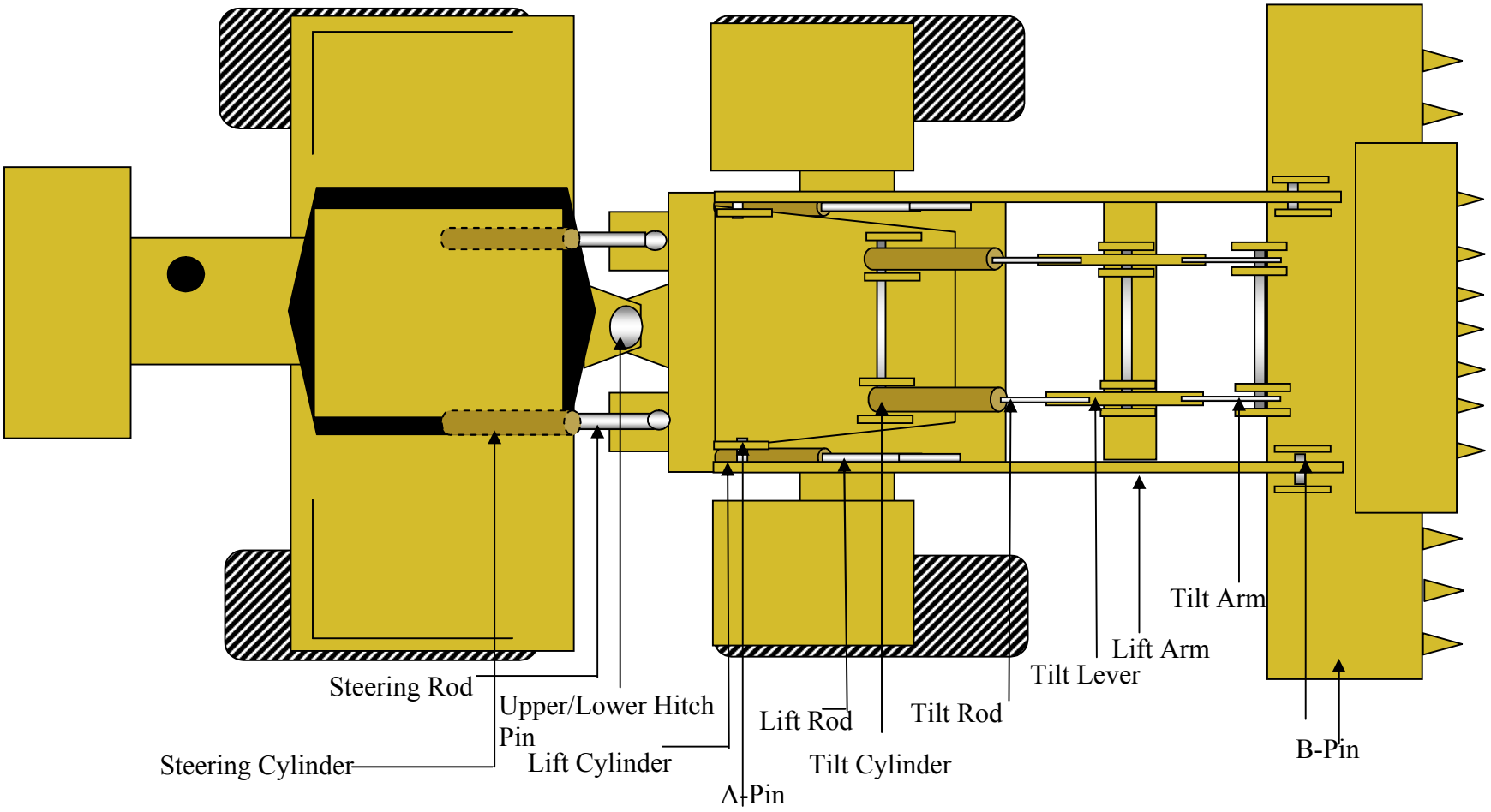

Figure A-1. Top View Layout of 980G II Wheel Loader

Kinematic Joint Definitions (Top View)

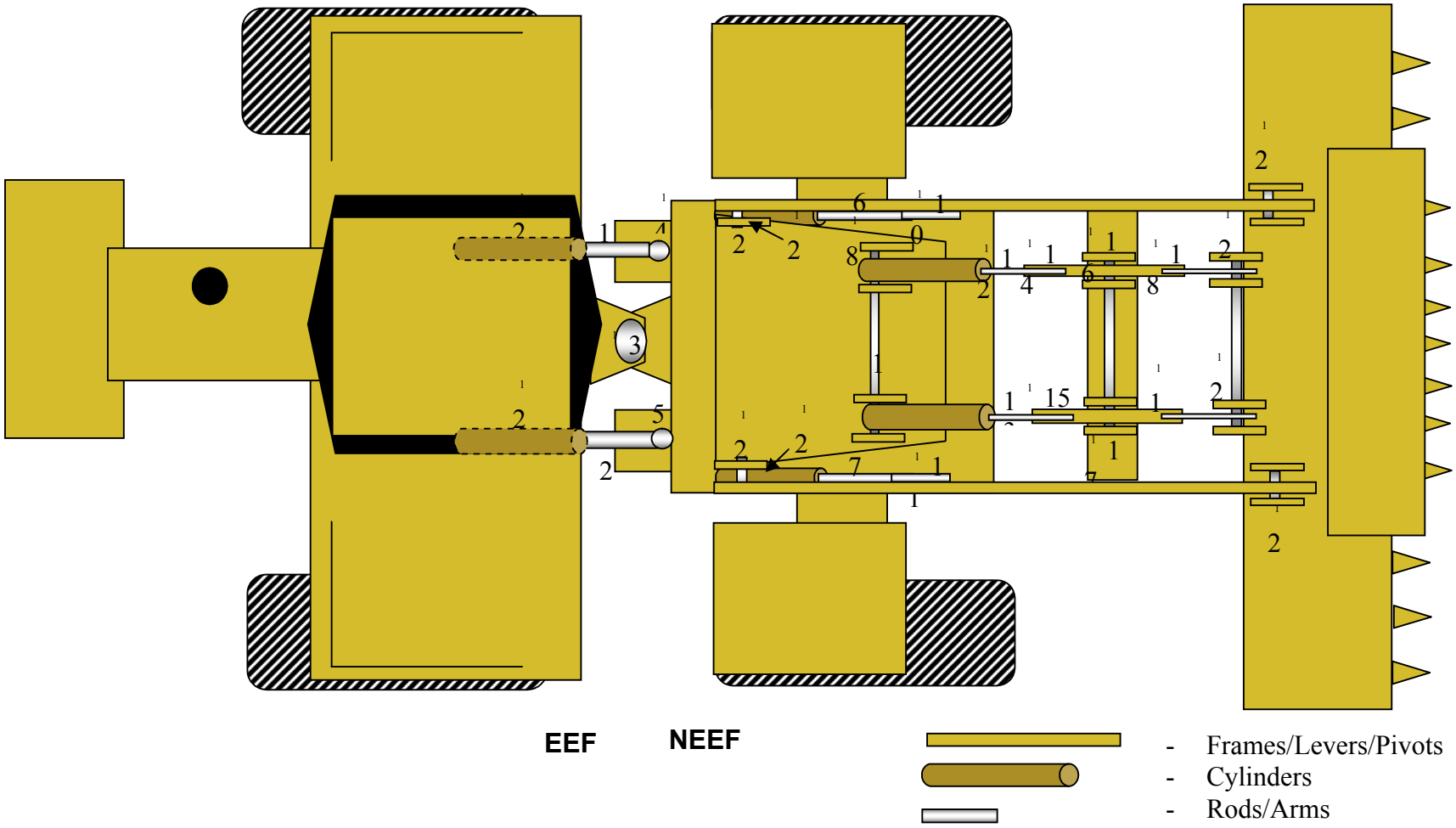

Figure A-2. Top View Layout of 980G II Wheel Loader

Table A-1. Kinematic Nomenclature for the 980G II Wheel Loader

Position	Description	Constraints
1	Left Steering Cylinder to rod slider	Slider Constraints/ Translational Joint
2	Right steering Cylinder to rod slider	Slider Constraints/ Translational Joint
3	Lower Hitch Pin/ Upper Hitch Pin	Revolute Constraint
4	Left steering rod to NEEF	Revolute Constraint
5	Right steering rod to NEEF	Revolute Constraint
6	Left lift cylinder to lift rod	Slider Constraints
7	Right lift cylinder to lift rod	Slider Constraints
8	NEEF to left tilt cylinder	Revolute Constraints
9	NEEF to right tilt cylinder	Revolute Constraints
10	Left lift rod to liftarm	Revolute Constraints
11	Right lift rod to liftarm	Revolute Constraints
12	Left tilt cylinder to left tilt rod	Slider Constraints/ Translational Joint
13	Right tilt cylinder to right tilt rod	Slider Constraints/ Translational Joint
14	Left lift rod to tilt lever	Revolute Constraints
15	Right lift rod to tilt lever	Revolute Constraints
16	Liftarm to left tilt lever	Revolute/ Cylindrical Constraints
17	Liftarm to right tilt lever	Revolute/ Cylindrical Constraints
18	Left tilt lever to left tilt arm	Revolute Constraints
19	Right tilt lever to right tilt arm	Revolute Constraints
20	Left tilt arm to bucket	Revolute Constraints
21	Right tilt arm to bucket	Revolute Constraints
22	Left B pin. Bucket to liftarm	Revolute Constraints
23	Right B pin. Bucket to liftarm	Revolute Constraints
24	Left A pin Liftarm to NEEF	Revolute Constraints
25	Right A pin Liftarm to NEEF	Revolute Constraints
26	Left steering cylinder to EEF	Revolute Constraints
27	Right steering cylinder to EEF	Revolute Constraints
28	Left lift cylinder to NEEF	Revolute Constraints
29	Right lift cylinder to NEEF	Revolute Constraints
30	6 DOF ground to Bucket	Spherical Constraints

31	Left tilt arm to right tilt arm weld	Moves as one body (may be redundant)
32	Left tilt am to left tilt lever weld	Moves as one body (may be redundant)
33	Dummy Roll to EEF slider	Slider Constraints+ integrated accelerometer data for bounce
34	Dummy Pitch to Dummy Roll pin joint	Pin constraints+ roll angle from inclinometer
35	Dummy Yaw to Dummy Pitch pin joint	Pin constraints+ pitch angle from inclinometer
36	Dummy Trans to Dummy Yaw pin joint	Pin constraints+ yaw angle from Equation 1
37	Ground to Dummy Trans	Horizontal translation from equation 2. Zero vertical translation. Zero rotations
38	Ground to NEEF free joint	3 Translational Constraints to center of left wheel (3d translation)
39	Ground to NEEF free joint	2 Translational Constraints to center of right wheel (3d translation)

APPENDIX B. MATLAB CODE

Matlab Routine for Generating Collocation Points for Rack-stop Force

```
clear all
close all

global number_terms_polychaos nColloc
global Acolloc    % output
global Distribution   % 1 = Uniform;  2 = Beta22;  5 = Beta55;  10 = Gaussian

%%%%%%%%%%%%%%%%%%%%%%%%%%%%%%%%%%%%%%%%%%%%%%%%%%%%%%%%%%%%%%%%%%%%%%%
% Input whatever you want for these 2 values
% (AverageValue(indtime)  and StandardDeviation(indtime) )
% Replace that by whatever values you have

tfinal = 0.07;
t = 0:0.01:tfinal;

rack-stop = load('rack-stop.mat')
mean=rack-stop.Rack-stop;
stdev=rack-stop.Rack-stopdev;

for indtime = 1:length(t)
    AverageValue(indtime) = mean(indtime,2);
    StandardDeviation(indtime) = stdev(indtime,2);
end

%%%%%%%%%%%%%%%%%%%%%%%%%%%%%%%%%%%%%%%%%%%%%%%%%%%%%%%%%%%%%%%%%%%%%%%
```

```
% 10: Gaussian
Distribution = 10;

number_terms_polychaos = 5;
nColloc = 15;

% Matrix for collocation, will be called Acolloc, and comes from the code in
this line below (generateAcolloc .m)
generateAcolloc
```

```
   Figure(1)
   plot(zeros(size(Mu)), Mu, '.')
   axis([-3 3 -3 3])
   ylabel('Psi (Psi = 1 is the stdev)')
   title('Collocation Points - Gaussian Distribution')
```

```
Values = zeros(nColloc,length(t));
Values_polychaos = zeros(number_terms_polychaos,length(t));


for indtime = 1:length(t)

for iColloc = 1:nColloc     % iColloc = 1:nColloc

     psi1 = Mu(iColloc,1);


if (Distribution == 10)     % 1 = Uniform  or  2 = Beta11;  10 = Gaussian
     Values(iColloc,indtime) =  AverageValue(indtime) + psi1  *
StandardDeviation(indtime);
end


 end    %   for iColloc = 1:nColloc     % iColloc = 1:nColloc

 Values_polychaos(1:number_terms_polychaos, indtime) =
Acolloc\Values(1:nColloc, indtime);

end % for indtime = 1:length(t)

%%%%%%%%%%%%%%%%%%%%%%%%%%%%%%%%%%%%%%%%%%%%%%%%%%%%%%%%%%%%%%%%%%%%%%%%%%%%%%%
%  YOU WANT TO PLAY WITH THESE PARAMETERS TO MAKE THE PLOTS LOOK BETTER
pointsforhist = 4000;   % number of points used to draw a histogram, which
represents a PDF when very high
NumberBins = 100;




if (Distribution == 10)    % 10 = Gaussian

% From generateAcolloc
% % Inverse Cumulative Distribution Function of Gaussian distribution
% Hammersley_GaussianDist = sqrt(2)*erfinv(2*Ham-1);

WholePsi1Gaussian = zeros(pointsforhist, 1) ;    %  I'm just checking that
looks like a Gaussian dist


 for indhist1 = 1:pointsforhist

% You do not wantg to use  psi1 = ((indhist1-1)/(pointsforhist-1)) for a
Gaussian distribution
% becuase psi1 = -1 and psi1 = 1 do not have an inverse CDF
     psi1 = (indhist1/(pointsforhist+1));
```

```
     % We take the inverse CDF of the Gaussian distribution
        psi1 = sqrt(2)*erfinv(2*psi1-1);

     % To get rid of the 0.000*i each time so that it cannot be seen as a
complex number
        psi1 = real(psi1);

      WholePsi1Gaussian(indhist1,1) = psi1 ;        %  I'm just checking that
looks like a Gaussian dist

%  To check it looks like Beta:
plot(ones(1,pointsforhist),real(WholePsi1Gaussian),'.')


         for itime = 1:length(t)

        Values_hist(itime,indhist1) = ...
                        Values_polychaos(1,itime)*phiPC(1,psi1)+...
                        Values_polychaos(2,itime)*phiPC(2,psi1)+...
                        Values_polychaos(3,itime)*phiPC(3,psi1)+...
                        Values_polychaos(4,itime)*phiPC(4,psi1)+...
                        Values_polychaos(5,itime)*phiPC(5,psi1);

         end

     % to see how far I am in this code
     if( mod(indhist1,100)==0), disp(indhist1); end

 end

end     % if (Distribution == 10)



N_Values = zeros(length(t)-1,NumberBins);
X_Values = zeros(length(t)-1,NumberBins);

 for itime = 1:length(t)

  [N_Values(itime,1:NumberBins),X_Values(itime,1:NumberBins)] = ...
                    hist(Values_hist(itime,1:pointsforhist), NumberBins);

 end

 N_Values_normalized = zeros(size(rack-stop.Rack-stop,1), NumberBins);

for ind = 1:size(rack-stop.Rack-stop,1)
    N_Values_normalized(ind,:) = N_Values(ind,:)/((max(X_Values(ind,:))-
min(X_Values(ind,:)))*pointsforhist/NumberBins) ;
end
% Size of the rectangles you want to plot in your PDF
% Fr2xRange = -2.5:0.01:2.5;
```

```
% Fr2yRange = 8:0.01:11.5;

Nrange = 500;
ValuesRange = min(min(X_Values)):(max(max(X_Values))-
min(min(X_Values)))/Nrange: max(max(X_Values));


 for i=1:length(t)-1

     AValues(:,i) =
interp1(X_Values(i,:)',N_Values(i,:)',ValuesRange','nearest');

 end


% Figure(10)
% mesh(t(2:length(t)),ValuesRange,AValues); view(2)
% % YOU WANT TO PLAY WITH THE HIGHER NUMBER TO MAKE THE PLOTS LOOK BETTER
%  set(gca,'CLim',[min(min(AValues)), max(max(AValues))]); colorbar; hold on
%  % set(gca,'CLim',[1, 60]); colorbar; hold on
%
% title('PDF for our values')
%
% % I changed the line below, because the Range can be incoherent when for 1
time point,
% % all the values are exactly the same
% %  axis([0 t(length(t)) min(Fr2xRange)-0.1 max(Fr2xRange)+0.1])
%
% % the -0.1 and + 0.1 is just to leave some white space above and below the
plots
%  axis([0 t(length(t)) min(min(ValuesRange))-1 max(max(ValuesRange))+1])
%
% xlabel('Time [s]')
% ylabel('Values')
%
%%%%%%%%%%REAL PLOTS

Figure(12)
subplot(1,2,1)
hist(Values_hist(1,:),100)
axis([min(X_Values(1,:)) max(X_Values(1,:)) 0 max(N_Values(1,:))])
title('Histogram of Rack-stop Force at 26.78(s)')
xlabel('Force (N)')
ylabel('Occurrences')


subplot(1,2,2)
plot(X_Values(1,:),N_Values_normalized(1,:))
axis([min(X_Values(1,:)) max(X_Values(1,:)) 0 max(N_Values_normalized(1,:))])
title('PDF of Rack-stop Force at 26.78(s)')
xlabel('Force (N)')
ylabel('PDF')

Figure(13)
subplot(1,2,1)
```

```
hist(Values_hist(2,:),100)
axis([min(X_Values(2,:)) max(X_Values(2,:)) 0 max(N_Values(2,:))])
title('Histogram of Rack-stop force at 26.8(s)')
xlabel('Force (N)')
ylabel('Occurrences')

subplot(1,2,2)
plot(X_Values(2,:),N_Values_normalized(2,:))
axis([min(X_Values(2,:)) max(X_Values(2,:)) 0 max(N_Values_normalized(2,:))])
title('PDF of Rack-stop Force at 26.8(s)')
xlabel('Force (N)')
ylabel('PDF')


Figure(14)
subplot(1,2,1)
hist(Values_hist(3,:),100)
axis([min(X_Values(3,:)) max(X_Values(3,:)) 0 max(N_Values(3,:))])
title('Histogram of Rack-stop force at 50.16(s)')
xlabel('Force (N)')
ylabel('Occurrences')

subplot(1,2,2)
plot(X_Values(3,:),N_Values_normalized(3,:))
axis([min(X_Values(3,:)) max(X_Values(3,:)) 0 max(N_Values_normalized(3,:))])
title('PDF of Rack-stop Force at 50.16(s)')
xlabel('Force (N)')
ylabel('PDF')


Figure(15)
subplot(1,2,1)
hist(Values_hist(4,:),100)
axis([min(X_Values(4,:)) max(X_Values(4,:)) 0 max(N_Values(4,:))])
title('Histogram of Rack-stop Force at 50.18(s)')
xlabel('Force (N)')
ylabel('Occurrences')


subplot(1,2,2)
plot(X_Values(4,:),N_Values_normalized(3,:))
axis([min(X_Values(4,:)) max(X_Values(4,:)) 0 max(N_Values_normalized(4,:))])
title('PDF of Rack-stop Force at 50.18(s)')
xlabel('Force (N)')
ylabel('PDF')

Figure(16)
subplot(1,2,1)
hist(Values_hist(5,:),100)
axis([min(X_Values(5,:)) max(X_Values(5,:)) 0 max(N_Values(5,:))])
title('Histogram of Rack-stop Force at 70.26(s)')
xlabel('Force (N)')
ylabel('Occurrences')
```

```
subplot(1,2,2)
plot(X_Values(5,:),N_Values_normalized(5,:))
axis([min(X_Values(5,:)) max(X_Values(5,:)) 0 max(N_Values_normalized(5,:))])
title('PDF of Rack-stop Force at 70.26(s)')
xlabel('Force (N)')
ylabel('PDF')

Figure(17)
subplot(1,2,1)
hist(Values_hist(6,:),100)
axis([min(X_Values(6,:)) max(X_Values(6,:)) 0 max(N_Values(6,:))])
title('Histogram of Rack-stopForce at 70.28(s)')
xlabel('Force (N)')
ylabel('Occurrences')


subplot(1,2,2)
plot(X_Values(6,:),N_Values_normalized(6,:))
axis([min(X_Values(6,:)) max(X_Values(6,:)) 0 max(N_Values_normalized(6,:))])
title('PDF of Rack-stop Force at 70.28(s)')
xlabel('Force (N)')
ylabel('PDF')

Figure(18)
subplot(1,2,1)
hist(Values_hist(7,:),100)
axis([min(X_Values(7,:)) max(X_Values(7,:)) 0 max(N_Values(7,:))])
title('Histogram of Rack-stop Force at 92.06(s)')
xlabel('Force (N)')
ylabel('Occurrences')


subplot(1,2,2)
plot(X_Values(7,:),N_Values_normalized(7,:))
axis([min(X_Values(7,:)) max(X_Values(7,:)) 0 max(N_Values_normalized(7,:))])
title('PDF of Rack-stop Force at 92.06(s)')
xlabel('Force (N)')
ylabel('PDF')

Figure(19)
subplot(1,2,1)
hist(Values_hist(8,:),100)
axis([min(X_Values(8,:)) max(X_Values(8,:)) 0 max(N_Values(8,:))])
title('Histogram of Rack-stop Force at 92.08(s)')
xlabel('Force (N)')
ylabel('Occurrences')


subplot(1,2,2)
plot(X_Values(8,:),N_Values_normalized(8,:))
axis([min(X_Values(8,:)) max(X_Values(8,:)) 0 max(N_Values_normalized(8,:))])
title('PDF of Rack-stop Force at 92.08(s)')
xlabel('Force (N)')
ylabel('PDF')
```

APPENDIX C. ADDITIONAL SIMULATION RESULTS

Additional plots obtained with the stochastic collocation analysis performed on the rack-stop force and for the B-Pin X force are included in this appendix for the 980G II wheel loader.

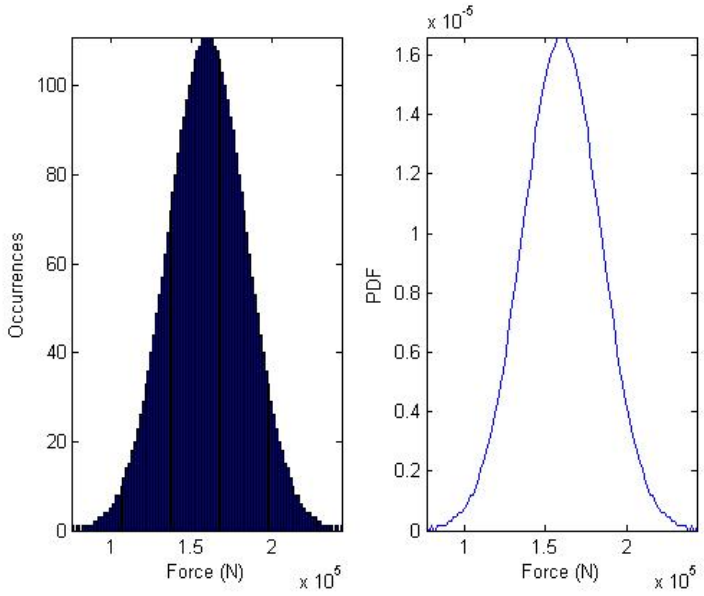

Figure C-1. Histogram and PDF of uncertain rack-stop force at t=70.26 sec

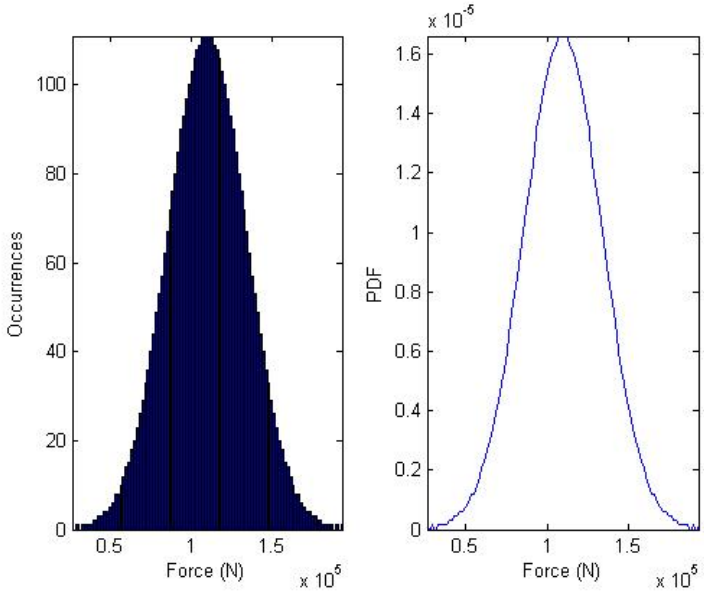

Figure C-2. Histogram and PDF of uncertain rack-stop force at t=70.28 sec

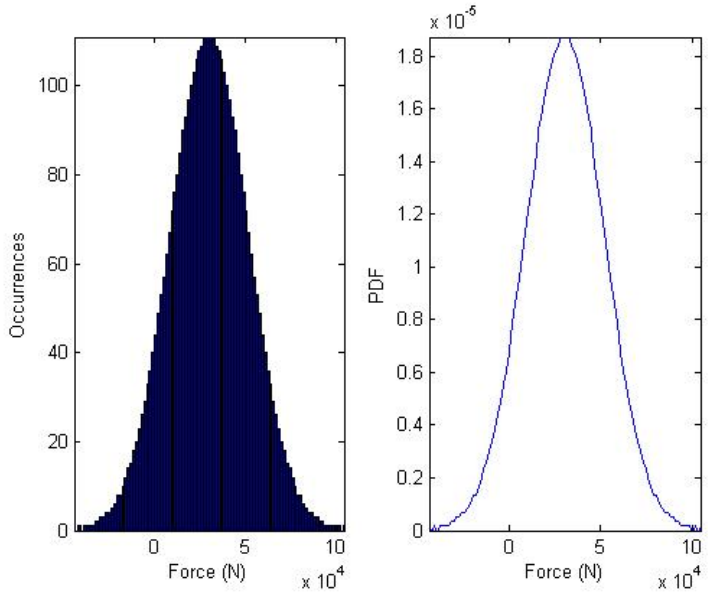

Figure C-3. Histogram and PDF of uncertain rack-stop force at t=92.06 sec

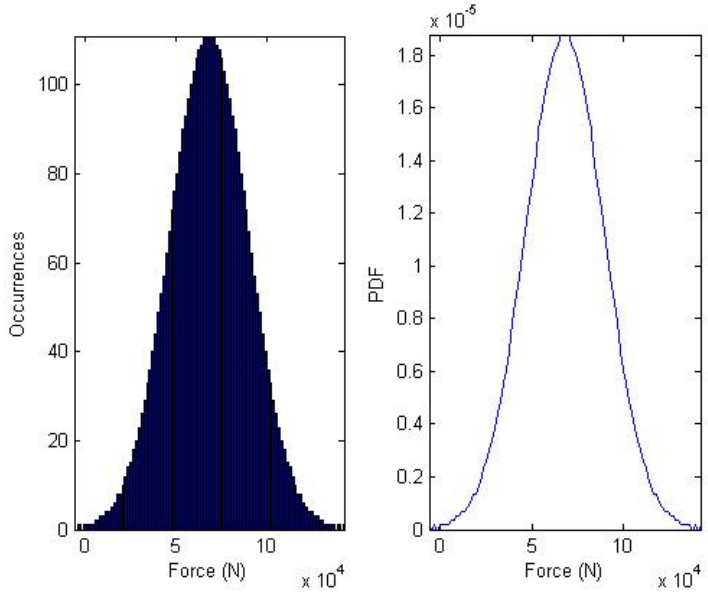

Figure C-4. Histogram and PDF of uncertain rack-stop force at t=92.08 sec

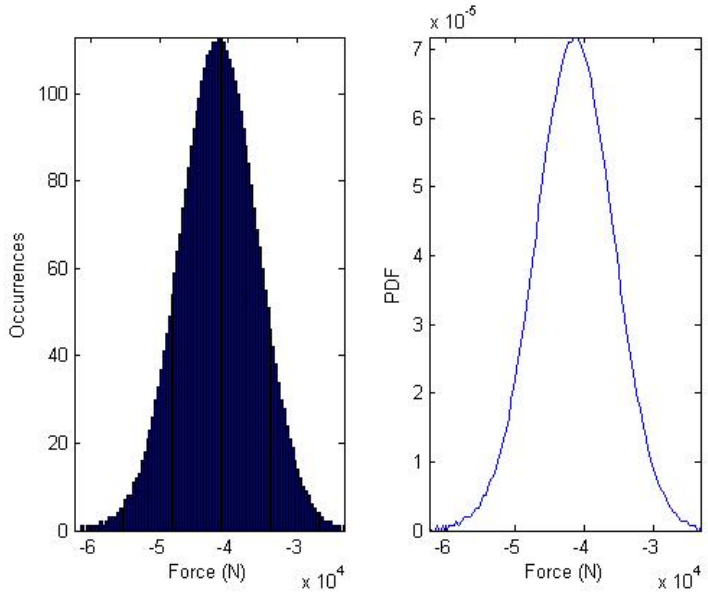

Figure C-5. Histogram and PDF of uncertain B-Pin X force at t=70.26 sec

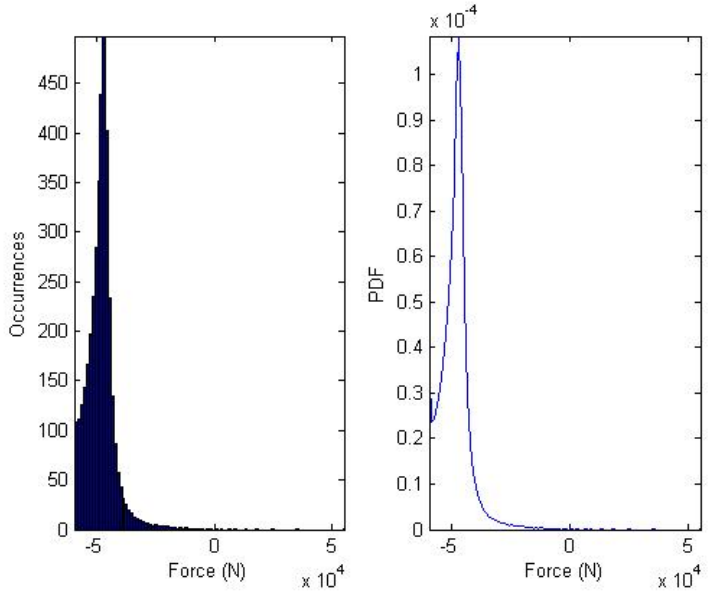

Figure C-6. Histogram and PDF of uncertain B-Pin X force at t=70.28 sec

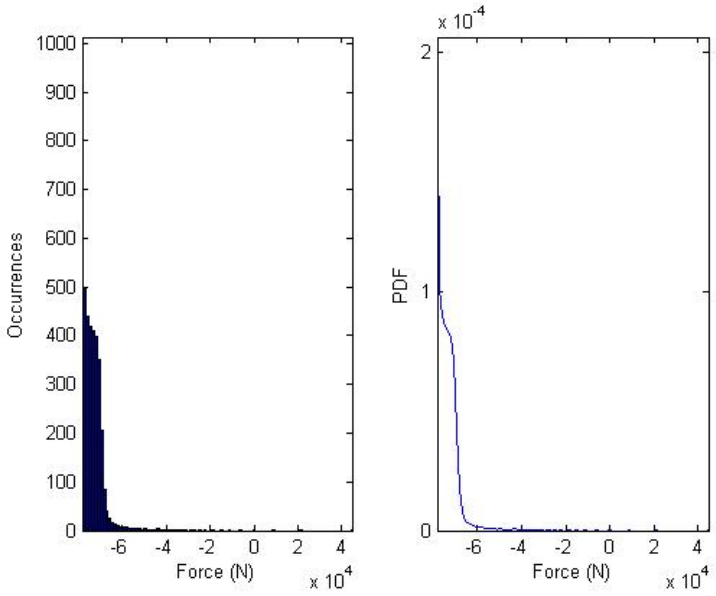

Figure C-7. Histogram and PDF of uncertain B-Pin X force at t=92.06 sec

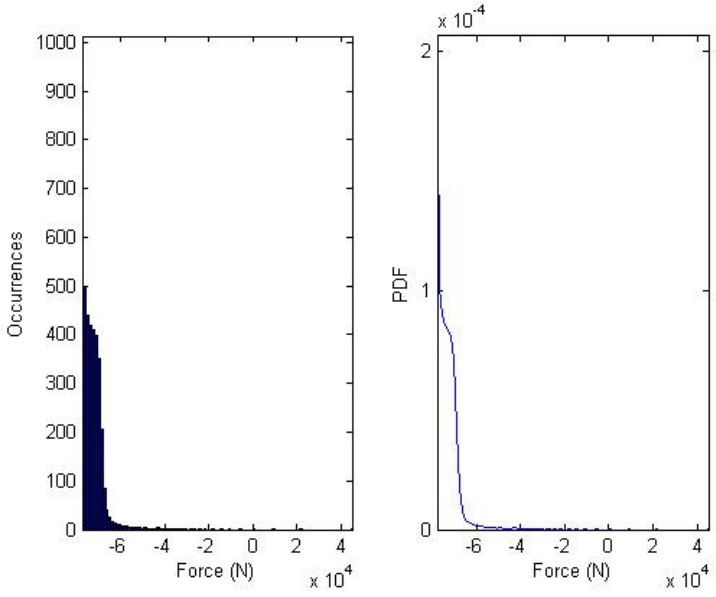

Figure C-8. Histogram and PDF of uncertain B-Pin X force at t=92.08 sec

REFERENCES

[1] Rehnburg, Adam. Vehicle Dynamic Analysis of Wheel Loaders with Supsended Axles. Licentiate Thesis. Royal Institute of Technology, 2008.

[2] B. McCunn, "Modeling the Resistive Forces on Wheel Loader Bucket During Digging" M.S. in *Mechanical and Industrial Engineering*. Urbana-Champaign: University of Illinois. 1996.

[3] Vail, Rob. "Validation of a Caterpillar Virtual Prototyping Wheel Loader Model." Master's of Science. The University of Iowa. 1998.

[4] Zhang, Rongm Carter, E. Don, Alleyne, G. Andrew. "Multivariable Control of an Earthmoving Vehicle Powertrain Experimentally Validated in an Emulated Working Cycle." 2003 ASME International Mechanical Engineering Congress and Exposition, Proceeding of IMECE'03, 2003.

[5] Ericsson, Allan. A Model for Predicting Digging Forces when Workingin Gravel or orther Granulated Material. 15th ADAMS European Users Conference, Rome. Mechanical Dynamics-Digging Forces in Gravel, pp. 1-9, 2000.

[6] Andersson1, Kjell, and Sellgren2, Ulf - *Reality-driven virtual wheel loader operation. Proceedings of Virtual Concept.* 2005 Biarritz, France, November 8th – November 10th, 2005.

[7] Hemami, Ahmad. Motion Trajectory Study in the Schooping Operation of anLHD-Loader. IEE Transactions on Industry Applications, vol, 30, no, 5, September/October 1994.

[8] Fales, Roger and Kelkar, Atul - *Robust Control Design for a Wheel Loader Using Mixed Sensitivity H-infinity and Feedback Linearization Based Methods.* 2005 American Control Conference June 8-10, 2005. Portland, OR, USA

[9] Sundermeyer, Jeffry N. - *The Characterization of Load Uncertainty via Probability Density Functions as an Enabler of Hypothesis Testing of Finite Element Models.* May 10, 2006.

[10] Ghanem, R., and Spanos, P., *Stochastic Finite Elements: A Spectral Approach*, Springer Verlag, 1991.

[11] Ghanem, R., and Spanos, P.; A Spectral Stochastic Finite Element Formulation for Reliability Analysis; *J. of Engineering Mechanics, ASCE* **117(10)**, 1991, 2338--2349.

[12] Dorf, R.C. and Bishop, R.H., *Modern Control Systems*, 9th ed., Prentice Hall, New Jersey, 2001.

[13] Trefethen, L.N., and Baw, D., III, *Spectral Methods in MATLAB*, SIAM, 1998.

[14] Tatang, M.A., Pan, W., Prinn, R.G., and McRae, G.J.; An efficient method for parametric uncertainty analysis of numerical geophysical models; *J. Geophy. Res*. **102**, 1997, 21925--21931.

[15] Isukapalli, S.S., Roy, A., and Georgopoulos, P.G.; Stochastic Response Surface Methods (SRSMs) for Uncertainty Propoagation: Application to Environmental and Biological Systems; 1998, http://www.ccl.rutgers.edu/~ssi/ srsmreport/srsm.html.

[16] Isukapalli, S.S., and Georgopoulos, P.G.; Development and Application of Methods for Assessing Uncertainty in Photochemical Air Quality Problems; *Interim Report*, prepared for the U.S.EPA National Exposure Research Laboratory, under Cooperative Agreement CR 823467, 1998.

[17] Sandu, A., Sandu, C., and Ahmadian, M. – "Modeling Multibody Dynamic Systems With Uncertainties. Part I: Theoretical and Computational Aspects", Multibody System Dynamics, Publisher: Springer Netherlands, ISSN: 1384-5640 (Paper) 1573-272X (Online), DOI 10.1007/s11044-006-9007-5, pp. 1-23 (23), June 29, 2006.

[18] Sandu, C., Sandu, A., and Ahmadian, M. – "Modeling Multibody Dynamic Systems With Uncertainties. Part II: Numerical Applications", Multibody System Dynamics, Publisher: Springer Netherlands, ISSN: 1384-5640 (Paper) 1573-272X (Online), DOI: 10.1007/s11044-006-9008-4, Vol. 15, No. 3, pp. 241 - 262 (22), April 2006.

[19] D. Negrut, G. Ottarson, R. Rampalli, and A. Sajdak, "On an Implementation of the Hilber-Hughes-Taylor Method in the Context of Index 3 Differential-Algebraic Equations of Multibody," *Journal of Computational and Nonlinear Dynamics,* vol. 2, pp. 73 – 85, 2007.

[20] H. Chang and A. Sandu, "Uncertainty Quantification and Apportionment of Air Quality Models using the Polynomial Chaos Method", Computer Science Technical Report TR-07-37, Virginia Tech, 2007.